EQUIVALENCE MEASUREMENT STUDIES (SECTIONS 5 - 6 AND APPENDIXES A, B AND C)

Phillip A. Bello, et al

CNR, Incorporated

Prepared for:

Rome Air Development Center

April 1975

DISCLAIMER NOTICE

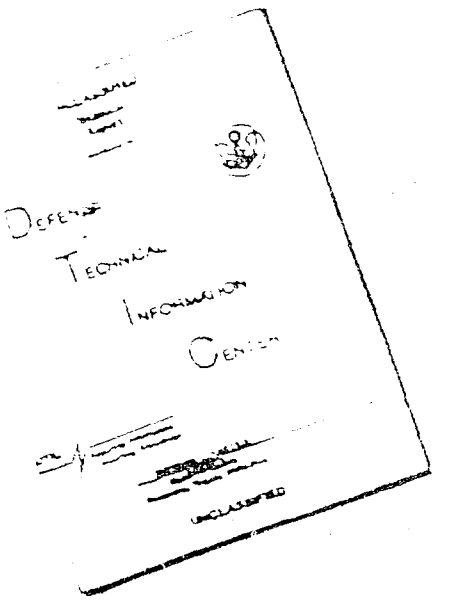

THIS DOCUMENT IS BEST QUALITY AVAILABLE. THE COPY FURNISHED TO DTIC CONTAINED A SIGNIFICANT NUMBER OF PAGES WHICH DO NOT REPRODUCE LEGIBLY.

RADC-TR-75-95, Volume II (of two)
Final Technical Report
April 1975

EQUIVALENCE MEASUREMENT STUDIES
(Sections 5 - 6 & Appendixes A, B & C)

CNR, Inc.

Rome Air Development Center
Air Force Systems Command
Griffiss Air Force Base, New York 13441

UNCLASSIFIED

SECURITY CLASSIFICATION OF THIS PAGE *(When Data Entered)*

REPORT DOCUMENTATION PAGE		READ INSTRUCTIONS BEFORE COMPLETING FORM
1. REPORT NUMBER RADC-TR-75-95, Volume II (of two)	2. GOVT ACCESSION NO.	3. RECIPIENT'S CATALOG NUMBER
4. TITLE *(and Subtitle)* EQUIVALENCE MEASUREMENT STUDIES (Sections 5 - 6 & Appendixes A, B & C)		5. TYPE OF REPORT & PERIOD COVERED Final Technical Report April 1973 - May 1974 6. PERFORMING ORG. REPORT NUMBER N/A
7. AUTHOR(s) Phillip A. Bello Louis A. Jankauskas Leslie W. Pickering		8. CONTRACT OR GRANT NUMBER(s) F30602-73-C-0267
9. PERFORMING ORGANIZATION NAME AND ADDRESS CNR, Inc. 20 Wells Ave. Newton, MA 02159		10. PROGRAM ELEMENT, PROJECT, TASK AREA & WORK UNIT NUMBERS 62702F 45191812
11. CONTROLLING OFFICE NAME AND ADDRESS Rome Air Development Center (DCLD) Griffiss AFB, NY 13441		12. REPORT DATE April 1975 13. NUMBER OF PAGES 168
14. MONITORING AGENCY NAME & ADDRESS*(if different from Controlling Office)* Same		15. SECURITY CLASS. *(of this report)* UNCLASSIFIED 15a. DECLASSIFICATION/DOWNGRADING SCHEDULE N/A

16. DISTRIBUTION STATEMENT *(of this Report)*

Approved for public release; distribution unlimited.

17. DISTRIBUTION STATEMENT *(of the abstract entered in Block 20, if different from Report)*

Same

18. SUPPLEMENTARY NOTES

RADC Project Engineer:
Charles N. Meyer (DCLD)
AC 315 330-2859

19. KEY WORDS *(Continue on reverse side if necessary and identify by block number)*

Channel Quality Monitoring; HF Channel; Troposcatter Channel; Line-of-sight Microwave Relay Channel; Satellite Ionospheric Scintillation Channel; Advanced Data Transmission Modems

20. ABSTRACT *(Continue on reverse side if necessary and identify by block number)*

This report describes the results of an investigation concerned with developing and evaluating concepts for channel quality monitoring of advanced digital data transmission techniques over four fading dispersive channels of interest to military communications: the line-of-sight ground point-to-point microwave relay, troposcatter, satellite ionospheric scintillation, and high-frequency long haul channels. The study emphasis is on a monitoring subsystem called the Media Quality Unit (MQU) which continually estimates long- and short-term error rates for a nondegraded receiver and by comparison with actual error rate as

DD FORM 1 JAN 73 1473 EDITION OF 1 NOV 65 IS OBSOLETE

UNCLASSIFIED

SECURITY CLASSIFICATION OF THIS PAGE *(When Data Entered)*

PRICES SUBJECT TO CHANGE

measured by a Performance Monitor Unit (PMU) allows estimation of receiver degradation trends and classification of outages into receiver-, media, or interference-caused. Major effort was devoted to development and analysis of MQU techniques which utilize the received information-bearing signal alone as a source of channel information since continuous on-line operation is possible and no special probing signals are required. However, some attention is given to special probing signals and their application to each of the channels of interest. For all channel parameter and error rate estimation techniques, the measurement accuracy was determined as a function of processing bandwidth, averaging time, and channel parameters. Consideration is given to implementation alternatives for the MQU in terms of analog, digital hardware, and small computer processing.

PREFACE

This final report, covering the period April 1973 to May 1974, was prepared by CNR, Inc., of Newton Massachusetts, under Contract F30602-73-C-0267 with Rome Air Development Center, Griffiss Air Force Base, New York.

This study was carried out by Dr. P. A. Bello, Dr. L. E. Jankauskas, and Dr. L. W. Pickering. The project was directed by Dr. P. A. Bello.

The authors wish to acknowledge the ready and willing assistance of RADC project engineer, Mr. C. N. Meyer. The project was originally administered by the Signal Processing Section of RADC under the direction of Mr. Miles Bickelhaupt and subsequently transferred to the Digital Technical Control Group under Mr. D. Iram.

Because of the size of this report, it has been divided into 2 volumes. Vol I contains Sections 1 through 4. Vol II contains Sections 5 through 6 and Appendixes A, B & C.

This report has been reviewed by the RADC Information Office (OI) and is releasable to the National Technical Information Service (NTIS). At NTIS it will be releasable to the general public, including foreign nations.

This technical report has been reviewed and approved for publication.

APPROVED: Charles N Meyer

CHARLES N. MEYER
Project Engineer

APPROVED: Fred I Diamond

FRED I. DIAMOND,
Technical Director
Communications & Navigation Division

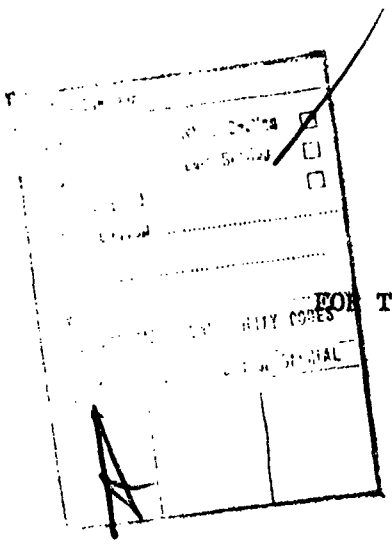

FOR THE COMMANDER: John P Huss

JOHN P. HUSS
Acting Chief, Plans Office

Do not return this copy. Retain or destroy.

SECTION 5

ERROR RATE ESTIMATION UTILIZING CHANNEL MEASUREMENTS BASED UPON RECEIVED SIGNALS ALONE

This section of the report deals with the specification and analysis of techniques for predicting error rates for the fading channels of interest. A variety of techniques are considered varying in complexity and performance. It has been pointed out in Section 2 that the LOS channel should be analyzed on a quasi-stationary basis because bad performance occurs only during deep fades which, by link design, are (hopefully) made to be rare. It is more meaningful, for channel quality monitoring of LOS channels, to estimate the error rate at each instant of time due to the observed channel strength and frequency selectivity, than to average over an assumed stationary fading channel because the fading is too slow to obtain meaningful averages over the time duration of the fading state. Thus, the results here should be regarded as applicable to the HF, Troposcatter, and Satellite Scintillation channels although strictly for comparison purposes we have presented average error rate estimates for the LOS channel also. When the fading is flat over the typical DCS LOS bandwidth of 14 MHz, a very reliable estimate of quasi-stationary error rate is obtainable by using the measured $|T(f,t)|^2$ in an appropriate error rate formula. The existence of frequency selectivity may be determined from measurements of $|T(kF,t)|^2$ but quasi-stationary error rates cannot be estimated knowing $|T(f,t)|^2$ alone. Special probing signals are required to estimate $T(f,t)$.

The discussion below is divided into six sections. Sections 5.1 - 5.3 analyze three classes of techniques for average error rate estimation due to flat fading in diversity-combining receivers. An appropriate "instantaneous" error rate is determined and then averaged over the fading for the techniques of Section 5.1. In Section 5.2, the probabilities that instantaneous SNR's are below thresholds are measured and related to the desired error probabilities. For Section 5.3 a formula is assumed relating average error rate to SNR and to diversity branch correlation. Measurements of the latter are used in the formulas to estimate error rate. Section 5.4 presents examples of the estimation of irreducible error rate due to fast fading and frequency-selective fading. Section 5.5 considers the estimation of error rate for an FDM-FM data transmission system. Section 5.6 discusses the error rate estimation problem for advanced anti-multipath modems which employ in-band diversity. Finally, Section 5.7 deals with the analysis of error rate estimation techniques when interference is present. In all analyses complex Gaussian fading statistics are assumed.

5.1 Flat Fading Error Rate Estimation by Averaging "Instantaneous" Error Rates

5.1.1 Introduction

In this section we address the problem of estimating the error rate of a flat fading channel by averaging instantaneous error rate estimates. Two techniques are examined. The first technique uses estimates of the instantaneous SNR on each diversity branch to form error rate estimates for each of the diversity branches. The branch error rate estimates are then used to estimate the channel error rate, assuming independently fading diversity channels. The second technique that is examined is to use instantaneous SNR estimates to estimate the SNR at the output of the diversity combiner. The combiner output SNR is used to estimate an error rate at that instant. These instantaneous error rates are averaged to form an estimate of the channel error rate. This technique does not require the assumption of independently fading diversity channels. However, it is more difficult to estimate error rates when the modem error rate is low. A technique is proposed for alleviating this problem by amplifying the apparent error rate and extrapolating to the correct value.

Finally, a technique is studied for predicting short-term error bursts.

5.1.2 Use of Diversity Branch Error Rate Estimates for Error Rate Prediction

In this section we consider the problem of estimating the error rate of a flat fading channel from estimates of the instantaneous error rate on each diversity branch, assuming independently fading diversity branches. Figure 5.1 is a block diagram of the system to be analyzed. The estimation procedure is as follows. The data signal is transmitted over the diversity channel, picked off at RF (or IF) in the receiver, and sent to a magnitude-squared channel transfer function estimator of the type analyzed in Section 4.1. The output of the estimator is sampled and combined with an estimate of the noise power to form an estimate of the instantaneous SNR. From this instantaneous SNR estimate, we obtain an estimate of the instantaneous error rate for that diversity branch. These are averaged to form an estimate of the average error rate, which are combined with the average error rate estimates of the other diversity branches to give a channel error rate estimate. A possible correction for the bias in the error probability estimator is shown in dashed lines.

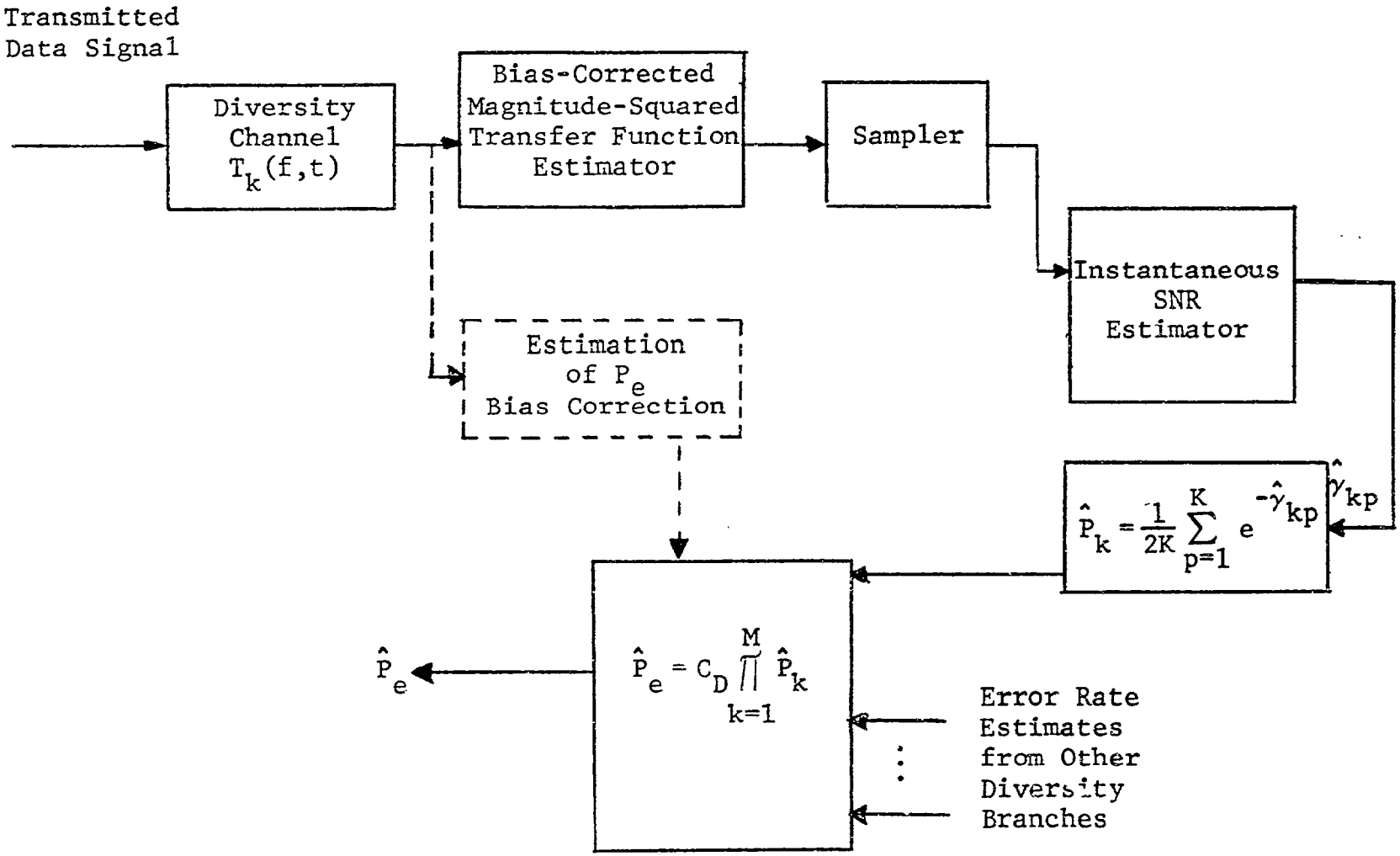

Figure 5.1 Block Diagram of Error Rate Estimator 1

For analysis purposes, a 2-phase DCPSK system is used. This scheme is sufficiently similar to other signaling schemes so that the results of this section can be used for comparison purposes. For a 2-phase DCPSK system and Gaussian noise, the error rate conditioned upon the SNR is given by

$$P = \frac{1}{2} e^{-\gamma} \tag{5.1}$$

where γ is the SNR. From (5.1) and estimates of the signal-to-noise ratio on the k^{th} diversity branch and in the p^{th} sampling instant, we can form an estimate of what the ensemble error rate would be on this branch and at this sampling instant if the other branches were not there:

$$\hat{P}_{kp} = \frac{1}{2} e^{-\hat{\gamma}_{kp}} \tag{5.2}$$

where $\hat{\gamma}_{kp}$ is an estimate of the SNR on the k^{th} branch and at the p^{th} instant. Assuming stationarity, the error rate on the k^{th} branch can be formed by averaging the above estimates. This gives an estimate of the error rate for the k^{th} branch acting alone:

$$\hat{P}_k = \frac{1}{2K} \sum_{p=1}^{K} e^{-\hat{\gamma}_{kp}} \tag{5.3}$$

For many diversity combining techniques, it is possible to express the error rate of the channel approximately in terms of the error rates of the particular branches acting alone when independent fading occurs on the diversity branches. For example, with M the order of diversity, we can express the error rate by [5.1]

$$P_e \approx C \prod_{k=1}^{M} P_k \tag{5.4}$$

where

$$C = \begin{cases} \dfrac{M^M \sqrt{\pi}}{2\left(M - \frac{1}{2}\right)!} & \text{for equal gain combining} \\ M!\ 2^{M-1} & \text{for selection combining} \\ 2^{M-1} & \text{for maximal ratio combining} \end{cases}$$

Equation (5.4) is exactly true for maximal ratio combining, asymptotically true for low error rates, but still useful for error rates up to 10^{-2} to 10^{-1} for the other combining techniques. From (5.4) we can estimate the error rate by

$$\hat{P}_e = C \prod_{k=1}^{M} \hat{P}_k \tag{5.5}$$

The ability of (5.5) to estimate the error rate will be determined. From (4.250) of Section 4.3, the estimate of the SNR on the k^{th} diversity branch and at the p^{th} sampling instant can be approximately represented by

$$\hat{\gamma}_{kp} = (1+\epsilon_{kp})\,\gamma_{kp} + \delta_{kp} \tag{5.6}$$

where γ_{kp} is the actual instantaneous SNR, and ϵ_{kp} and δ_{kp} are independent estimate errors with first- and second-order error moments approximately given by

$$\begin{aligned} \overline{\epsilon_{kp}} &= \overline{\delta_{kp}} = 0 \\ \overline{\epsilon_{kp}^2} &= \epsilon^2 \\ \overline{\delta_{kp}^2} &= \epsilon_S^2 \Gamma_k^2 \end{aligned} \tag{5.7}$$

where, for the estimator of Figure 4.1, ϵ and ϵ_S are, respectively, given by (4.57) and (4.100). In (5.7), Γ_k is the mean SNR of the k^{th} diversity branch. Using (5.6) in (5.3), the estimate of the error rate on the k^{th} diversity branch acting alone is given by

$$\hat{P}_k = \frac{1}{2K} \sum_{p=1}^{K} e^{-\left[(1+\epsilon_{kp})\gamma_{kp}+\delta_{kp}\right]} \tag{5.8}$$

Averaging over the instantaneous SNR estimation errors and channel fluctuations gives

$$E\left\{\hat{P}_k\right\} = \frac{1}{2K} \sum_{p=1}^{K} E\left\{ e^{-\left[(1+\epsilon_{kp})\gamma_{kp}+\delta_{kp}\right]} \right\} \tag{5.9}$$

Since the estimation errors due to the channel selectivity, δ_{kp}, are independent of the errors due to noise and data, ϵ_{kp},

$$E\left\{\hat{P}_k\right\} = \frac{1}{2K} \sum_{p=1}^{K} E\left\{e^{-\delta_{kp}}\right\} E\left\{e^{-(1+\epsilon_{kp})\gamma_{kp}}\right\} \tag{5.10}$$

For zero mean complex Gaussian channels, γ_{kp} has a one-sided exponential distribution with mean Γ_k. Therefore, performing the average over the channel fluctuations gives

$$E\left\{\hat{P}_k\right\} = \frac{1}{2K} \sum_{p=1}^{K} E\left\{e^{-\delta_{kp}}\right\} E\left\{\frac{1}{\Gamma_k + 1 + \epsilon_{kp}\Gamma_k}\right\} \tag{5.11}$$

The channels studied have allowed sufficiently accurate estimation of the magnitude squared of the channel transfer function so that $E\left\{\hat{P}_k\right\}$ can be accurately expressed in terms of the first- and second-order moments of the error. Therefore, we can approximate (5.11) by

$$E\left\{\hat{P}_k\right\} = \frac{\left[1 + \frac{\epsilon_S^2}{2}\Gamma_k^2 + \frac{\epsilon^2\Gamma_k^2}{(\Gamma_k+1)^2}\right]}{2(\Gamma_k+1)} \tag{5.12}$$

Noting that for the system considered we have [5.1] for the average error rate of the k^{th} diversity branch acting alone

$$P_k = \frac{1}{2(\Gamma_k+1)} \tag{5.13}$$

and upper bounding slightly the term in ϵ^2 by assuming $\Gamma_k/(\Gamma_k+1) = 1$, it immediately follows that

$$\boxed{E\left\{\hat{P}_k\right\} \approx P_k\left[1 + \frac{\epsilon_S^2}{2}\Gamma_k^2 + \epsilon^2\right]} \tag{5.14}$$

Hence, the diversity branch error rate estimator is biased. The quantity ϵ is known and σ_ϵ will normally be measured. If ϵ_S^2 could be estimated, the bias could be corrected. While insufficient time was available to study this question, it appears that ϵ_S can be measured.

The error variance in estimating P_k will be determined next. Squaring (5.8) and averaging gives for the second moment of the estimate of the error rate for the k^{th} diversity branch acting alone

$$E\left\{\hat{P}_k^2\right\} = \frac{1}{4K^2} \sum_{p=1}^{K} \sum_{q=1}^{K} E\left\{e^{-\left[(1+\epsilon_{kp})\gamma_{kp}+\delta_{kp}+(1+\epsilon_{kq})\gamma_{kq}+\delta_{kq}\right]}\right\} \tag{5.15}$$

To evaluate the above expectation, the joint density of γ_{kp} and γ_{kq} must be known. For a complex Gaussian channel, the joint density is a function of the correlation coefficient of the channel complex envelope. In particular, defining

$$\rho_{pq} \triangleq \frac{\left|E\left\{T_k^*(F,t_p)T_k(F,t_q)\right\}\right|}{E\left\{|T_k(f,t)|^2\right\}} \tag{5.16}$$

where $T_k(f,t)$ is the time-varying channel transfer function of the k^{th} diversity branch, then the joint density of γ_{kp} and γ_{kq} can be expressed as [5.2]

$$p(\gamma_{kp},\gamma_{kq}) = \frac{1}{\Gamma_k^2\left(1-\rho_{pq}^2\right)} I_0\left(\frac{2\rho_{pq}\sqrt{\gamma_{kp}\gamma_{kq}}}{\Gamma_k\left(1-\rho_{pq}^2\right)}\right) e^{-\left[\frac{\gamma_{kp}+\gamma_{kq}}{\Gamma_k(1-\rho_{pq}^2)}\right]} \tag{5.17}$$

Using (5.17) to perform the average over γ_{kp} and γ_{kq} gives for the second moment of the error rate estimate on the k^{th} diversity branch acting alone

$$E\left\{\hat{P}_k^2\right\} = \frac{1}{4K^2} \sum_{p=1}^{K} \sum_{q=1}^{K} E\left\{ \frac{e^{-(\delta_{kp}+\delta_{kq})}}{\Gamma_k^2(1+\epsilon_{kp})(1+\epsilon_{kq})(1-\rho_{pq}^2) + \Gamma_k(2+\epsilon_{kp}+\epsilon_{kq}) + 1} \right\} \tag{5.18}$$

Expressing $E\left\{\hat{P}_k^2\right\}$ in terms of the first- and second-order moments of the errors gives

$$E\left\{\hat{P}_k^2\right\} = \frac{1 + 2\epsilon_S^2\Gamma_k^2 + \epsilon^2}{4K(2\Gamma_k + 1)} + \frac{1 + \epsilon_S^2\Gamma_k^2 + 2\epsilon^2}{4K^2} \sum_{\substack{p=1 \\ p\neq q}}^{K} \sum_{q=1}^{K} \frac{1}{(\Gamma_k+1)^2 - (\rho_{pq}\Gamma_k)^2} \tag{5.19}$$

where the errors at different sampling times were assumed to be independent.

To simplify notation, we define $\Phi(\rho_{pq})$ as

$$\Phi(\rho_{pq}) \triangleq \frac{(\rho_{pq}\Gamma_k)^2}{(\Gamma_k+1)^2 - (\rho_{pq}\Gamma_k)^2} \tag{5.20}$$

where we note that $\Phi(\rho_{pq}) \to 0$ as $\rho_{pq} \to 0$. Figure 5.2 presents typical time dependencies for the functions discussed in this section.

Substituting the above expression for $\Phi(\rho_{pq})$ into Eq. (5.19) and using the expression for P_k given by (5.13) gives approximately for $E\left\{\hat{P}_k^2\right\}$

$$E\left\{\hat{P}_k^2\right\} = \frac{1 + 2\epsilon_S^2\Gamma_k^2 + \epsilon^2}{4K(2\Gamma_k + 1)} + P_k^2 \frac{\left(1 + \epsilon_S^2\Gamma_k^2 + 2\epsilon^2\right)}{4K^2} \sum_{\substack{p=1 \\ p\neq q}}^{K} \sum_{q=1}^{K} \left[\Phi(\rho_{pq}) + 1\right] \tag{5.21}$$

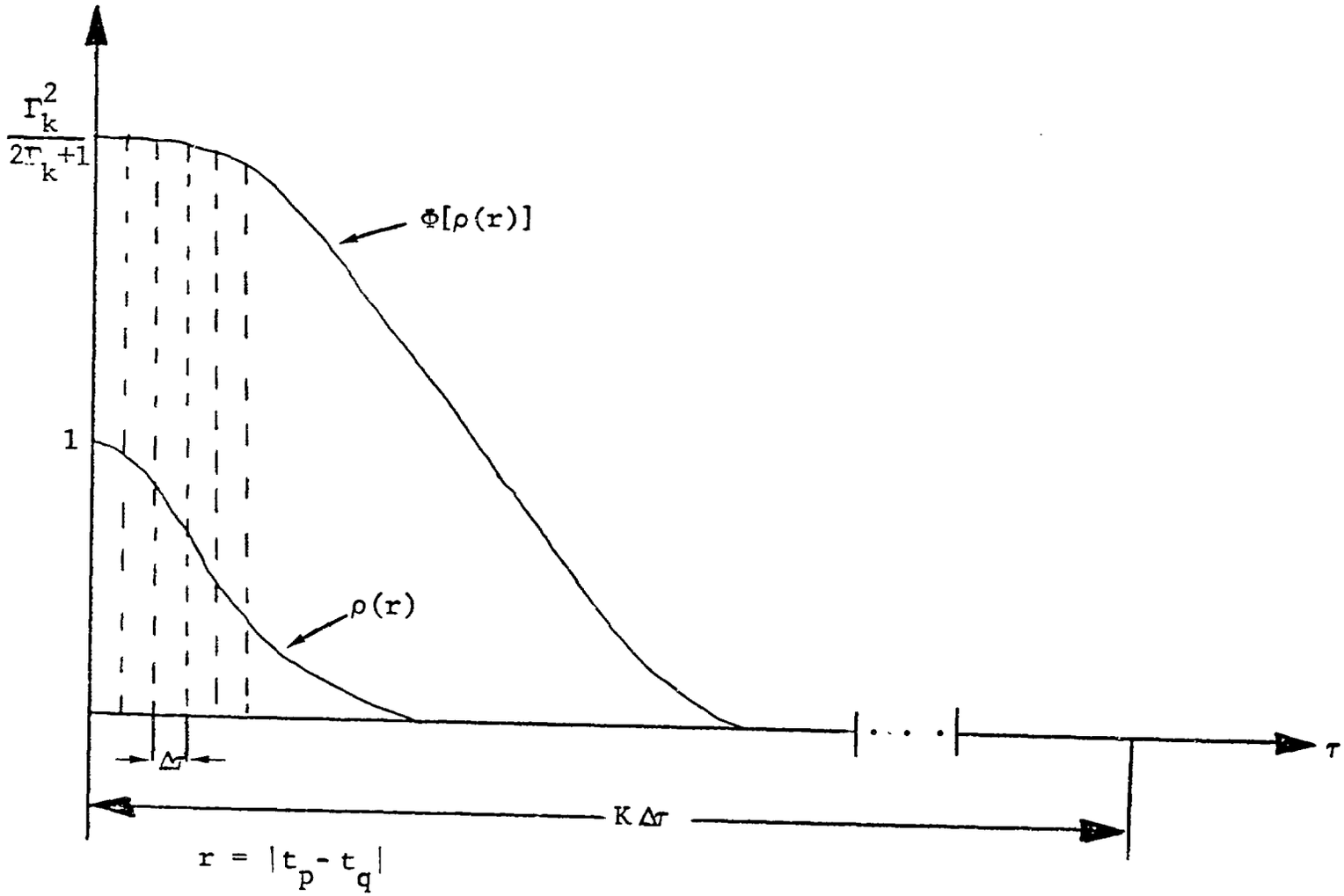

$r = |t_p - t_q|$

$\rho(r) = \rho_{pq}$

$\Delta\tau = t_{p+1} - t_p$

Figure 5.2 Time Dependence of Various Functions

Using (5.12) and (5.21) to evaluate the variance of the error rate estimate of the k^{th} diversity branch acting alone gives

$$\sigma^2_{\hat{P}_k} = \frac{1+2\epsilon^2_S\Gamma_k^2+\epsilon^2}{4K(2\Gamma_k+1)} - \frac{1+\epsilon^2_S\Gamma_k^2+2\epsilon^2}{K} P_k^2 + \frac{1+\epsilon^2_S\Gamma_k^2+2\epsilon^2}{K^2} P_k^2 \sum_{\substack{p=1 \\ p\neq q}}^{K} \sum_{q=1}^{K} \Phi(\rho_{pq}) \tag{5.22}$$

where higher than second-order error moments were considered negligible.

For stationary scatter channels, ρ_{pq} can be expressed in terms of $|t_p-t_q|$ and, for equally spaced samples, ρ_{pq} can be expressed in terms of $|p-q|$. Thus, for this case, the double sum of (5.22) can be written as a single sum giving

$$\sigma^2_{\hat{P}_k} = \frac{1+2\epsilon^2_S\Gamma_k^2+\epsilon^2}{4K(2\Gamma_k+1)} - \frac{1+\epsilon^2_S\Gamma_k^2+2\epsilon^2}{K} P_k^2 + \frac{1+\epsilon^2_S\Gamma_k^2+2\epsilon^2}{K^2} 2P_k^2 \sum_{r=1}^{K-1} (K-r)\, \Phi[\rho(r)] \tag{5.23}$$

where $\rho(r) = \rho_{pq}$ with $r = |p-q|$.

When K is large, $\Phi[\rho(r)]$ contributes to the above sum only when $K-r \approx K$. Furthermore, the second term is negligible for all cases of practical interest. Therefore, the variance of the estimator is closely given by

$$\boxed{\sigma^2_{\hat{P}_k} \approx \frac{1+2\epsilon^2_S\Gamma_k^2+\epsilon^2}{4K(2\Gamma_k+1)} + \frac{1+\epsilon^2_S\Gamma_k^2+2\epsilon^2}{K} 2P_k^2 \sum_{r=1}^{K-1} \Phi[\rho(r)]} \tag{5.24}$$

Therefore, from (5.14) and (5.24) we can express the estimate of the error rate of the k^{th} diversity branch acting alone by by

$$\hat{P}_k = P_k(1+\omega_k) \tag{5.25}$$

where

$$\bar{\omega}_k = \frac{\epsilon_S^2 \Gamma_k^2}{2} + \epsilon^2$$

$$\sigma^2_{\omega_k} = \frac{\sigma^2_{\hat{P}_k}}{P_k^2}$$

Substituting (5.25) into the pression for the error rate estimate of (5.5) gives

$$\hat{P}_e = C\left(\prod_{k=1}^{M} P_k\right) \prod_{k=1}^{M} (1+\omega_k) \tag{5.26}$$

One may readily compute the mean and variance of $\hat{P}_e$ (5.26). For small ω_k

$$\boxed{E\{\hat{P}_e\} \approx P_e\left(1 + M\epsilon^2 + \frac{\epsilon_S^2}{2} \sum_{k=1}^{M} \Gamma_k^2\right)} \tag{5.27}$$

for independent diversity channels.

The estimator of the error rate is biased. For the systems of interest, the effect of this bias should be assessed and, if the bias is unacceptable, the filter parameters of the magnitude-squared channel transfer function estimator of Figure 4.1 can be chosen to reduce this bias for the expected range of Γ_k's.

From (5.26) and (5.27) the variance of the error rate estimate for small ω_k is given by

$$\boxed{\sigma^2_{\hat{P}_e} = P_e^2 \sum_{k=1}^{M} \frac{\sigma^2_{\hat{P}_k}}{P_k^2}} \tag{5.28}$$

Examples are presented in Section 5.1.5 to illustrate the effectiveness of the error rate estimator analyzed above.

While the above calculations of error bias and variance assumed Gaussian noise, it appears that the results will not differ significantly for atmospheric noise. (Calculations of error rate with atmospheric rather than Gaussian noise have been carried out by Bello [5.17].) This may be deduced by noting that the curves of error rate vs. SNR for atmospheric noise (see Figures 2 and 3 of [5.17]) are similar to those for Gaussian noise. These comments apply to all the error rate estimation techniques and will not be repeated.

5.1.3 Use of Diversity Combiner Output Instantaneous SNR Estimates for Error Rate Prediction

In this section we address the problem of estimating the error rate for a flat fading channel by averaging instantaneous error rate estimates determined after pseudo-diversity combining. Figure 5.3 is a functional block diagram of the error rate estimator to be considered. The estimation procedure is as follows. The data signal is transmitted over the diversity channel, picked off at RF (or IF) in the receiver, and sent to a magnitude-squared channel transfer function estimator of the type analyzed in Section 4.1. The output of this estimator is sampled and combined with an estimate of the noise power to form an estimate of the instantaneous SNR. This instantaneous SNR estimate, along with instantaneous SNR estimates from the other diversity branches, is sent to a simulated diversity combiner. This simulated combiner produces an estimate of the combiner output SNR at that instant. An instantaneous error rate is then computed and averaged to give an error rate estimate.

For analysis purposes, the modem is chosen to be a two-phase DCPSK system employing M^{th} order maximal ratio combining. A statististically stationary channel with independent fading on diversity branches will be assumed to simplify calculation. However, it should be noted that the method does not require any assumption about the dependence or statistics of the fading. It requires only that the additive noises be Gaussian and independent.

For ideal maximal ratio combining and independently fading diversity branches, the instantaneous SNR at the combiner output is the sum of the input SNR's [5.1]. Hence, the SNR at the combiner output and at the p^{th} sampling instant will be estimated by

$$\hat{\gamma}_p = \sum_{k=1}^{M} \hat{\gamma}_{kp} \tag{5.29}$$

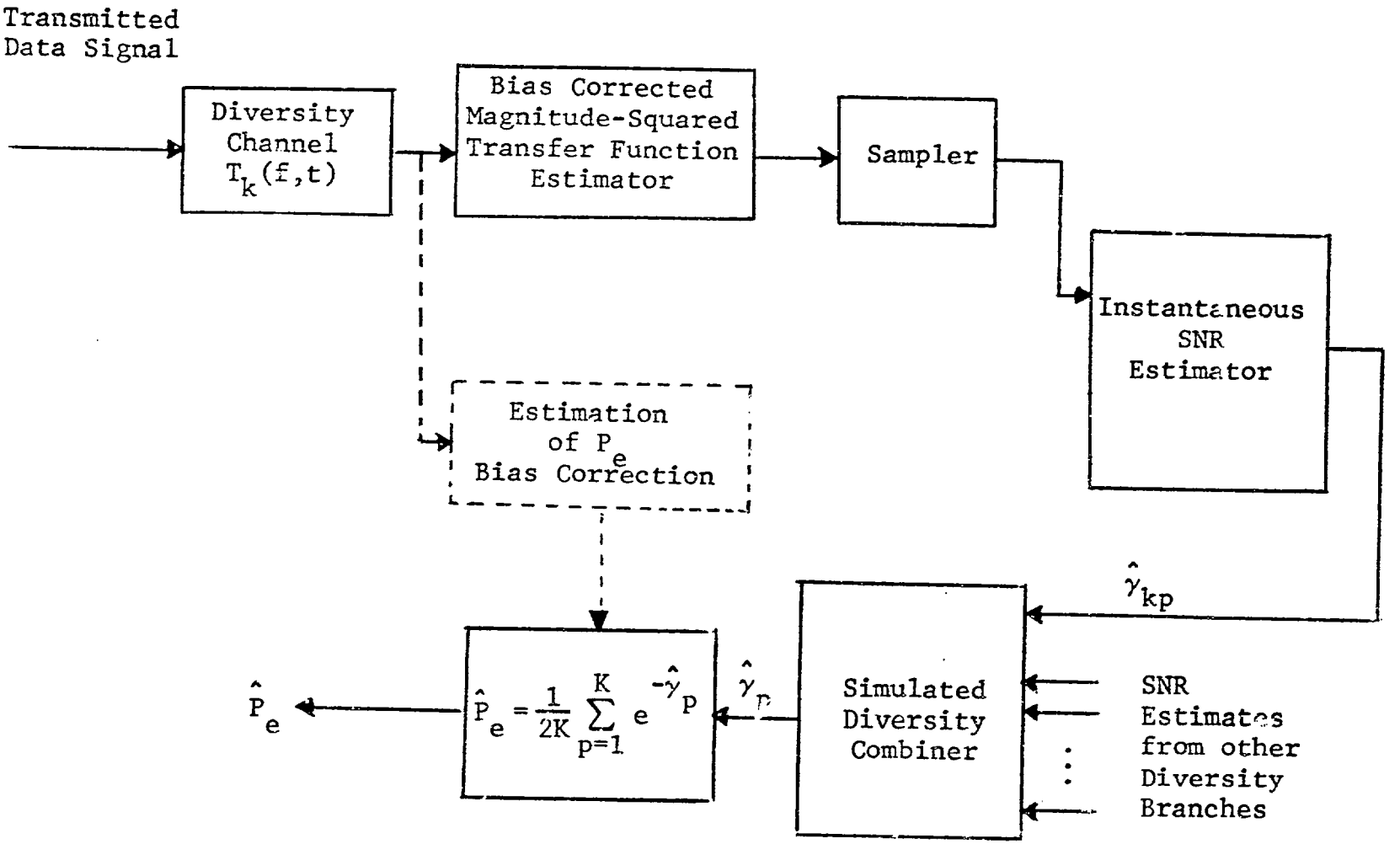

Figure 5.3 Block Diagram of Error Rate Estimator 2

where $\hat{\gamma}_{kp}$ are the estimates of the SNR on the k^{th} diversity branch and at the p^{th} sampling instant.

Furthermore, recalling [from (5.1)] the expression for the error rate of a two-phase DCPSK system in Gaussian noise, we can form an estimate of what the ensemble error rate would be at the p^{th} sampling instant:

$$\hat{P}_e(p) = \frac{1}{2} e^{-\hat{\gamma}_p} \tag{5.30}$$

An estimate of the average error rate can be obtained by averaging these instantaneous error rates. Hence, the average error rate estimate is given by

$$\hat{P}_e = \frac{1}{2K} \sum_{p=1}^{K} e^{-\sum_{k=1}^{M} \hat{\gamma}_{kp}} \tag{5.31}$$

Representing the estimated instantaneous SNR's by Eq. (5.6), the error rate estimate becomes

$$\hat{P}_e = \frac{1}{2K} \sum_{p=1}^{K} e^{-\sum_{k=1}^{M} \gamma_{kp}(1+\epsilon_{kp})+\delta_{kp}} \tag{5.32}$$

where ϵ_{kp} and δ_{kp} are errors in estimating γ_{kp}.

The effectiveness of the above error rate estimate is determined by evaluating its bias and rate of convergence. We will assume that the errors are independent of each other and of γ_{kp}. Furthermore, the diversity branches will be assumed to fade independently in the evaluation of estimator performance. Note, however, that the technique itself is valid for dependent diversity channels since conditional error rates are computed only with the diversity combined SNR. Therefore, we can write

$$E\left\{\hat{P}_e\right\} = \frac{1}{2K} \sum_{p=1}^{K} \prod_{k=1}^{M} E\left\{e^{-\delta_{kp}}\right\} E\left\{e^{-\gamma_{kp}(1+\epsilon_{kp})}\right\} \tag{5.33}$$

Using (5.7) to represent the moments of the errors, then in a manner similar to that shown in Section 5.1.2, it can be shown that $E\{\hat{P}_e\}$ can be closely approximated by

$$E\{\hat{P}_e\} = \left[1+\frac{\epsilon_S^2}{2}\sum_{k=1}^{M}\Gamma_k^2+M\epsilon^2\right]P_e \tag{5.34}$$

where higher than second-order moments of the error were neglected and where, for the system analyzed, the error rate that we are estimating is given by $\dfrac{1}{2\prod_{k=1}^{2}(\Gamma_k+1)}$.

Comparing (5.27) with (5.34), we note that the biases for the two error rate estimators considered in this section are identical.

The second moment of $\hat{P}_e$ is found by squaring and averaging (5.32) to give

$$E\{\hat{P}_e^2\} = \frac{1}{4K^2}\sum_{p=1}^{K}\sum_{q=1}^{K}E\left\{e^{-\left[\sum_{k=1}^{M}\gamma_{kp}(1+\epsilon_{kp})+\gamma_{kq}(1+\epsilon_{kq})+\delta_{kp}+\delta_{kq}\right]}\right\} \tag{5.35}$$

Assuming that the errors in estimating the instantaneous SNR's at different sampling instants are independent, we have

$$E\{\hat{P}_e^2\} = \frac{1}{4K^2}\sum_{p=1}^{K}\prod_{k=1}^{M}\left[E\left\{e^{-2\delta_{kp}}\right\}E\left\{e^{-2\gamma_{kp}(1+\epsilon_{kp})}\right\}\right]$$
$$+\frac{1}{4K^2}\sum_{\substack{p=1\\p\neq q}}^{K}\sum_{q=1}^{K}\prod_{k=1}^{M}\left[E\left\{e^{-(\delta_{kp}+\delta_{kq})}\right\}E\left\{e^{-\gamma_{kp}(1+\epsilon_{kp})+\gamma_{kq}(1+\epsilon_{kq})}\right\}\right] \tag{5.36}$$

Performing the above averages and neglecting higher than second-order moments of the error, it follows that we can closely approximate the second moment of the error rate estimate by

$$E\left\{\hat{P}_e^2\right\} = \frac{1 + M\epsilon^2 + 2\epsilon_S^2 \sum_{k=1}^{M} \Gamma_k^2}{4K \prod_{k=1}^{M} (2\Gamma_k + 1)}$$

$$+ \frac{\left[1 + 2M\epsilon^2 + \epsilon_S^2 \sum_{k=1}^{M} \Gamma_k^2\right] P_e^2}{4K^2} \sum_{\substack{p=1 \\ p \neq q}}^{K} \sum_{q=1}^{K} \left[\Phi_1(\rho_{pq}) + 1\right] \qquad (5.37)$$

where ρ_{pq} is defined by (5.16) and where

$$P_e = \frac{1}{2 \prod_{k=1}^{M} (\Gamma_k + 1)}$$

$$\Phi_1(\rho_{pq}) \triangleq \prod_{k=1}^{M} \left[\frac{(\Gamma_k + 1)^2}{(\Gamma_k + 1)^2 - (\rho_{pq}\Gamma_k)^2}\right] - 1 \qquad (5.38)$$

Also, when $M = 1$, $\Phi_1(\rho_{pq})$ reduces to $\Phi(\rho_{pq})$ as given by (5.20). In fact, it is easy to see that when $M = 1$, the error rate estimates given by (5.5) and (5.31) are identical, as are the techniques given by Figures 5.1 and 5.3.

For a stationary scatter channel, the double sum of (5.37) can be reduced to a single sum by defining $\rho(r)$ as in the previous section. This gives for the variance of the estimate

$$\boxed{\sigma^2_{\hat{P}_e} = \frac{1 + M\epsilon^2 + 2\epsilon_S^2 \sum_{k=1}^{M} \Gamma_k^2}{4K \prod_{k=1}^{M} (2\Gamma_k + 1)} + \frac{2\left[1 + 2M\epsilon^2 + \epsilon_S^2 \sum_{k=1}^{M} \Gamma_k^2\right] P_e^2}{K} \sum_{r=1}^{K-1} \Phi_1[\rho(r)]} \qquad (5.39)$$

where the terms that fall off faster than $\frac{1}{K}$ and higher than second-order error moments were neglected.

For the usual case of not strongly correlated diversity branches, the error rate computed at the diversity combiner output will be very much lower than the error rate of each branch acting alone. As with an error counting procedure, the error rate estimate variance varies as the reciprocal of the error rate that it is desired to measure. Thus, the variance of the P_e estimate for method 2 will normally be much worse than for method 1.

A variant of method 2 was presented in Section 3 which reduces greatly the variance of the P_e estimate. Briefly, the apparent SNR is reduced by a factor r in the conditional error rate estimates. Because the apparent SNR is much less, the apparent error rate is higher and a much smaller variance of the error rate estimate (and bias) is achieved. The correct error rate is estimated by extrapolation with the aid of a theoretical error rate vs. SNR curve. It was shown in Section 2 that the procedure is exact at high SNR and will work for a wide class of fading statistics, additive noises, modulation techniques, and diversity combiners.

5.1.4 Error Burst Estimation

In this section we examine the problem of estimating error bursts from estimates of the instantaneous error rate. The error burst estimates can be used to distinguish error bursts caused by the channel from those caused by the equipment.

The estimator given by Figure 5.3 will be examined for its ability to estimate short-term error bursts. A two-phase DCPSK system employing maximal ratio combining will be used for the analysis. For this system, the error rate estimate is given by [repeating (5.32)]

$$\hat{P}_e = \frac{1}{2K} \sum_{p=1}^{K} e^{-\sum_{k=1}^{M} \gamma_{kp}(1+\epsilon_{kp})+\delta_{kp}} \tag{5.40}$$

where M is the order of diversity, γ_{kp} is the SNR on the k^{th} diversity branch at the p^{th} sampling instant, and ϵ_{kp} and δ_{kp} are errors in estimating γ_{kp} due to noise, data, and the selectivity of the channel.

It will be assumed that the samples are taken close enough together such that the SNR can be considered to be constant in each sampling interval. Since the fading rate of the channel is much slower than the data rate, many data bits will be received between samples of the output of the magnitude-squared channel transfer function estimator. We will assume that N data bits are received for each SNR sample. Therefore, since, from (5.40), there are K SNR samples on each branch, NK data bits are received in the time interval over which we are estimating error bursts.

The fraction of data bits received in error during the observation interval is given by

$$P_C = \frac{1}{NK} \sum_{p=1}^{K} \sum_{\ell=1}^{N} \beta(p,\ell) \tag{5.41}$$

where

$$\beta(p,\ell) = \begin{cases} 1, & \text{if the } \ell^{th} \text{ data bit in the } p^{th} \\ & \text{sampling interval is in error} \\ 0, & \text{otherwise} \end{cases}$$

In this section, we will examine the use of the error rate estimate given by (5.40) as a means of estimating P_C given by (5.41). The effectiveness of this estimator is determined by the mean-squared difference given by

$$MSD = E\left\{\left(P_C - \hat{P}_e\right)^2\right\} \tag{5.42}$$

By direct substitution, MSD can be expressed as

$$MSD = E\left\{\left(\frac{1}{NK} \sum_{p=1}^{K} \sum_{\ell=1}^{N} \beta(p,\ell) - \frac{1}{2K} \sum_{k=1}^{K} e^{-\sum_{k=1}^{M} \gamma_{kp}(1+\epsilon_{kp})+\delta_{kp}}\right)^2\right\} \tag{5.43}$$

To evaluate the MSD, we will first find the MSD conditioned upon $\{\epsilon_{kp}, \gamma_{kp}, \delta_{kp}\}$. This conditional mean-squared difference is given by

$$\mathrm{MSD}_{\{\gamma_{kp},\epsilon_{kp},\delta_{kp}\}} = \frac{1}{(NK)^2} \sum_{p=1}^{K} \sum_{q=1}^{K} \sum_{\ell=1}^{N} \sum_{n=1}^{N} E\left\{\beta(p,\ell)\beta(q,n)\left|\left[\gamma_{kp},\epsilon_{kp},\delta_{kp}\right]\right.\right\}$$

$$- \frac{1}{2NK^2} \sum_{p=1}^{K} \sum_{q=1}^{K} \sum_{\ell=1}^{N} e^{-\sum_{k=1}^{M} \gamma_{kq}(1+\epsilon_{kq})+\delta_{kq}} E\left\{\beta(p,\ell)\left|\left[\gamma_{kp},\epsilon_{kp},\delta_{kp}\right]\right.\right\}$$

$$- \frac{1}{2NK^2} \sum_{p=1}^{K} \sum_{q=1}^{K} \sum_{n=1}^{N} e^{-\sum_{k=1}^{M} \gamma_{kp}(1+\epsilon_{kp})+\delta_{kp}} E\left\{\beta(q,n)\left|\left[\gamma_{kp},\epsilon_{kp},\delta_{kp}\right]\right.\right\}$$

$$+ \frac{1}{4K^2} \sum_{p=1}^{K} \sum_{q=1}^{K} e^{-\sum_{k=1}^{M} \gamma_{kp}(1+\epsilon_{kp})+\delta_{kp}+\gamma_{kq}(1+\epsilon_{kq})+\delta_{kq}} \qquad (5.44)$$

Recalling the assumption that the SNR estimates are taken close enough together such that the SNR can be assumed constant in a sampling interval and also recalling (5.1), then for the two-phase DCPSK system considered, the required expectations are given by

$$E\left\{\beta(p,\ell)\left|\left[\gamma_{kp},\epsilon_{kp},\delta_{kp}\right]\right.\right\} = \frac{1}{2} e^{-\sum_{k=1}^{M} \gamma_{kp}} \qquad (5.45)$$

$$E\left\{\beta(p,\ell)\beta(q,n)\left|\left[\gamma_{kp},\epsilon_{kp},\delta_{kp}\right]\right.\right\} = \begin{cases} \frac{1}{2} e^{-\sum_{k=1}^{M} \gamma_{kp}} & \text{, if } p=q \text{ and } \ell=n \\ \frac{1}{4} e^{-\sum_{k=1}^{M} \gamma_{kp}+\gamma_{kq}} & \text{, otherwise} \end{cases} \qquad (5.46)$$

Substituting (5.45) and (5.46) into (5.44) gives for the conditional mean-squared difference

$$\mathrm{MSD}_{\{\gamma_{kp},\epsilon_{kp},\delta_{kp}\}} = \frac{1}{4K^2}\sum_{p=1}^{K}\sum_{q=1}^{K}\left[e^{-\sum_{k=1}^{M}\gamma_{kp}+\gamma_{kq}} - e^{-\sum_{k=1}^{M}\gamma_{kp}(1+\epsilon_{kp})+\delta_{kp}+\gamma_{kq}} - e^{-\sum_{k=1}^{M}\gamma_{kq}(1+\epsilon_{kq})+\delta_{kq}+\gamma_{kp}} + e^{-\sum_{k=1}^{M}\gamma_{kp}(1+\epsilon_{kp})+\delta_{kp}+\gamma_{kq}(1+\epsilon_{kq})+\delta_{kq}}\right]$$

$$+ \frac{1}{K^2N}\sum_{p=1}^{K}\left[\frac{1}{2}e^{-\sum_{k=1}^{M}\gamma_{kp}} - \frac{1}{4}e^{-2\sum_{k=1}^{M}\gamma_{kp}}\right] \qquad (5.47)$$

Using the joint probability density function for γ_{kp} and γ_{kq} given by (5.17), the conditional mean-squared difference given above can be averaged over the instantaneous signal-to-noise ratio samples to give the mean-squared difference conditional upon the instantaneous SNR estimation errors. Performing this average gives

$$\text{MSD}_{\{\epsilon_{kp},\delta_{kp}\}} = \frac{1}{4K^2}\sum_{p=1}^{K}\sum_{q=1}^{K}\left\{\frac{1}{\prod_{k=1}^{M}\left[\Gamma_k^2(1-\rho_{pq}^2)+2\Gamma_k+1\right]}\right.$$

$$-\frac{e^{-\sum_{k=1}^{M}\delta_{kp}}}{\prod_{k=1}^{M}\left[\Gamma_k^2(1-\rho_{pq}^2)(1+\epsilon_{kp})+\Gamma_k(2+\epsilon_{kp})+1\right]}$$

$$-\frac{e^{-\sum_{k=1}^{M}\delta_{kq}}}{\prod_{k=1}^{M}\left[\Gamma_k^2(1-\rho_{pq}^2)(1+\epsilon_{kq})+\Gamma_k(2+\epsilon_{kq})+1\right]}$$

$$\left.+\frac{e^{-\sum_{k=1}^{M}\delta_{kp}+\delta_{kq}}}{\prod_{k=1}^{M}\left[\Gamma_k^2(1-\rho_{pq}^2)(1+\epsilon_{kp})(1+\epsilon_{kq})+\Gamma_k(2+\epsilon_{kp}+\epsilon_{kq})+1\right]}\right\}$$

$$+\frac{1}{KN}\left[\frac{1}{2\prod_{k=1}^{M}(\Gamma_k+1)}-\frac{1}{4\prod_{k=1}^{M}(2\Gamma_k+1)}\right] \qquad (5.48)$$

where Γ_k is the mean SNR on the k^{th} diversity branch and ρ_{pq} is the channel correlation coefficient defined by (5.16). The mean-squared difference can be closely approximated by the first- and second-order moments of ϵ_{kp} and δ_{kp}. Therefore, averaging (5.48) over the errors in estimating the magnitude squared of the channel transfer function gives for the mean-squared difference

$$MSD = \frac{1}{KN}\left[P_e - \frac{1}{4\prod_{k=1}^{M}(2\Gamma_k+1)}\right] + \frac{\epsilon^2\sum_{k=1}^{M}\frac{\Gamma_k^2}{(2\Gamma_k+1)^2} + \epsilon_S^2\sum_{k=1}^{M}\Gamma_k^2}{2K\prod_{k=1}^{M}(2\Gamma_k+1)} \qquad (5.49)$$

where

$$P_e = \frac{1}{2\prod_{k=1}^{M}(\Gamma_k+1)}$$

is the average error rate of the system.

It should be noted that as $K \to \infty$, the mean-squared difference given by (5.49) goes to zero. However, from (5.34), the estimate given by (5.40) is a biased estimate of error rate and, since P_C given by (5.41) converges to the error rate, then P_e is also a biased estimate of P_C. This bias can be included in the expression for the MSD to obtain

$$MSD = \frac{1}{KN}\left[P_e - \frac{1}{4\prod_{k=1}^{M}(2\Gamma_k+1)}\right] + \frac{\epsilon^2\sum_{k=1}^{M}\frac{\Gamma_k^2}{(2\Gamma_k+1)^2} + \epsilon_S^2\sum_{k=1}^{M}\Gamma_k^2}{2K\prod_{k=1}^{M}(2\Gamma_k+1)} + P_e^2\left[\frac{\epsilon_S^2}{2}\sum_{k=1}^{M}\Gamma_k^2 + M\epsilon^2\right]^2 \qquad (5.50)$$

The performance of the error burst estimator considered in this section will be discussed in the following section along with the performance of the error rate estimators previously considered.

5.1.5 Estimator Performance

In this section, the performance of the estimation techniques analyzed in the previous sections will be presented. For illustrative purposes, the channel models (HF, LOS, Tropo, and Satellite) used in Section 4.1 to analyze the performance of the magnitude-squared channel transfer function estimator will also be used in the examples of this section.

From (5.24), (5.28), and (5.39) the determination of the error rate estimator performances requires the functional description of the channel correlation function. To illustrate the performance of these estimators, two representations for $\rho(r)$ were used; one is the Gaussian correlation function and is given by

$$\rho_G(r) = e^{-\frac{\pi^2 B^2 r^2 (\Delta\tau)^2}{2}} \tag{5.51}$$

and the second is the double pole correlation function given by

$$\rho_{DP}(r) = [1 + \pi|r| B \Delta\tau] e^{-\pi|r| B \Delta\tau} \tag{5.52}$$

where

B is the channel rms Doppler spread

$\Delta\tau$ is the time between samples

It should be reiterated that the above representations for the channel correlation function are for illustrative purposes only, and are not meant to represent the actual correlation functions for the various channels. It was found in the examples that the performance of the error rate estimators is relatively invariant for the above two correlation functions and, thus, the performance of the estimators may be robust with respect to the shape of the correlation function. The performance presented is for the double pole correlation functio. .

Figure 5.4 and 5.5 present the error rate estimator performance for the estimator analyzed in Section 5.1.2, while Figures 5.6 and 5.7 illustrate the performance of the estimator analyzed in Section 5.1.3. The estimation errors $\sigma_{\hat{P}_e}$ given by

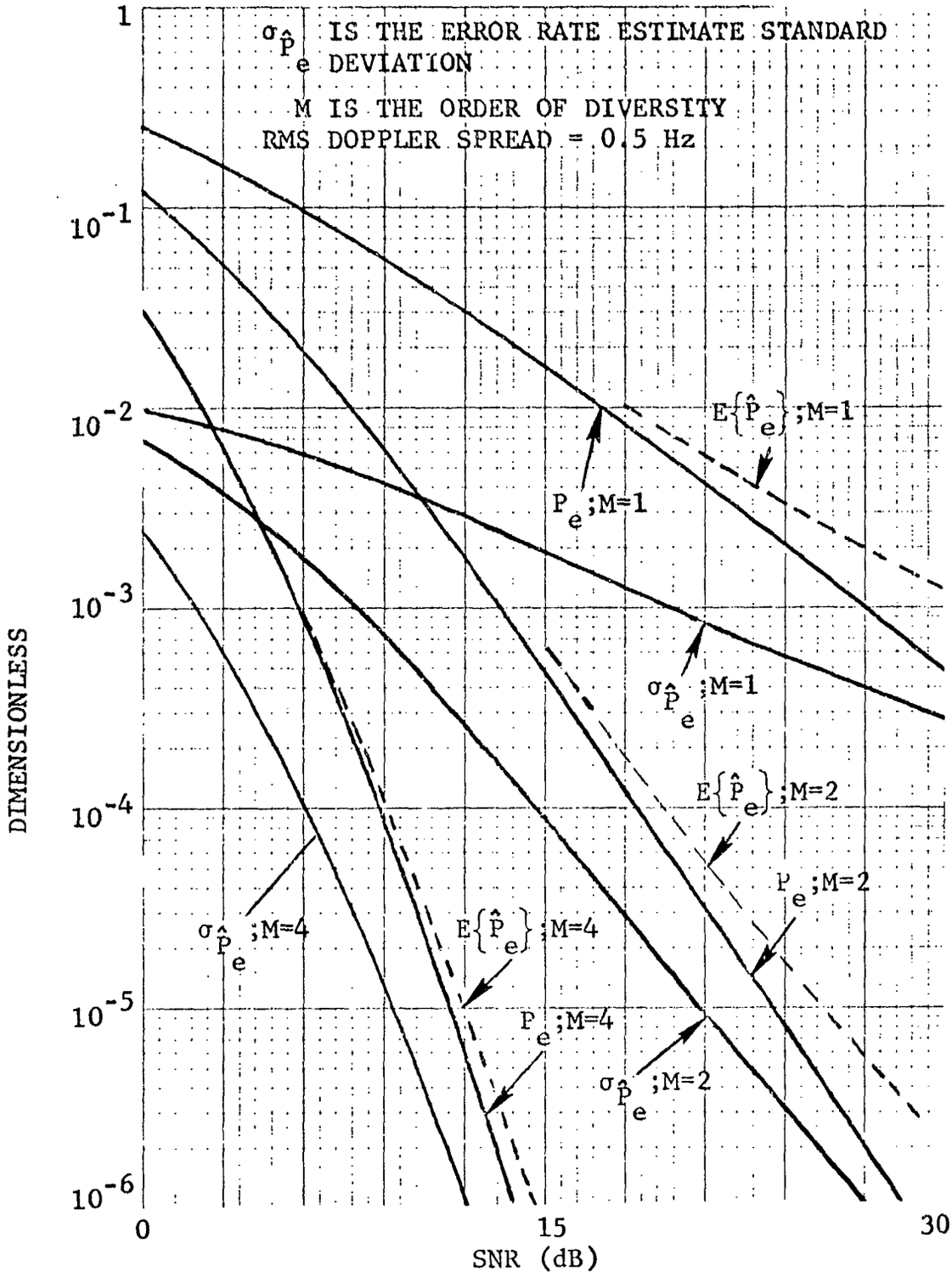

Figure 5.4 Performance of Error Rate Estimator 1 for HF Channel (10-minute Estimation Time)

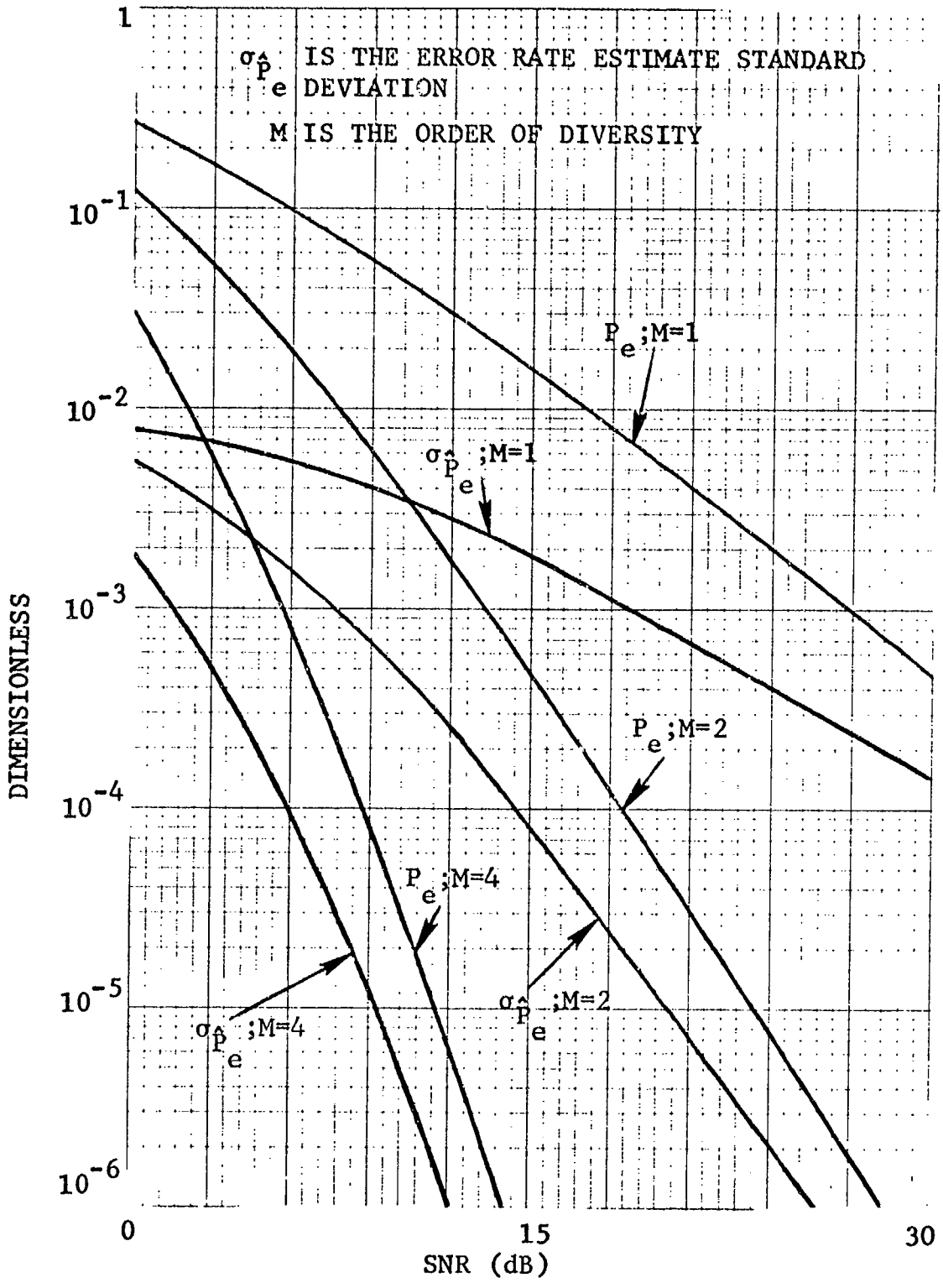

Figure 5.5 Performance of Error Rate Estimator 1 for Satellite, Tropo, and LOS Channels

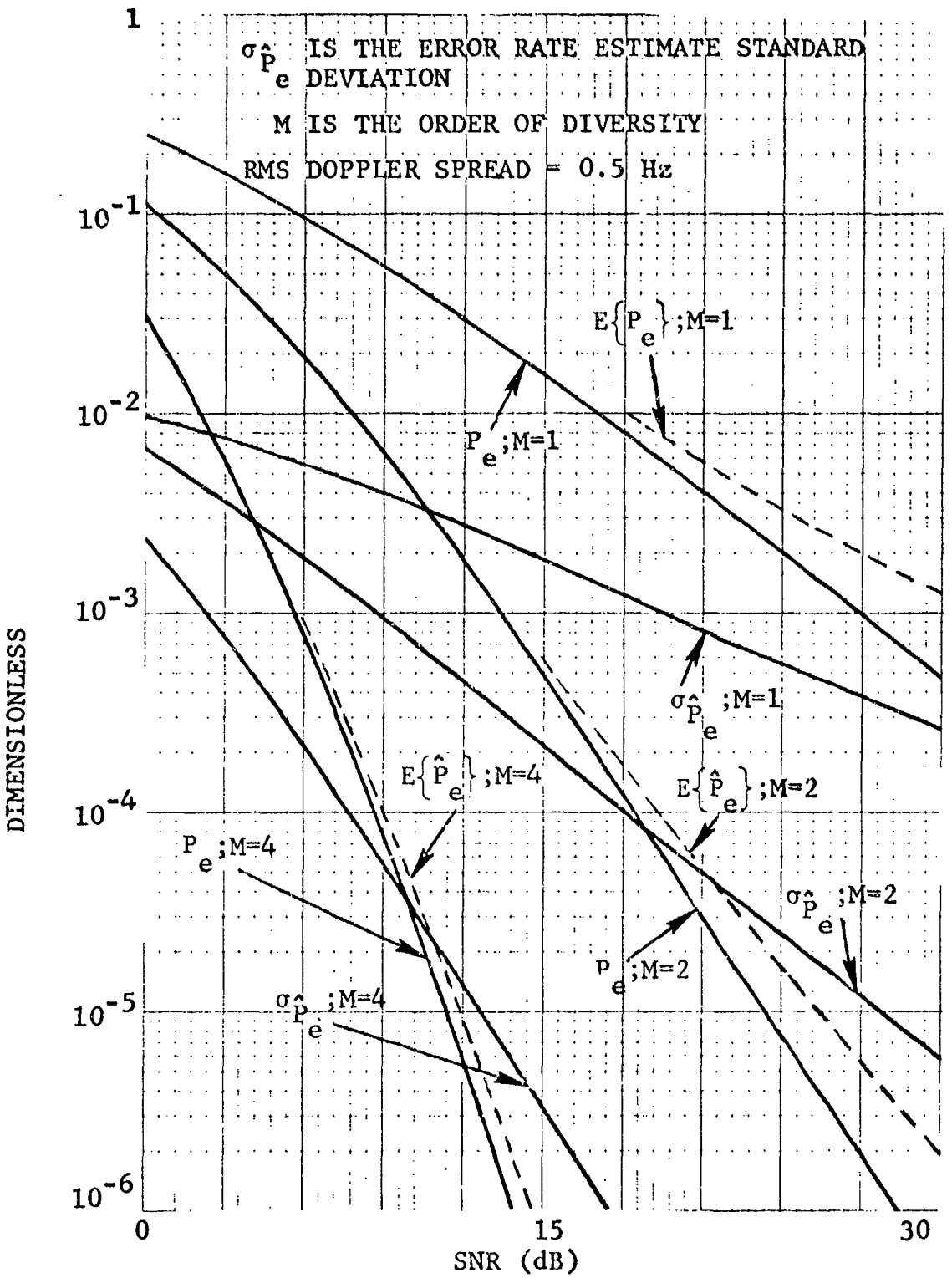

Figure 5.6 Performance of Error Rate Estimator 2 for HF Channel (10-minute Estimation Time)

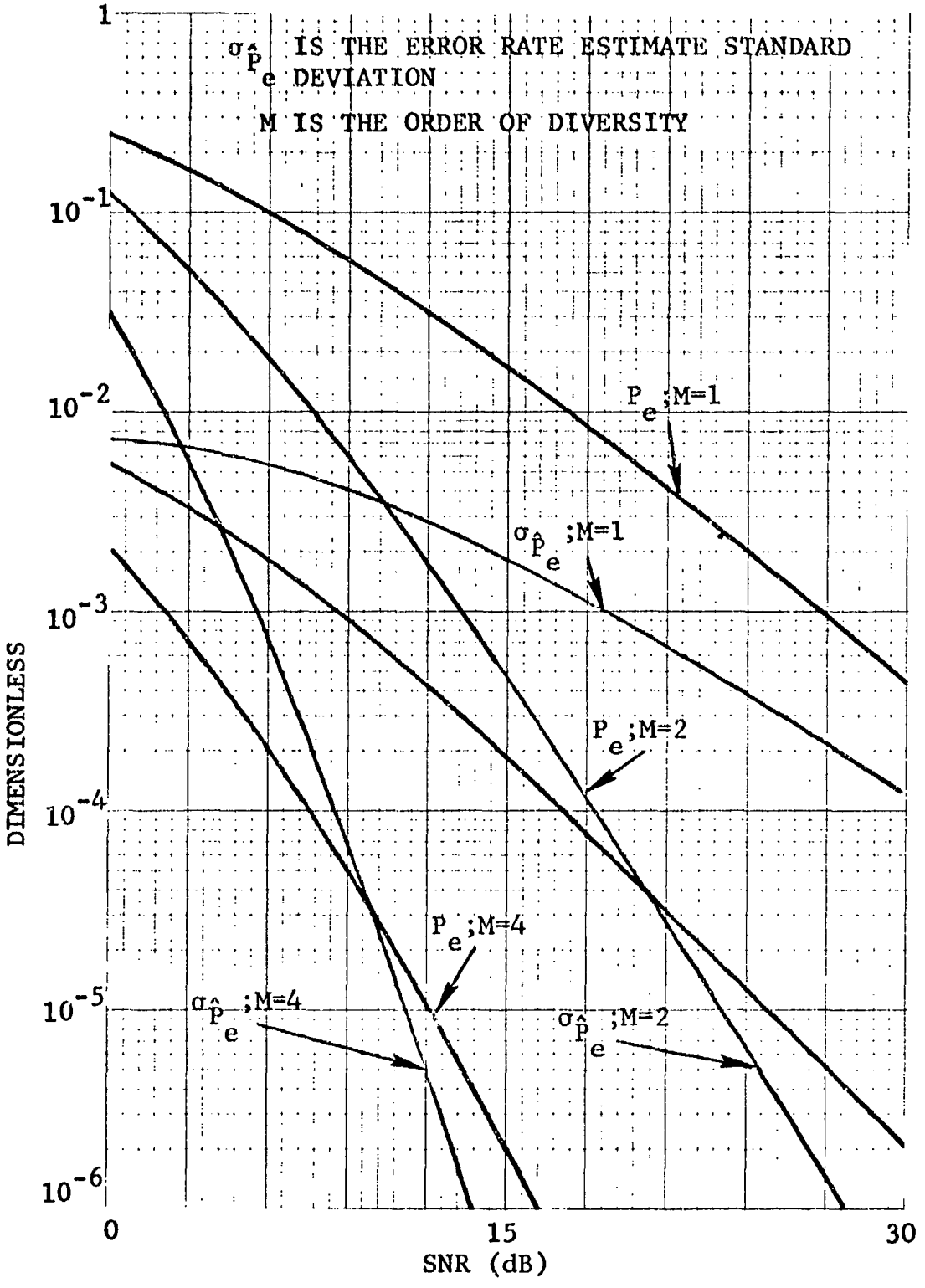

Figure 5.7 Performance of Error Rate Estimator 2 for Satellite, Tropo, and LOS Channels

(5.28) and (5.39) are used as the measure of the estimator performance. The performance of the estimators for other time intervals, still large such that the sums in (5.24) and (5.39) do not change appreciably, can be determined from these figures by noting that $\sigma_{\hat{p}_e}$ decreases as the inverse of the square root of the number of samples. Thus, if the performance for a time interval of four times the specified time is desired, it can be determined by decreasing $\sigma_{\hat{p}_e}$ by a factor of 2 from the performance presented.

Table 5-1 presents the parameters used to evaluate the error rate estimation techniques. As pointed out in Section 2, the LOS channel should be analyzed on a quasi-stationary basis. The LOS channel has been included in Table 5-1 to make clear that reliable average error rate measurements on LOS links are meaningless because of the long measurement time required — 1667 minutes.

From Figures 5.4 to 5.7, we note that the estimator of Section 5.1.2 is superior to the estimator of Section 5.1.3. Since the bias of Error Rate Estimators 1 and 2 can be significant for HF channels, it is shown on these performance curves. This bias was calculated using estimator filter parameters for which the bias is minimized at each SNR. Therefore, this represents an upper bound on performance. Due to this bias, these estimators are not recommended for use on HF channels. For the other channels of interest, the bias can be made negligible by proper filter parameter selection. Use of the error amplification technique presented in Section 3 will also reduce the error rate bias significantly.

Figures 5.8 - 5.11 present the performance of the error burst estimation technique analyzed in Section 5.1.4. A short time interval (15 seconds) is used in the example because good short-term error burst estimates can aid an operator in quickly distinguishing an error burst due to the channel fading from one due to equipment failure.

From the figures we note that the best error burst estimates (small MSD) are obtained for the channels for which good estimates of the instantaneous SNR are possible (LOS, Satellite, Tropo). For the channels that do not allow good estimation of the instantaneous SNR, the error burst estimator of Section 5.1.4 is of questionable usefulness.

TABLE 5-1

PARAMETERS USED TO EVALUATE ERROR RATE ESTIMATION TECHNIQUES

Parameter / Channel	Estimation Time (s)	RMS Doppler Spread (Hz)
Tropo	5	1.0
HF	10	0.5
Satellite Ionospheric Scintillation	25	0.2
LOS	1667	0.003

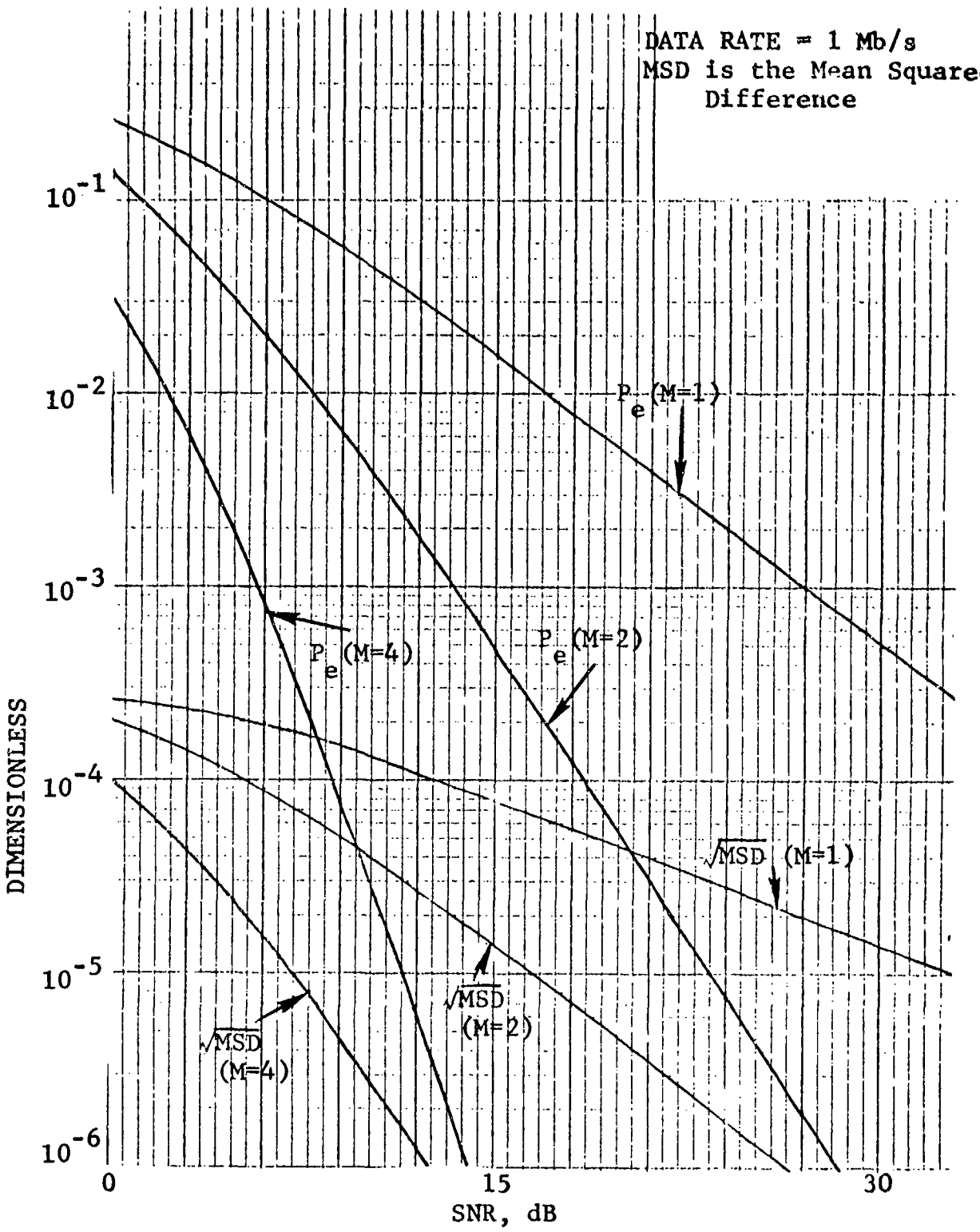

Figure 5.8 Performance of Error Burst Estimator for Tropo Channels (15-second Estimation Time)

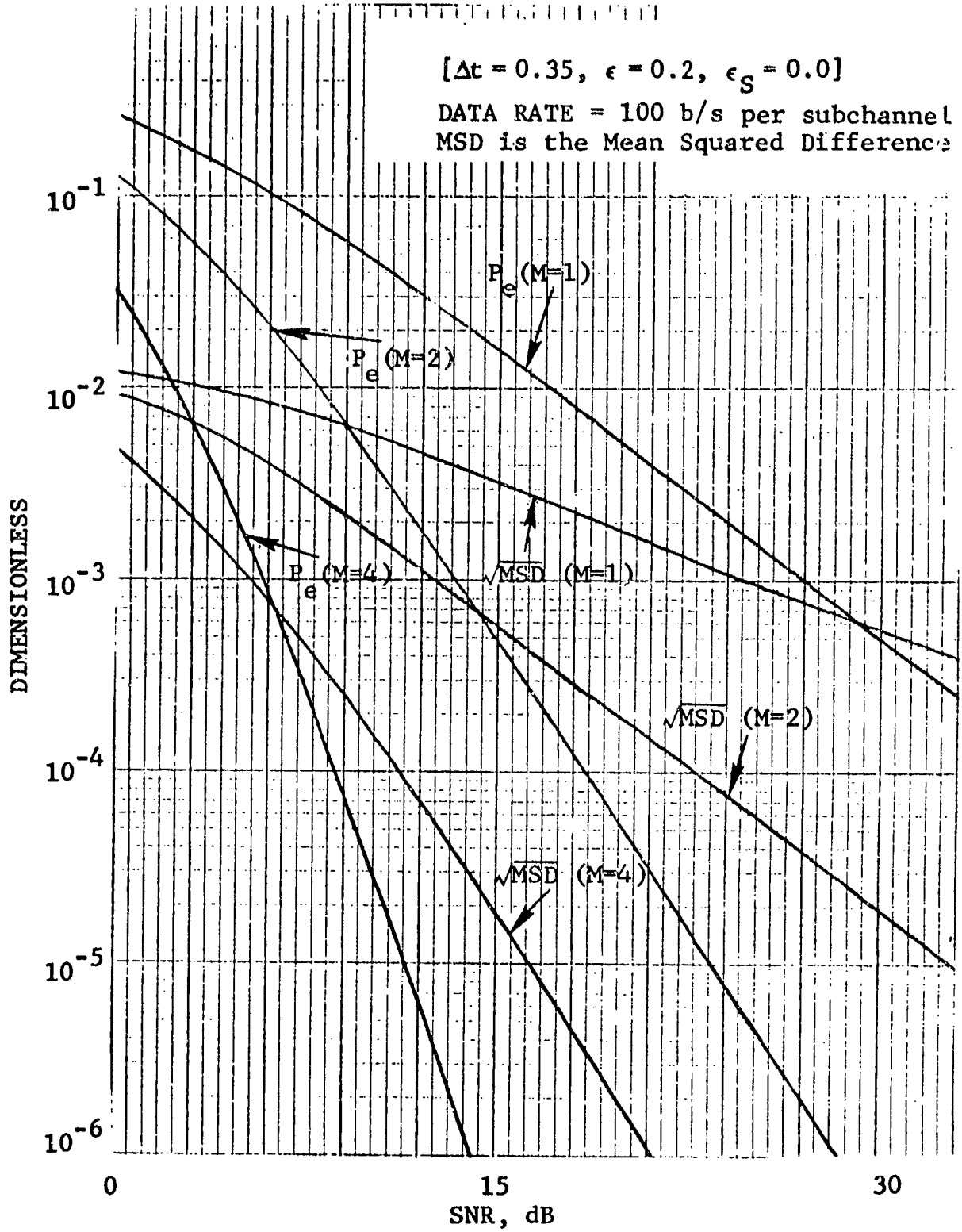

Figure 5.9 Performance of Error Burst Estimator for HF Channel (15-second Estimation Time)

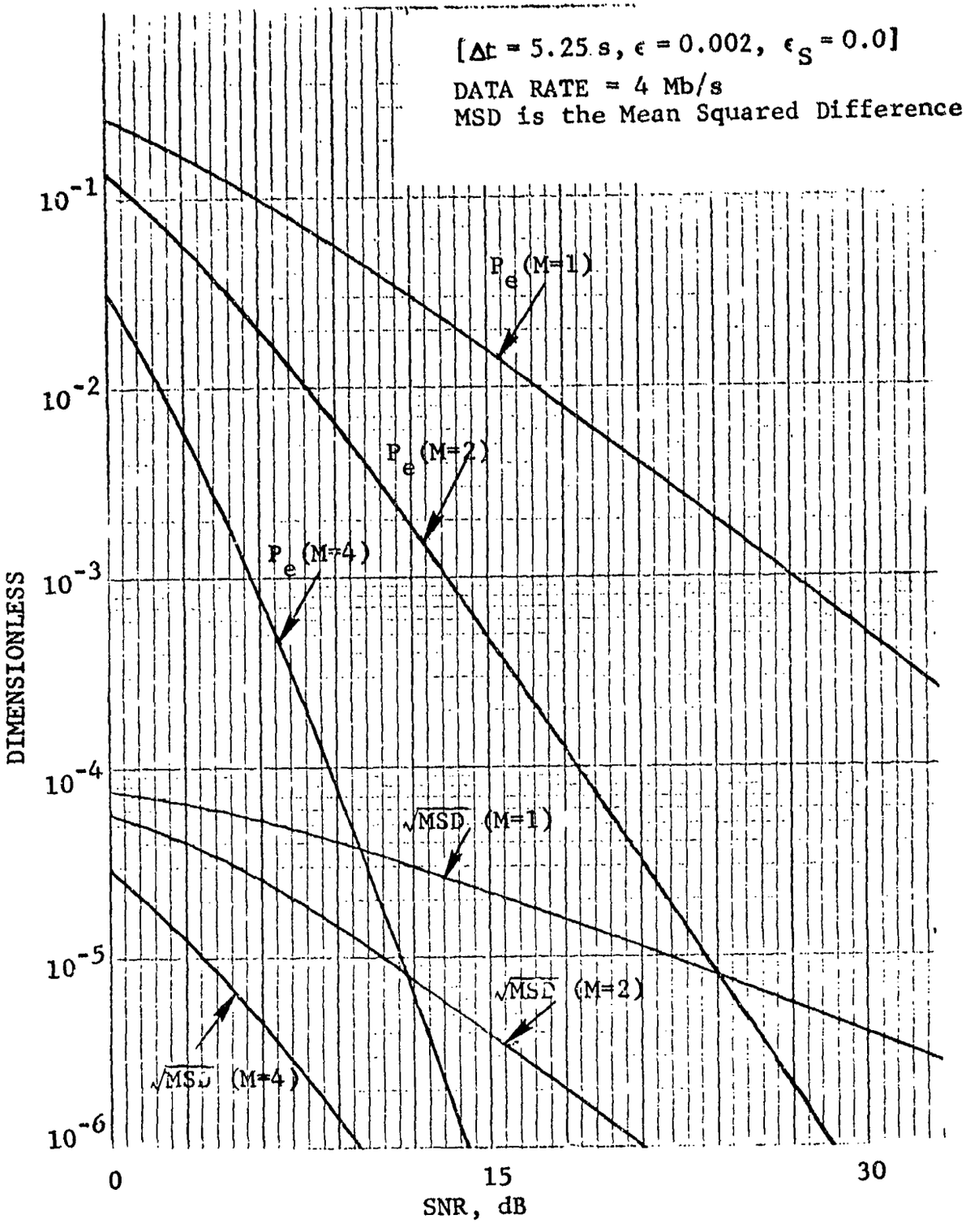

Figure 5.10 Performance of Error Burst Estimator for LOS Channel (15-second Estimation Time)

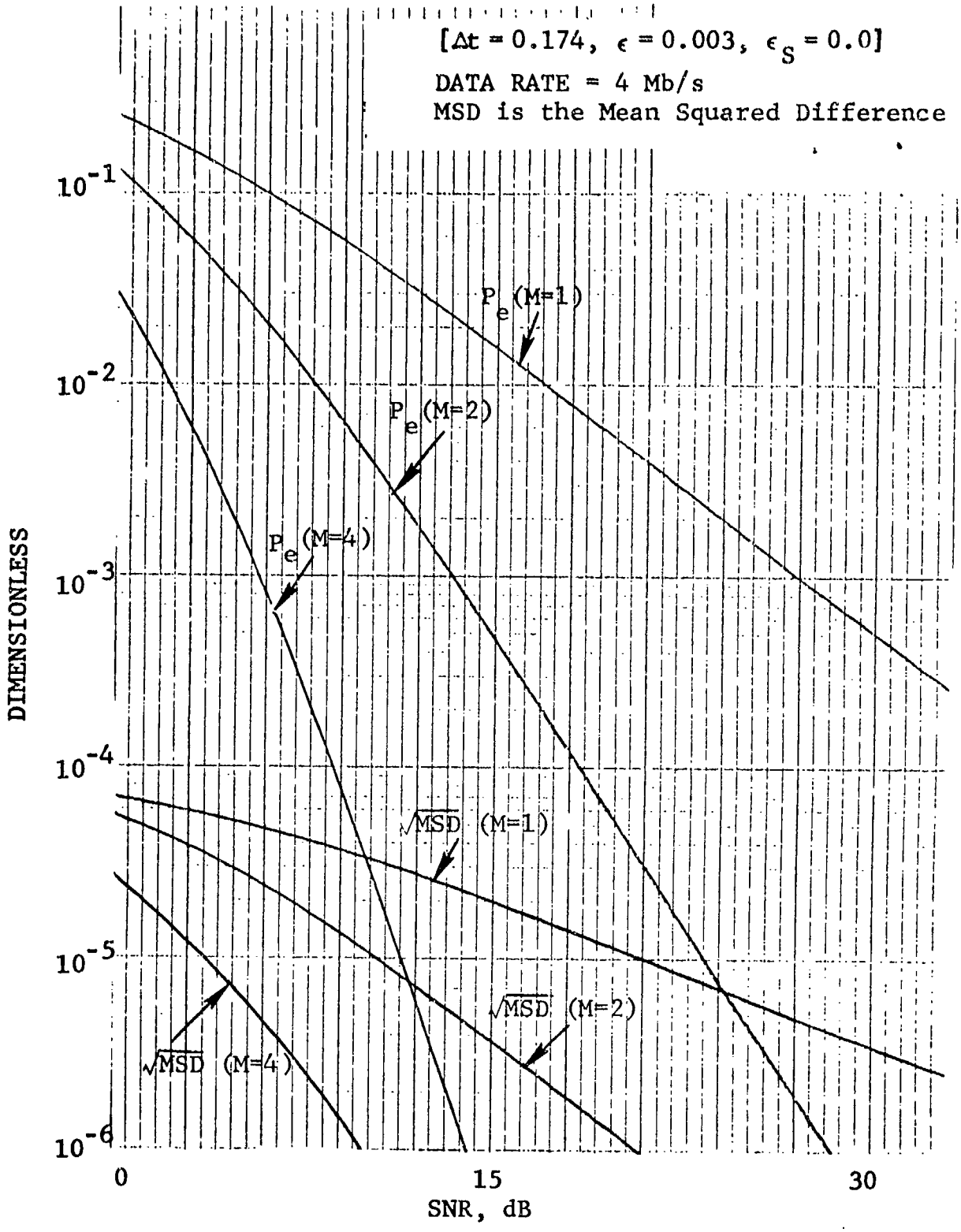

Figure 5.11 Performance of Error Burst Estimator for Satellite Channel (15-second Estimation Time)

5.2 Flat Fading Error Rate Estimation from Measured Fade Probabilities

5.2.1 Introduction

For a flat fading Rayleigh fading channel, the probability that the signal-to-noise ratio fades below a level can be related to the average error rate of the channel. In this section, we use measured fade probabilities as a means of estimating the error rate of a flat fading channel. Two techniques for estimating the error rate are considered. The first technique uses the fade probabilities to form estimates of the error rate each diversity branch would have if acting alone, and then uses these estimates of branch error rates to estimate the error rate of the channel. The second technique uses the fade probabilities of the output of the diversity combiner to estimate the average error rate. While simpler to implement than the techniques described in Section 5.1, these techniques are approximate, requiring that the SNR be large compared to unity.

5.2.2 Relationship Between Fade Probabilities and Error Rate

For a nonselective Rayleigh fading channel, the error rate for many modems can be directly related to the probability that the signal-to-noise ratio fades below a level. In this section, we will determine this relationship.

The error rate for many modems operating over a nonselective Rayleigh fading channel can be approximated by [see Ref. 5.1, chapter 10]:

$$P_e \approx \frac{S}{\prod_{k=1}^{M} \Gamma_k} \quad ; \quad \Gamma_k >> 1 \tag{5.53}$$

where M is the order of diversity and Γ_k is the mean SNR on the k^{th} diversity branch. Equation (5.53) is a good approximation when $\Gamma_k \gg 1$. The constant S is dependent upon the order of diversity, the type of combining, and the modulation technique. Table 5-2 gives values of S for some modulation schemes and diversity combiner techniques.

The probability that the SNR at the output of the diversity combiner is below a level is approximately given by [see Ref. 5.1, chapter 10]

TABLE 5-2

VALUES OF S SUCH THAT $P_e \approx \frac{S}{\prod_{k=1}^{M} \Gamma_k}$

Modulation Scheme \ Combining Technique	Maximal Ratio Combining	Selection Combining	Equal Gain Combining
Coherent PSK	$\frac{(M-\frac{1}{2})!}{M!\,2\sqrt{\pi}}$	$\frac{(M-\frac{1}{2})!}{2\sqrt{\pi}}$	$\frac{\left(\frac{M}{2}\right)^M}{M!\,2}$
Coherent FSK	$\frac{2^{M-1}(M-\frac{1}{2})!}{M!\,\sqrt{\pi}}$	$\frac{2^{M-1}(M-\frac{1}{2})!}{\sqrt{\pi}}$	$\frac{M^M}{2\,M!}$
Differentially Coherent PSK	$\frac{1}{2}$	$\frac{M!}{2}$	$\frac{\left(\frac{M}{2}\right)^M \sqrt{\pi}}{2(M-\frac{1}{2})!}$
Noncoherent FSK	2^{M-1}	$2^{M-1}\,M!$	$\frac{M^M \sqrt{\pi}}{2(M-\frac{1}{2})!}$

Γ_k is the mean SNR on the k^{th} diversity branch

M is the order of diversity

$$\text{Prob.}\left\{\gamma \le X\right\} \approx \frac{V X^M}{\prod_{k=1}^{M} \Gamma_k} \quad ; \quad \text{for } X \ll \Gamma_k, \; k=1,\ldots,M \; (X>1) \tag{5.54}$$

where

$V = \frac{1}{M!}$ for maximal ratio combining

$V = 1$ for selection combining

$V = \frac{\left(\frac{M}{2}\right)^M \sqrt{\pi}}{M!\ (M-\frac{1}{2})!}$ for equal gain combining

The fade probability given by (5.54) is a good approximation when $X \ll \Gamma_k$. Combining Eqs. (5.53) and (5.54), it follows that

$$\text{Prob.}\left\{\gamma \le X\right\} \approx \frac{P_e V X^M}{S} \quad ; \quad \text{for } X \ll \Gamma_k, \; k=1,\ldots,M \; (X>1) \tag{5.55}$$

From the expressions for V and S, it is easy to show that for the three combining techniques considered, the ratio $\frac{V}{S}$ is the same for all combiners. In particular, for DCPSK and noncoherent FSK, the fade probability is given by

$$\text{Prob.}\left\{\gamma \le X\right\} \approx \frac{2\alpha^M X^M P_e}{M!} \quad ; \quad \text{for } X \ll \Gamma_k, \; k=1,\ldots,M \; (X>1) \tag{5.56}$$

where $\alpha = 1$ for DCPSK, $\alpha = \frac{1}{2}$ for noncoherent FSK. For the coherent detection techniques

$$\text{Prob.}\left\{\gamma \le X\right\} \approx \frac{2\sqrt{\pi}\ \beta^M X^M P_e}{(M-\frac{1}{2})!} \; ; \; \text{for } X \ll \Gamma_k, \; k=1,\ldots,M \; (X>1) \tag{5.57}$$

where $\beta = 1$ for PSK, $\beta = \frac{1}{2}$ for FSK.

Therefore, the probability that the SNR at the output of the combiner falls below a level is directly related to the probability of error. In Sections 5.2.3 and 5.2.4, we will examine two techniques for estimating error rate from measured fade probabilities.

5.2.3 Use of Fade Probabilities on Each Diversity Branch for Error Rate Estimation

In this section, we will use error rate estimates for each diversity branch to predict the system error rate. The error rates of the diversity branches are estimated from their fade probabilities. Figure 5.12 is the block diagram of the estimator to be analyzed. The estimation procedure is as follows. The data signal is transmitted over the diversity channel, picked off at RF (or IF) in the receiver, and sent to the magnitude-squared channel transfer function estimator of the type analyzed in Section 4.1. The output of this estimator is sampled and combined with an estimate of the noise power to form an estimate of the instantaneous SNR. This instantaneous SNR estimate is then compared with a threshold, quantized and summed to form an estimate of the error rate on the k^{th} diversity branch. This error rate estimate, combined with error rate estimates from the other diversity branches, is then used to estimate the average error rate.

To estimate the error rate for one diversity branch acting alone from fade probabilities, either (5.56) or (5.57) should be used with $M = 1$. Therefore, the ensemble error rate on the k^{th} diversity branch, assuming the other diversity branches are not there, can be approximately related to the fade probability by

$$P_k = \frac{A \text{ Prob.}\left\{\gamma_k \le X\right\}}{X} \tag{5.58}$$

where γ_k is the instantaneous SNR on the k^{th} diversity branch and A can be found from (5.56) or (5.57) for the modems considered.

In implementing the technique to estimate the error rate on the k^{th} diversity branch acting alone, the fade probabilities will be estimated from the instantaneous SNR estimates by

$$\tilde{\text{Prob.}}\left\{\gamma_k \le X\right\} = \frac{1}{K} \sum_{p=1}^{K} b_p \tag{5.59}$$

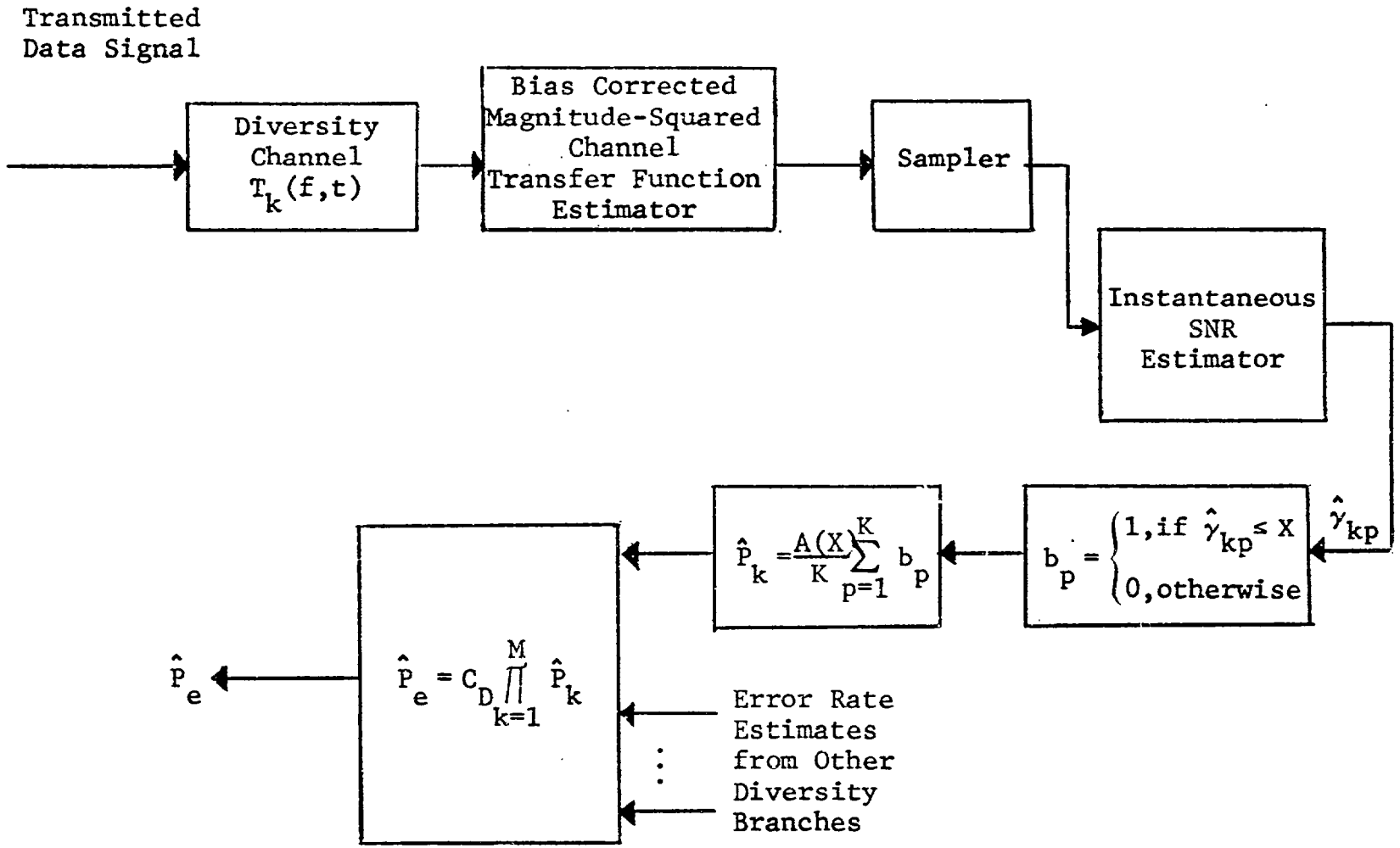

Figure 5.12 Block Diagram of Error Rate Estimator 3

where

$$b_p = \begin{cases} 1, & \text{if } \hat{\gamma}_{kp} \le X \\ 0, & \text{otherwise} \end{cases}$$

and $\hat{\gamma}_{kp}$ is an estimate of γ_k at the p^{th} sampling instant.

Therefore, the error rate on the k^{th} diversity branch will be estimated by

$$\hat{P}_k = \frac{A}{KX} \sum_{k=1}^{K} b_p \tag{5.60}$$

To evaluate the effectiveness of the error rate estimator given in Figure 5.12 to estimate error rate, we must determine the convergence of $\hat{P}_k$ to P_k. From Eq. (5.6), for the magnitude-squared transfer function estimator of Section 4.1, the estimate of the instantaneous SNR can be expressed as

$$\hat{\gamma}_{kp} = \gamma_{kp}(1 + \epsilon_{kp}) + \delta_{kp} \tag{5.61}$$

where γ_{kp} is the actual signal-to-noise ratio on the k^{th} diversity branch and at the p^{th} sampling instant. The parameters ϵ_{kp} and δ_{kp} are errors in estimating γ_{kp} due to noise, data, and the selectivity of the channel.

From (5.59) and (5.60), the expected value of $\hat{P}_k$ can be given by

$$E\{\hat{P}_k\} = \frac{A}{KX} \sum_{p=1}^{K} \text{Prob.}\left\{\gamma_k \le \frac{X - \delta_{kp}}{1 + \epsilon_{kp}}\right\} \tag{5.62}$$

Using (5.58) to express the above probability, averaging over the error parameters gives

$$E\{\hat{P}_k\} = P_k(1 + \epsilon^2) \tag{5.63}$$

where the moments of the errors in estimating γ_{kp} are given by (5.7) and higher than second-order terms of these errors are considered negligible.

Therefore, the estimate of the error rate on the k^{th} diversity branch is biased due to the error in estimating the magnitude squared of the channel transfer function. The second moment of $\hat{P}_k$ can be found from (5.60) to be given by

$$E\left\{\hat{P}_k^2\right\} = \frac{A^2}{X^2K^2} E\left\{\sum_{p=1}^{K}\sum_{q=1}^{K} b_p b_q\right\} \tag{5.64}$$

From the definition of b_p, and noting that $b_p^2 = b_p$, it immediately follows that

$$E\left\{\hat{P}_k^2\right\} = \frac{A}{KX} P_k(1+\epsilon^2) + \frac{A^2}{X^2K^2} \sum_{\substack{p=1 \\ p\neq q}}^{K}\sum_{q=1}^{K} \text{Prob.}\left\{\gamma_{kp} \le \frac{X-\delta_{kp}}{1+\epsilon_{kp}}, \gamma_{kq} \le \frac{X-\delta_{kq}}{1+\epsilon_{kq}}\right\} \tag{5.65}$$

With the joint density of the SNR samples $p(\gamma_{kp},\gamma_{kq})$ given by (5.17), we have

$$\text{Prob.}\left\{\gamma_{kp} \le \frac{X-\delta_{kp}}{1+\epsilon_{kp}}, \gamma_{kq} \le \frac{X-\delta_{kq}}{1+\epsilon_{kq}}\right\} = \int_0^{\frac{X-\delta_{kp}}{1+\epsilon_{kp}}} \int_0^{\frac{X-\delta_{kq}}{1+\epsilon_{kq}}} p(\gamma_{kp},\gamma_{kq})\, d\gamma_{kp}\, d\gamma_{kq} \tag{5.66}$$

For analysis purposes, we will assume that the SNR samples are spaced far enough apart in time such that for all $\gamma_{kp} \le X$, $\gamma_{kq} \le X$, we have

$$\frac{2\rho_{pq}\sqrt{\gamma_{kp}\gamma_{kq}}}{\Gamma_k\left(1-\rho_{pq}^2\right)} \quad \text{small}$$

$$\frac{\gamma_{kp}+\gamma_{kq}}{\Gamma_k\left(1-\rho_{pq}^2\right)} \quad \text{small} \tag{5.67}$$

With the above assumptions, then $p(\gamma_{kp},\gamma_{kq})$ can be closely approximated by

$$p(\gamma_{kp},\gamma_{kq}) \approx \frac{1}{\Gamma_k^2\left(1-\rho_{pq}^2\right)} \qquad \gamma_{kp},\gamma_{kq} \le X \tag{5.68}$$

Since in order for the error rate to be related to the fade probability we must have $X \ll \Gamma_k$, then the small argument approximation of (5.67) will be valid if ρ_{pq} is not too near 1. Substituting (5.68) into (5.67), integrating with respect to γ_{kp} and γ_{kq}, and averaging over the errors give for the joint fade probability

$$\text{Prob.}\left\{\gamma_{kp} \le \frac{X-\delta_{kp}}{1+\epsilon_{kp}},\gamma_{kq} \le \frac{X-\delta_{kq}}{1+\epsilon_{kq}}\right\} \approx \frac{X^2(1+2\epsilon^2)}{\Gamma_k^2\left(1-\rho_{pq}^2\right)} \tag{5.69}$$

Substituting (5.69) into (5.65) gives after some simplification

$$E\left\{\hat{P}_k^2\right\} \approx \frac{A}{KX}\,P_k(1+\epsilon^2) + \frac{P_k^2(1+2\epsilon^2)}{K^2}\sum_{\substack{p=1\\p\neq q}}^{K}\sum_{q=1}^{K}\frac{1}{1-\rho_{pq}^2} \tag{5.70}$$

For a stationary scatter channel and equal spacing between samples, we can express ρ_{pq} in terms of $r = p-q$. Therefore, letting $\rho(r) = \rho_{pq}$ in (5.70), the double sum can be replaced by a single sum to give for the variance of $\hat{P}_k$

$$\sigma^2_{\hat{P}_k} \approx \frac{A}{KX}\,P_k(1+\epsilon^2) - \frac{P_k^2(1+2\epsilon^2)}{K} + \frac{2P_k^2(1+2\epsilon^2)}{K^2}\sum_{r=1}^{K-1}\psi[\rho(r)](K-r) \tag{5.71}$$

where

$$\psi[\rho(r)] \triangleq \frac{\rho^2(r)}{1-\rho^2(r)}$$

If $\psi[\rho(r)]$ contributes significantly to the sum only when $r \ll K$ and if (as should be the case) the second term is negligible, then the variance of $\hat{P}_k$ is

$$\sigma^2_{\hat{P}_k} \approx \frac{A P_k}{K X}(1+\epsilon^2) + \frac{2P_k^2(1+2\epsilon^2)}{K} \sum_{r=1}^{K-1} \psi[\rho(r)] \tag{5.72}$$

From (5.60) and (5.72), the estimate of the error rate on the k^{th} diversity branch acting alone can be expressed as

$$\hat{P}_k = P_k(1+\Omega_k) \tag{5.73}$$

where

$$E\{\Omega_k\} = \epsilon^2$$

$$\sigma^2_{\Omega_k} = \frac{\sigma^2_{\hat{P}_k}}{P_k^2}$$

Proceeding as in (5.25) to (5.28), the mean and variance for estimating the error rate with the technique of Figure 5.16 is

$$\bar{\hat{P}}_e = P_e(1 + M\epsilon^2)$$

$$\sigma^2_{\hat{P}_e} = P_e^2 \sum_{k=1}^{M} \frac{\sigma^2_{\hat{P}_k}}{P_k^2} \tag{5.74}$$

The performance of this estimator will be illustrated in Section 5.2.5. However, it should be noted that in implementing the error rate estimator analyzed in this section, a choice of the level must be made. From Section 5.2.2, the level on each diversity branch must be much less than the mean SNR of that branch. This allows us to relate the fade probability on that branch to the error rate of that diversity branch acting alone.

Furthermore, from (5.72) the rate of convergence of the estimator increases as the level, X, increases.

5.2.4 Use of Combiner Output Fade Probabilities for Error Rate Estimation

5.2.4.1 Introduction

As was shown in Section 5.2.2, for high SNR the probability that the instantaneous SNR at the output of the diversity combiner is below a level is directly related to the average probability of error. Figure 5.13 is a block diagram of an error rate estimator that utilizes the above-mentioned relationship. Up to the estimation of the instantaneous SNR at the diversity combiner output, the estimation procedure is identical to that of Error Rate Estimator 2 discussed in Section 5.1.3. However, instead of estimating the instantaneous error rate, the error rate estimator of Figure 5.17 compares an estimate of the instantaneous SNR at the diversity combiner output with a level to form an estimate of a fade probability. These fade probability estimates are then used to estimate the average probability of error of the channel.

From Eqs. (5.56) and (5.57), the error rate of the systems considered can be estimated by

$$\hat{P}_e = \frac{B\ \tilde{\text{Prob.}}\{\gamma \le X\}}{X^M} \tag{5.75}$$

where B is a constant dependent upon the particular modulation scheme used, M is the order of diversity, and γ is the instantaneous SNR at the output of the diversity combiner. The probability that the SNR at the combiner output fades below a level X will be estimated by

$$\tilde{\text{Prob.}}\{\gamma \le X\} = \frac{1}{K} \sum_{p=1}^{K} b_p \tag{5.76}$$

where

$$b_p = \begin{cases} 1, & \text{if } \hat{\gamma}_p \le X \\ 0, & \text{otherwise} \end{cases}$$

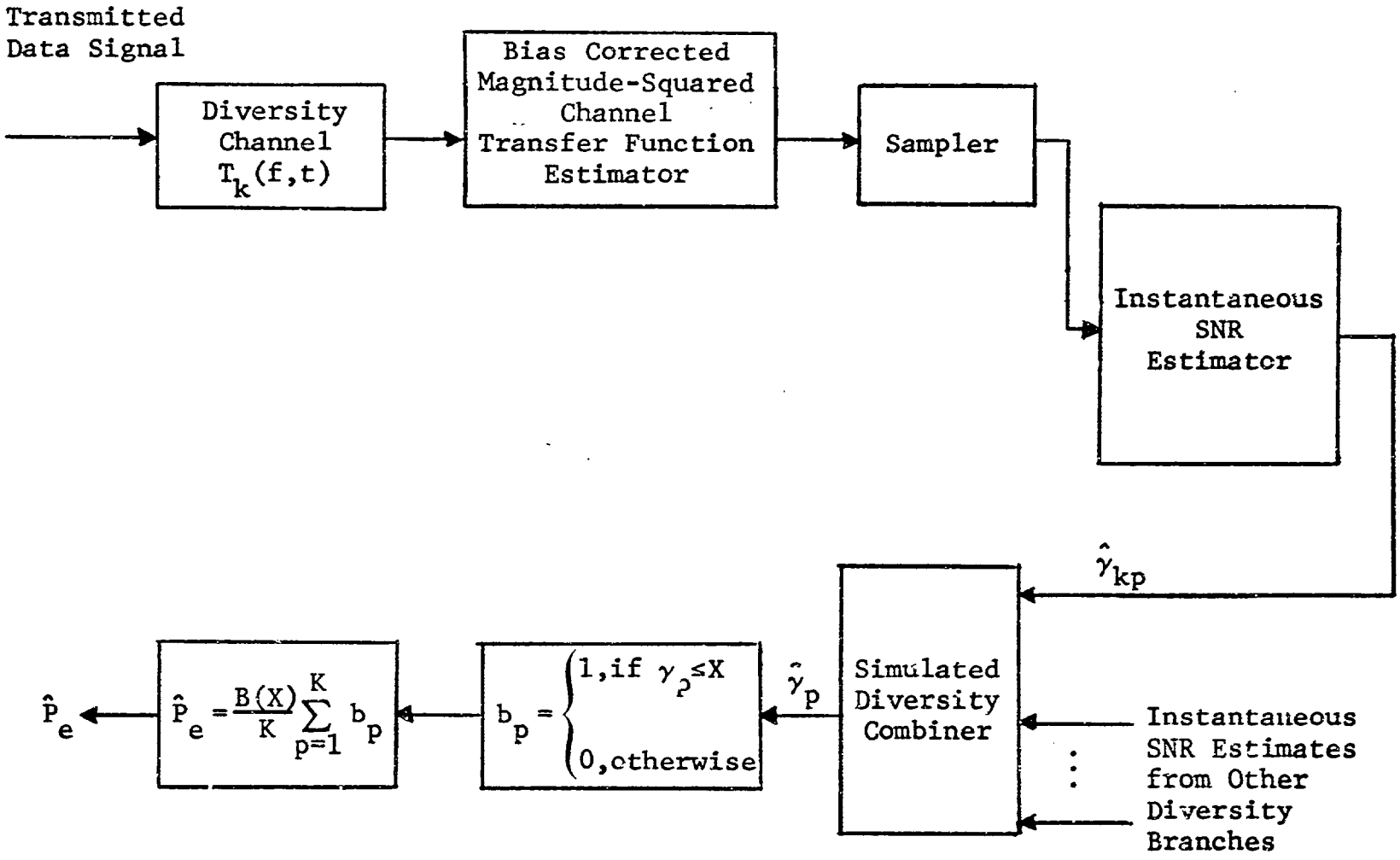

Figure 5.13 Block Diagram of Error Rate Estimator 4

and $\hat{\gamma}_p$ is the estimate of the SNR in the p^{th} sampling interval. Substituting Eq. (5.73) into (5.72) gives

$$\hat{P}_e = \frac{B \sum_{p=1}^{K} b_p}{X^M K} \tag{5.77}$$

5.2.4.2 Instantaneous Combiner Output SNR

To evaluate the effectiveness of $\hat{P}_e$ given by (5.77) to estimate the average error rate, it is necessary to relate the estimate of the instantaneous SNR at the output of the combiner to its actual value. We will derive this relationship for two of the combining techniques considered in Section 5.2.2. It will be assumed that [see Eqs. (4.250), (5.6)]

$$\hat{\gamma}_{kp} = \gamma_{kp}(1 + \epsilon_{kp}) + \delta_{kp} \tag{5.78}$$

where γ_{kp} is the actual SNR on the k^{th} diversity branch and at the p^{th} sampling instant, and $\hat{\gamma}_{kp}$ is the estimate of γ_{kp}.

For selection combining, the combiner output SNR is the largest of the input SNR. With small errors in estimating the magnicude squared of the channel transfer function, the diversity branch with the largest estimated SNR will usually have the largest instantaneous SNR. Therefore, we can relate the estimated and actual SNR at the output of the diversity combiner at the p^{th} sampling instant by

$$\hat{\gamma}_p = \gamma_p(1 + \epsilon_p) + \delta_p \tag{5.79}$$

where

$$E\{\epsilon_p\} = E\{\delta_p\} = 0$$

$$E\{\epsilon_p^2\} = \epsilon^2$$

$$E\{\delta_p^2\} = \epsilon_S^2 \Gamma_p^2$$

and ϵ and ϵ_S are the errors in estimating the magnitude squared of the channel transfer function and Γ_p is the mean SNR of the diversity branch with the largest SNR at p^{th} sampling instant.

For maximal ratio combining, the instantaneous SNR at the output of the diversity combiner is the sum of the instantaneous SNR's at the input to the combiner. Therefore, the estimate of the SNR at the output of a maximal ratio combiner at the p^{th} sampling instant is given by

$$\hat{\gamma}_p = \sum_{k=1}^{M} \hat{\gamma}_{kp} \tag{5.80}$$

where M is the order of diversity.

Using (5.78) to express the estimates of the instantaneous SNR, it follows that

$$\hat{\gamma}_p = \sum_{k=1}^{M} \gamma_{kp}(1+\epsilon_{kp}) + \delta_p \tag{5.81}$$

where

$$\delta_p = \sum_{k=1}^{M} \delta_{kp} \tag{5.82}$$

5.2.4.3 Error Rate Estimation

The performance of the error rate estimator presented in Figure 5.17 will be determined in this section. Since the fade probabilities for equal gain, maximal ratio, and selection combining are approximately related by (5.54), the error rate for these combining techniques can be estimated by simulating a selection combiner and then adjusting for the actual combiner employed. The error rate for selection combining and two-phase DCPSK modulation is found from (5.56) to be given by

$$P_S = \frac{M!\ \text{Prob.}\{\gamma_p \le X\}}{2X^M} \tag{5.83}$$

where γ_p is the instantaneous SNR at the output of the selection combiner. The fade probability will be estimated by

$$\tilde{\text{Prob.}}\{\gamma_p \le X\} = \frac{1}{K} \sum_{p=1}^{K} b_p \tag{5.84}$$

where

$$b_p = \begin{cases} 1 \text{ , if } \gamma_p \le X \\ \\ 0 \text{ , otherwise} \end{cases} \tag{5.85}$$

In (5.85), $\hat{\gamma}_p$ is the estimate of the selection combiner output at the p^{th} sampling instant, and can be represented by (5.79). To determine the performance of Error Rate Estimator 4, we will consider the case of equal mean SNR on each diversity branch. For this case, the estimate of the instantaneous SNR at the combiner output is given by

$$\hat{\gamma}_p = \gamma_p(1+\epsilon_p) + \delta_p \tag{5.86}$$

where

$$E\{\epsilon_p\} = E\{\delta_p\} = 0$$

$$E\{\epsilon_p^2\} = \epsilon^2$$

$$E\{\delta_p^2\} = \epsilon_S^2 \Gamma^2$$

and where Γ is the mean SNR on each of the diversity branches. From (5.83) and (5.84), the error rate for selection combining is estimated by

$$\hat{P}_S = \frac{M! \sum_{p=1}^{K} b_p}{2K X^M} \tag{5.87}$$

The mean value of the error rate estimate is given by

$$E\left\{\hat{P}_S\right\} = \frac{M! \sum_{p=1}^{K} \text{Prob.}\left\{\hat{\gamma}_p \le \frac{X - \delta_p}{1 + \epsilon_p}\right\}}{2K X^M} \tag{5.88}$$

Using (5.54) to express the fade probability, it follows that

$$E\left\{\hat{P}_S\right\} = \frac{M! \sum_{p=1}^{K} E\left\{\left(\frac{X - \delta_p}{1 + \epsilon_p}\right)^M\right\}}{2K X^M \Gamma^M} \tag{5.89}$$

From Table 5-2, we can approximate (5.89) by

$$E\left\{\hat{P}_S\right\} \approx P_S \frac{1}{K X^M} \sum_{p=1}^{K} E\left\{\left(\frac{X - \delta_p}{1 + \epsilon_p}\right)^M\right\} \tag{5.90}$$

and neglecting higher than second-order error moments, we can write

$$E\left\{\hat{P}_S\right\} \approx P_S\left[1 + \frac{M(M+1)}{2} \epsilon^2 + \frac{M(M-1)\epsilon_S^2 \Gamma^2}{2X^2}\right] \tag{5.91}$$

Therefore, the error rate estimate is biased due to the errors in estimating the magnitude squared of the channel transfer function. The second moment of the selection combiner error rate estimate is found from (5.87) to be given by

$$E\left\{\hat{P}_S^2\right\} = \frac{(M!)^2 \sum_{p=1}^{K} \sum_{q=1}^{K} E\left\{b_p b_q\right\}}{4K^2 X^{2M}} \tag{5.92}$$

Since $E\{b_p^2\} = E\{b_p\}$, then

$$E\{\hat{P}_S^2\} = \frac{M!}{2K X^M} P_S\left[1 + \frac{M(M+1)}{2}\left(\epsilon^2 + \frac{(M-1)\epsilon_S^2 \Gamma^2}{(M+1)X^2}\right)\right]$$

$$+ \frac{(M!)^2}{4X^{2M}K^2} \sum_{\substack{p=1 \\ p\neq q}}^{K} \sum_{q=1}^{K} \text{Prob.}\left\{\gamma_p \le \frac{X-\delta_p}{1+\epsilon_p}, \gamma_q \le \frac{X-\delta_q}{1+\epsilon_q}\right\} \tag{5.93}$$

To evaluate the joint probability that two samples of the combiner output SNR are below some levels, we first express this joint fade probability as

$$\text{Prob.}\{\gamma_p \le u, \gamma_q \le v\} = \int_0^u \int_0^v p(\gamma_p, \gamma_q)\, d\gamma_p\, d\gamma_q \tag{5.94}$$

Using the small argument approximation for the joint density of $p(\gamma_{kp}, \gamma_{kq})$ given by (5.68), we can obtain a small argument approximation for $p(\gamma_p, \gamma_q)$ by recalling that for selection combining the SNR at the output of the diversity combiner is equal to the largest of the input SNR's. Therefore, it follows that

$$p(\gamma_p, \gamma_q) \approx \frac{M^2\, \gamma_p^{M-1}\, \gamma_q^{M-1}}{\left(\prod_{k=1}^{M} \Gamma_k^2\right)\left(1-\rho_{pq}^2\right)^M} \tag{5.95}$$

Thus, we can write

$$\text{Prob.}\left\{\gamma_p \le \frac{X-\delta_p}{1+\epsilon_p}, \gamma_q \le \frac{X-\delta_q}{1+\epsilon_q}\right\} \approx \frac{E\left\{\left(\frac{X-\delta_p}{1+\epsilon_p}\right)^M \left(\frac{X-\delta_q}{1+\epsilon_q}\right)^M\right\}}{\left(\prod_{k=1}^{M} \Gamma_k^2\right)\left(1-\rho_{pq}^2\right)^M} \tag{5.96}$$

Performing the above expectations, neglecting their second-order error terms, and substituting the end result into (5.93), the variance of the error rate estimate is approximately given by

$$\sigma^2_{\hat{P}_S} \approx \frac{M!}{2K\,X^M} P_S\left[1 + \frac{M(M+1)}{2}\,\epsilon^2 + \frac{M(M-1)\epsilon_S^2 r^2}{2X^2}\right] + \frac{2P_S^2}{K}\left[1 + M(M+1)\,\epsilon^2 + \frac{M(M-1)\epsilon_S^2 r^2}{X^2}\right]\sum_{r=1}^{K-1}\psi_1[\rho(r)] \tag{5.97}$$

where

$$\psi_1[\rho(r)] \triangleq \frac{1}{\left[1-\rho^2(r)\right]^M} - 1$$

A stationary scatter channel with $\rho(r) = \rho_{pq}$ (where $r = |p-q|$) was assumed, where ρ_{pq} is the channel correlation coefficient defined by (5.16).

To estimate the error rate when maximal ratio diversity combining is used, it is only necessary to use Table 5-1 to determine that the error rate for maximal ratio combining is related to the error rate for selection combining by

$$P_{MR} = \frac{1}{M!} P_S \tag{5.98}$$

Therefore, the error rate for maximal ratio combining (similarly for equal gain combining) can be estimated by simulating a selection combiner. From (5.91), (5.97), and (5.98), it immediately follows that

$$E\left\{\hat{P}_{MR}\right\} = P_{MR}\left[1 + \frac{M(M+1)\epsilon^2}{2} + \frac{M(M-1)\epsilon_S^2\Gamma^2}{2X^2}\right]$$

$$\sigma_{\hat{P}_{MR}} = \frac{P_{MR}}{2KX^M}\left[1 + \frac{M(M+1)}{2}\epsilon^2 + \frac{M(M-1)\epsilon_S^2\Gamma^2}{2X^2}\right]$$

$$+ \frac{2P_{MR}^2}{K}\left[1 + M(M+1)\epsilon^2 + \frac{M(M-1)\epsilon_S^2\Gamma^2}{X^2}\right]\sum_{r=1}^{K-1}\psi_1[\rho(r)] \qquad (5.99)$$

A comparison of the flat fading error rate estimator analyzed in this section with the error rate estimators previously analyzed is most conveniently performed by considering examples. In the following section we will present examples to illustrate the performance of the estimators analyzed in Sections 5.2.3 and 5.2.4.

5.2.5 Performance of Error Rate Estimators

In this section we discuss the performance of the two error rate estimators analyzed in Sections 5.2.3 and 5.2.4. For the channel models considered in Section 4.1, examples will be presented to illustrate the effectiveness of using fade probabilities to estimate the error rate for a flat fading channel. Since a channel correlation function is required to evaluate the variance of the error rate estimates, we will use the correlation functions given by (5.51) and (5.52).

The comments of Section 5.1.5 regarding the channel correlation function and the time interval over which the error rate is measured also apply in this section. However, for some of the channel models considered, samples of the SNR spaced every T seconds, where T is the duration of the averaging filter of the magnitude-squared channel transfer function estimator will result in the small argument approximation [see Eq. (5.67)] not being valid. For these channels SNR samples spaced farther apart will be used.

For the examples, the level X was chosen to be equal to one-fourth of the mean SNR. With the level set as above, the assumption used in the derivations that $X \ll \Gamma$ should not result

in a large degradation of the error rate estimators. We should note that the level is an estimator parameter that affects the performance of the estimator and to achieve the performance predicted would necessitate prior estimation of the mean SNR.

Figures 5.14 and 5.15 demonstrate the performance of the Error Rate Estimators given by Figures 5.12 and 5.13, respectively. The rms Doppler spreads and the estimation times for the various channels are presented in Table 5-1 of Section 5.1. As previously mentioned in Section 5.1, the performance of the LOS channel is presented for comparison purposes only. The long estimation times required for the LOS channel make average error rate estimation impractical.

Comparing Figure 5.14 with 5.15, it is seen that Error Rate Estimator 3 is superior to Error Rate Estimator 4.

Comparison of the estimators analyzed in Section 5.2 with those of 5.1 will be delayed until the last flat fading error rate estimator is presented and analyzed in Section 5.3.

5.3 Flat Fading Error Rate Estimation from SNR Estimates

5.3.1 Introduction

For many systems it is possible to express the error rate of a flat fading channel in terms of the mean SNR on each of the diversity branches. In this section we examine the use of instantaneous SNR estimates to form estimates of the mean SNR. The error rate will be estimated from these mean SNR estimates.

Also, by using the estimate of the branch envelope correlation coefficient estimated in Section 4.3, the error rate for dependently fading diversity branches can be estimated.

5.3.2 Flat Fading Error Rate Estimation for Independently Fading Diversity Branches

The error rate for many digital systems can be expressed in terms of the mean SNR on each of the diversity branches. Therefore, for these systems, estimates of the mean SNR on each diversity branch can be used to estimate the error rate. Figure 5.16 is the block diagram of the error rate estimator that will be considered in this section. The estimation procedure is as follows. The data signal is transmitted over the diversity channel, picked

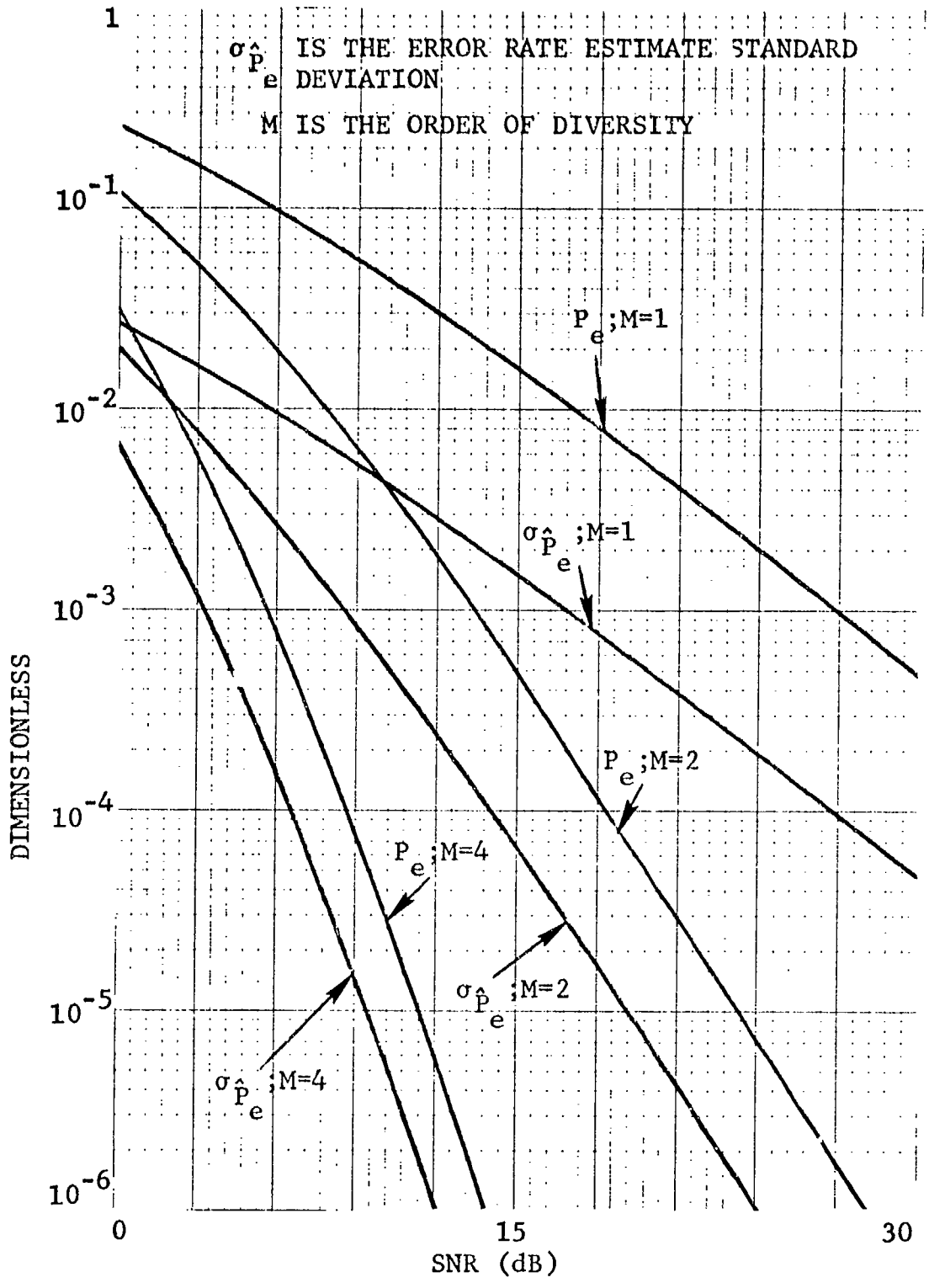

Figure 5.14 Performance of Error Rate Estimator 3 for Tropo, Satellite, LOS, and HF Channels

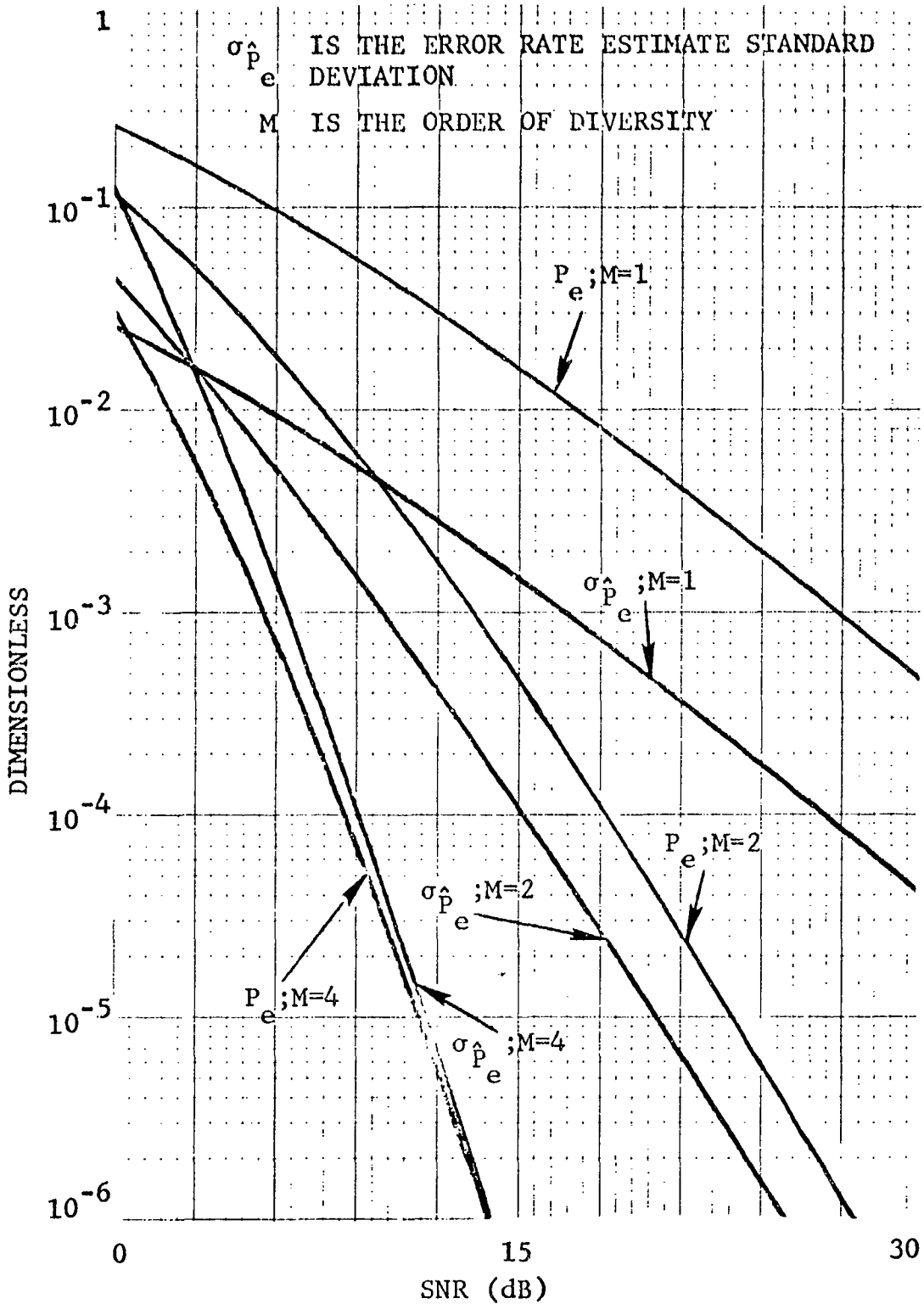

Figure 5.15 Performance of Error Rate Estimator 4 for Tropo, Satellite, LOS, and HF Channels

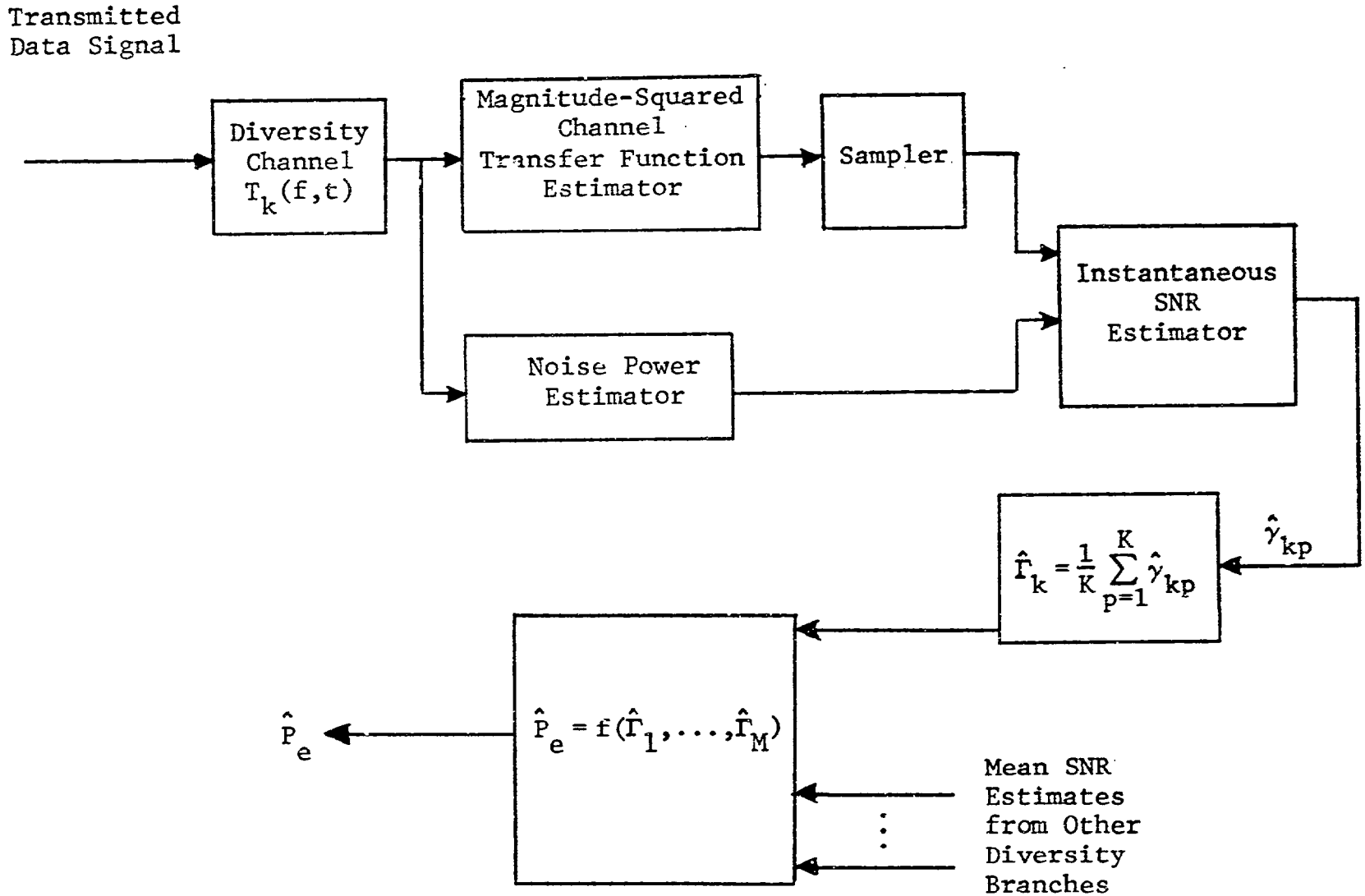

Figure 5.16 Block Diagram of Error Rate Estimator 5

off at RF (or IF) in the receiver, and sent to the magnitude-squared channel transfer function estimator analyzed in Section 4.1. The output of this estimator is sampled and combined with an estimate of the noise power to form an estimate of the instantaneous SNR. These instantaneous SNR estimates are then averaged to form an estimate of the mean SNR on each of the diversity branches. This mean SNR estimate, along with the mean SNR estimates on the other diversity branches, is used to form an estimate of the error rate.

Section 4.3.4 addressed the problem of estimating the mean SNR from the received data signal. From (4.253) and (4.256), an estimate of the mean SNR on the k^{th} diversity branch can be expressed as

$$\hat{\Gamma}_k = \Gamma_k(1+\beta_k) \tag{5.100}$$

where

$$\overline{\beta_k} = 0$$

$$\sigma^2_{\beta_k} = \frac{1}{K}\left[1+\epsilon_p^2+2\sum_{m=1}^{K-1}\rho^2(m)\right]$$

In (5.100), ϵ_p [see Eq. (4.104)] is the rms fractional error in estimating the magnitude squared of the channel transfer function, K is the number of instantaneous SNR samples, and $\rho(\cdot)$ [see Eq. (5.16)] is the normalized envelope correlation function evaluated at the spacing between samples.

For analysis purposes, we will evaluate the effectiveness of this error rate estimator for systems whose error rate can be closely represented by

$$P_e = \frac{S}{\prod_{k=1}^{M}\Gamma_k} \tag{5.101}$$

where M is the order of diversity and S is a constant dependent upon the type of combiner used and the particular modulation

scheme employed. Using (5.101) provides a conservative estimate of estimator accuracy at low SNR. Values of S for several common combining techniques and modulation schemes are given in Table 5-2 of Section 5.2.

From (5.101), the error rate can be estimated by

$$\hat{P}_e = \frac{S}{\prod_{k=1}^{M} \hat{\Gamma}_k} \tag{5.102}$$

Substituting the expression for the estimate of the mean SNR on the k^{th} diversity branch as given by (5.100) and averaging gives

$$\boxed{E\left\{\hat{P}_e\right\} = P_e\left[1 + \frac{M}{K}\left(1 + 2\epsilon_p^2 + 2\sum_{m=1}^{K-1} \rho^2(m)\right)\right]} \tag{5.103}$$

where β_n was assumed to be uncorrelated with β_ℓ if $n \neq \ell$, terms that decrease faster than 1/K where neglected, and only second-order error terms were considered to be significant.

From the above expression for $E\left\{\hat{P}_e\right\}$, we note that this error rate estimate is asymptotically unbiased. That is, as $K \to \infty$, $E\left\{\hat{P}_e\right\} \to P_e$.

The variance of the estimator can be found to be given by

$$\sigma^2_{\hat{P}_e} = \frac{P_e^2 M}{K}\left[1 + 2\epsilon_p^2 + 2\sum_{m=1}^{K-1} \rho^2(m)\right] \tag{5.104}$$

An rms fractional error for estimating error rate can be given by

$$\boxed{\frac{\sigma_{\hat{P}_e}}{P_e} \triangleq \left[\frac{2M}{K}\left(\frac{1}{2} + \epsilon_p^2 + \sum_{m=1}^{K-1} \rho^2(m)\right)\right]^{\frac{1}{2}}} \tag{5.105}$$

Therefore, the performance of the estimator does not depend upon the error rate to be estimated. It does depend upon the number of SNR samples K, the order of diversity M, rms fractional error in estimating the magnitude squared of the channel transfer function ϵ_p, and the correlation between instantaneous SNR samples.

Figure 5.17 illustrates the effectiveness of Error Rate Estimator 5 to estimate the flat fading error rate. As mentioned in Section 5.1, the performance of the LOS channel is for comparison purposes only. The long estimation time for the LOS channel makes average error rate estimation impractical.

5.3.3 Error Rate Estimation for Correlated Fading on Diversity Branches

Previously, we have assumed that the diversity branches have faded independently. For many systems, the branches do not fade independently and this dependent fading results in an increase in the error rate since the full diversity effect is not realized.

To determine the effect of dependent fading upon the error rate, we note that Pierce [5.3] has pointed out that the density function of the instantaneous SNR at the output of a maximal-ratio diversity combiner can be given for small γ by

$$p(\gamma) \approx \frac{1}{(M-1)!\ \det}\ \gamma^{M-1} \qquad (5.106)$$

where det is the determinant of the moment matrix of the set $\{T_k(f,t)\}$ of complex Gaussian random variables and $T_k(f,t)$ is the time varying transfer function on the k^{th} diversity branch.

At high mean SNR, most of the errors are caused by the occasional deep fades of the signal and a close approximation to the error rate is obtained by using (5.106). Bello [5.4] notes that this procedure yields asymptotically correct results for high SNR's and upper bounds for all SNR's. Using this approximation, we find that the error rate depends upon the diversity channel correlations only through the determinant. Thus, one may write

$$\frac{\text{error rate with correlated fading}}{\text{error rate with uncorrelated fading}} \approx \frac{\text{moment matrix determinant with uncorrelated fading}}{\text{moment matrix determinant with correlated fading}} \qquad (5.107)$$

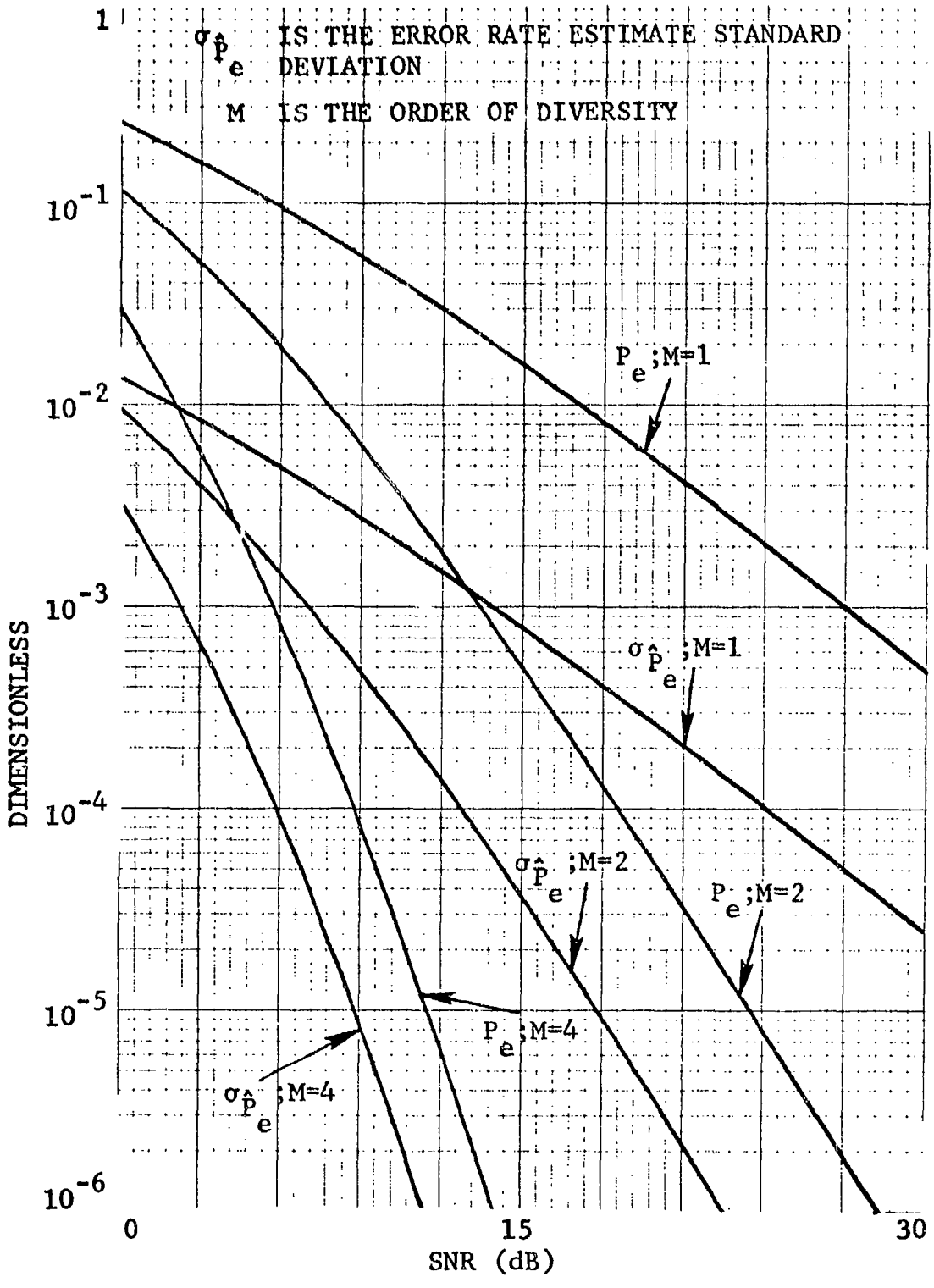

Figure 5.17 Performance of Error Rate Estimator 5 for Tropo, Satellite, LOS, and HF Channels

With P_U and P_C, respectively, the error rates with uncorrelated and correlated fading on diversity branches and with M_U and M_C, respectively, the moment matrix determinants with uncorrelated and correlated fading, we have

$$P_C \approx \frac{M_U}{M_C} P_U \tag{5.108}$$

The above moment matrix determinants are given by

$$M_U = C \prod_{k=1}^{M} \Gamma_k$$

$$M_C = C\left\{\prod_{k=1}^{M} \Gamma_k\right\} \det \begin{bmatrix} 1 & G_{12}^* & G_{13}^* & \cdots & \vdots \\ G_{12} & 1 & G_{23}^* & & \vdots \\ G_{13} & G_{23} & 1 & \ddots & \vdots \\ \vdots & & & 1 & G_{M-1,M}^* \\ \vdots & & & & \\ \cdots & \cdots & \cdots & G_{M-1,M} & 1 \end{bmatrix}$$

$$= C\left\{\prod_{k=1}^{M} \Gamma_k\right\} \det A_M \tag{5.109}$$

where C is a constant and G_{kj} is the complex branch correlation coefficient defined by (4.259); that is,

$$G_{kj} = \frac{E\left\{T_j^*(f,t)\, T_k(f,t)\right\}}{\left[E\left\{|T_j(f,t)|^2\right\} E\left\{|T_k(f,t)|^2\right\}\right]^{\frac{1}{2}}} \tag{5.110}$$

For the techniques involving the use of the magnitude-squared channel transfer function estimates, we are only able to estimate $|G_{kj}|$. The estimation of $\rho_{kj} = |G_{kj}|^2$ was presented and analyzed in Section 4.3.5. As will be demonstrated below, the error rate for a system with correlated fading only on "adjacent branches" is a function of ρ_{kj} and, thus, can be estimated from the estimates of the magnitude squared of the channel transfer function.

For the case of correlated fading only on adjacent diversity branches, it follows that

$$M_C = C\left\{\prod_{k=1}^{M}\right\}\Gamma_k \det A_M \tag{5.111}$$

where A_M is an M x M matrix given by

$$A_M = \begin{bmatrix} 1 & G_{12}^* & 0 & \cdots & 0 \\ G_{12} & 1 & G_{23}^* & \ddots & \vdots \\ 0 & G_{23} & 1 & \ddots & 0 \\ \vdots & \ddots & \ddots & \ddots & G_{M-1,M}^* \\ 0 & \cdots & 0 & G_{M-1,M} & 1 \end{bmatrix} \tag{5.112}$$

The determinant of A_M can be evaluated by expanding in terms of cofactors. This expansion yields a recursive formula for evaluating the determinant of A_M. In particular, it follows that

$$\det A_M = \det A_{M-1} - |G_{M-1,M}|^2 \det A_{M-2} \tag{5.113}$$

where

$$\det A_1 = 1$$

$$\det A_2 = 1 - |G_{12}|^2$$

are used to initiate the recursive relationship.

Since det A_M must be greater than zero, then the representation given by (5.112) implies that for M large that $|G_{jk}| \leq 1/2$. Of course, the above form should not be assumed unless $|G_{jk}| \leq 0.1$, or so.

For the cases of highly correlated fading, $|G_{jk}| \approx 0.9$, or so, then the above representation is not valid. However, it may be possible to upper and lower bound the moment matrix determinant.

Figure 5.18 presents a block diagram for estimating the error rate over a diversity system with correlated fading on the diversity branches.

The estimation procedure is as follows. The data signal is transmitted over the diversity channels and picked off at RF (or IF) in the receivers and sent to magnitude-squared channel transfer function estimators. The output of these estimators is sent to the error rate estimator analyzed in Section 5.3.2 to obtain an estimate of the error rate assuming uncorrelated fading on the diversity branches.

The estimates of the magnitude squared of the channel transfer function are also sent to branch envelope correlation coefficient estimators of the type proposed in Section 4.3.5. These branch envelope correlation coefficient estimates are used to estimate the determinant of the normalized moment matrix. This determinant estimate is then combined with the estimate of the error rate that assumed uncorrelated fading to estimate the error rate with correlated fading.

To illustrate the effectiveness of the error rate estimator given by Figure 5.18 to estimate the error rate for correlated fading on diversity branches, an example will be presented. For analysis purposes, a dual diversity system will be considered. For this system the error rate with correlated fading is closely approximated by

$$P_C = \frac{P_U}{1 - \rho_{12}} \tag{5.114}$$

where the estimation of ρ_{12} was considered in Section 4.3.5 and Appendix B. Therefore, the error rate with correlated fading will be estimated by

$$\hat{P}_C = \frac{\hat{P}_U}{1 - \hat{\rho}_{12}} \tag{5.115}$$

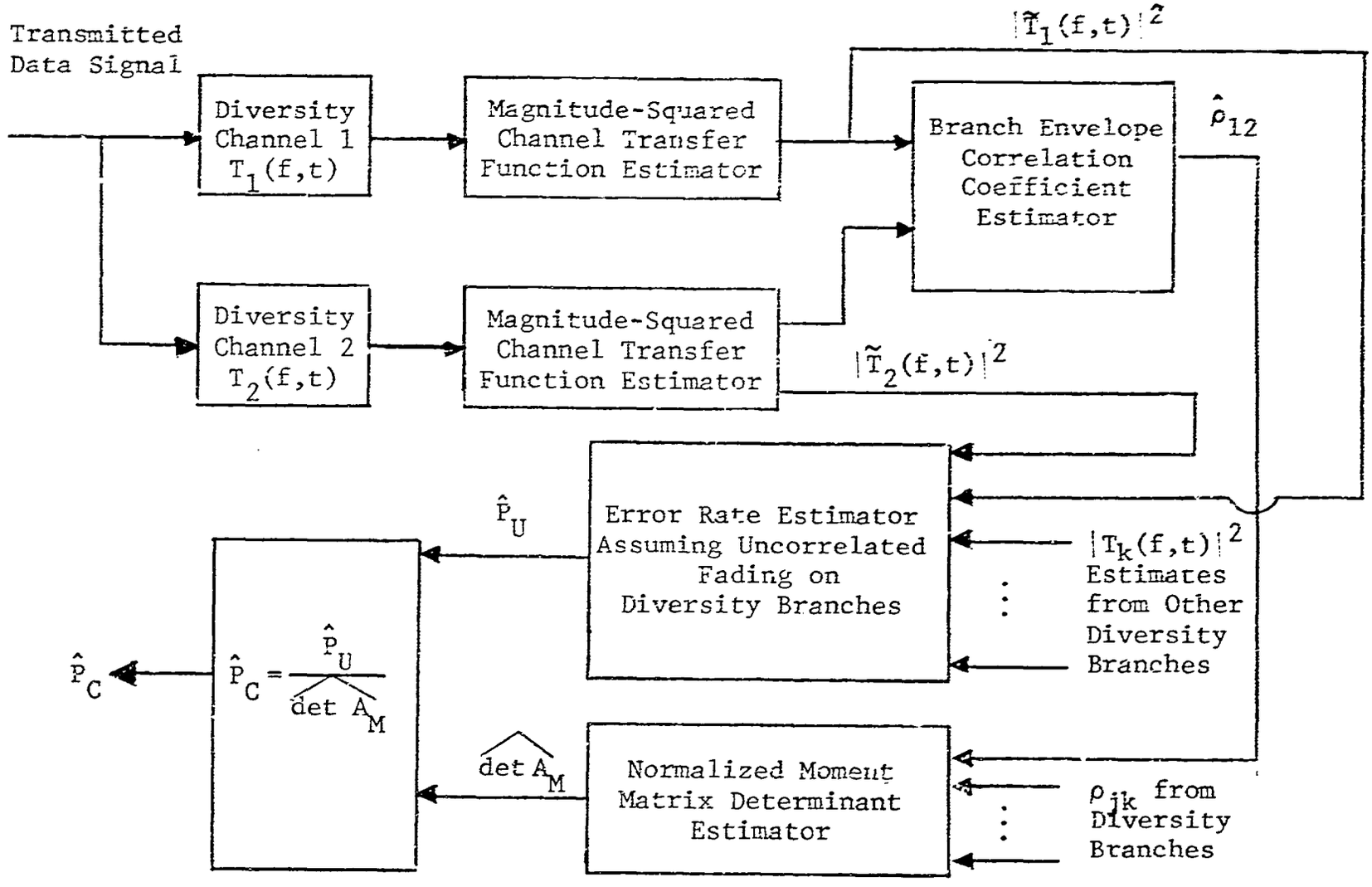

Figure 5.18 Error Rate Estimator for Correlated Fading on Diversity Branches

Assuming that the correlated fading on the diversity branches does not significantly affect the performance of the error rate estimator of Section 5.3.2, then

$$\hat{P}_U = P_U(1+\alpha) \tag{5.116}$$

where

$$E\{\alpha\} \to 0 \qquad \text{as K (the number of samples)} \to \infty$$

$$E\{\alpha^2\} = \frac{4}{K}\left[\frac{1}{2} + \epsilon_p^2 + \sum_{m=1}^{K-1} \rho^2(m)\right]$$

Furthermore, from (4.267) and (4.268) the estimate of the branch envelope correlation coefficient can be given by

$$\hat{\rho}_{12} = \rho_{12} + \beta \tag{5.117}$$

where

$$E\{\beta\} \to 0 \qquad \text{as J (number of independent samples)} \to \infty$$

$$E\{\beta^2\} = \frac{1}{J}\left(3 + 6\rho_{12} + \rho_{12}^2 + 6\rho_{12}^3\right)$$

The above expressions are applicable for the channels that allow an accurate estimation of $|T(f,t)|^2$.

Substituting (5.116) and (5.117) into (5.115) gives

$$\hat{P}_C = \frac{P_U(1+\alpha)}{1 - \rho_{12} - \beta} \tag{5.118}$$

With the number of samples large enough so that good estimates of P_U and ρ_{12} can be obtained, then the estimate of the error rate with correlated fading can be accurately expressed in terms of the first and second moments of α and β. Therefore, we can write

$$\hat{P}_C \approx P_C\left[1 + \alpha - \frac{\beta}{1-\rho_{12}} + \frac{\beta^2}{(1-\rho_{12})^2}\right] \tag{5.119}$$

and it follows that

$$E\{\hat{P}_C\} \approx P_C\left[1 + \frac{1}{J(1-\rho_{12})^2}\left(3 + 6\rho_{12} + \rho_{12}^2 + 6\rho_{12}^3\right)\right] \tag{5.120}$$

Thus, the estimate of the error rate with correlated fading on the diversity branches is asymptotically unbiased. The variance of $\hat{P}_C$ can be found from (5.119) to be given by

$$\sigma^2_{\hat{P}_C} = P_C^2\left\{\frac{4}{K}\left[\frac{1}{2} + \epsilon_p^2 + \sum_{m=1}^{K-1}\rho^2(m)\right] + \frac{1}{J(1-\rho_{12})^2}\left(3 + 6\rho_{12} + \rho_{12}^2 + 6\rho_{12}^3\right)\right\} \tag{5.121}$$

where α and β were assumed to be uncorrelated and higher than second-order moments of α and β were considered to be negligible.

Figure 5.19 shows the effectiveness of estimating the error rate with correlated fading on the diversity branches. In this figure, it was assumed that one independent sample of $|T(f,t)|^2$ can be taken every $1/B$ seconds. Furthermore, for this figure we let $K = J$, $\rho(m) = 0$ if $m \neq 0$. Therefore, from (5.121) we can approximate the rms fractional error by

$$\frac{\sigma_{\hat{P}_C}}{P_C} = \left[\frac{4\left(\epsilon_p^2 + \frac{1}{2}\right) + \frac{1}{(1-\rho_{12})^2}\left(3 + 6\rho_{12} + \rho_{12}^2 + 6\rho_{12}^3\right)}{BT}\right]^{1/2} \tag{5.122}$$

In Figure 5.19, $20 \log \left(P_C/\sigma_{\hat{P}_C}\right)$ vs. BT was plotted.

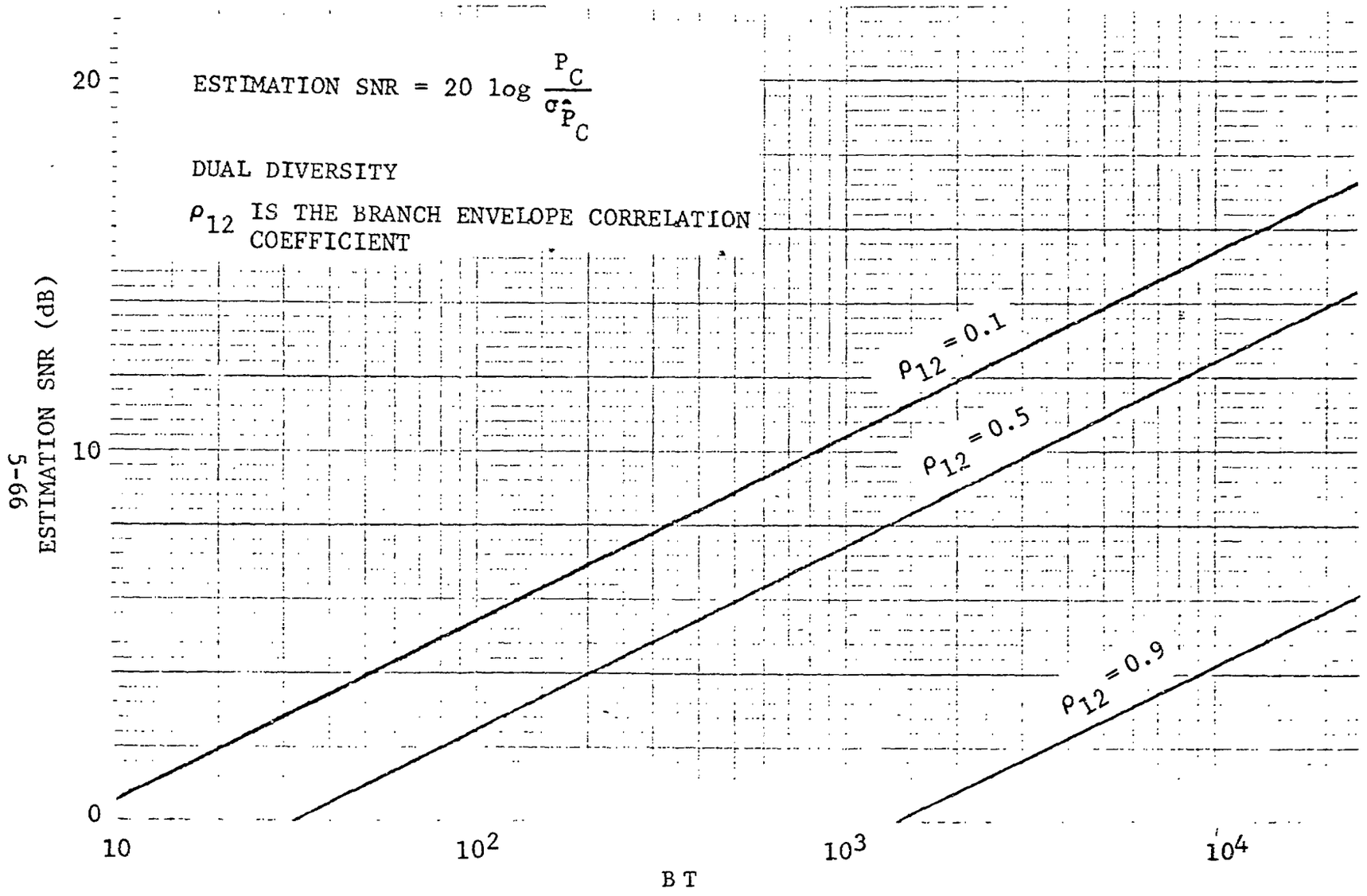

Figure 5.19 Performance of Error Rate Estimator with Correlated Fading on Diversity Branches

5.3.4 Comparison of Flat Fading Error Rate Estimation Techniques

In Sections 5.1 to 5.3, we proposed five techniques for estimating the flat fading error rate from the received data signal. The bias and convergence rate for these estimators were found and examples illustrating performance were presented.

Error Rate Estimators 1 and 2 used instantaneous error rate estimates to estimate the flat fading error rate. These estimators were found to be very sensitive to errors due to the selectivity of the channel, which does not allow accurate estimates of small instantaneous SNR's. For these error rate estimators, the bias in estimating error rate is highly dependent upon the error in estimating the instantaneous SNR due to the channel selectivity ϵ_S [see Eqs. (5.14) and (5.34)]. In Section 3, an error amplification technique using instantaneous SNR estimates is presented. This technique is less sensitive to selectivity-induced estimation errors.

Error Rate Estimators 3 and 4 used fade probabilities to estimate error rates. One problem that arose in implementing these techniques was the choice of a level which affected the performance of the estimators. These estimators were not as sensitive to channel selectivity (this may, in part, be due to the analysis that used a fade distribution linear with the level) and converged more rapidly at high SNR's than the corresponding technique of Error Rate Estimators 1 and 2.

Error Rate Estimator 5 used SNR estimates to estimate the flat fading error rate. This technique converged the fastest of all the techniques considered and was the least sensitive to channel selectivity induced errors. In fact, as shown in (5.105), the filter parameters of the magnitude-squared channel transfer function estimator should be chosen to minimize the rms fractional error given by (4.104).

In conclusion, Error Rate Estimator 5 is the recommended technique for estimating the flat fading error rate with independently fading diversity branches, and Error Rate Estimator 2 can be used to estimate error bursts for channels that allow accurate instantaneous SNR estimation.

5.4 Irreducible Error Rate Estimation Due to Time and Frequency Selective Fading

In this section, we address the problem of estimating the irreducible error rate due to time and frequency selective fading. The irreducible error rate is the error rate that cannot be reduced by increasing the signal-to-noise ratio.

Two types of systems will be considered. The first irreducible error rate to be estimated is that due to time-selective fading in differential phase-modulated systems. The second irreducible error rate is that due to frequency-selective fading in FDM-FM systems. The frequency-selective fading causes the appearance of an intermodulation distortion noise at the discriminator output which results in an irreducible error rate.

5.4.1 Irreducible Error Rate of Differential Phase Modulated Systems

Let the reference vector for the i^{th} tone be given by

$$V_i' = r_i' e^{j\varphi_i'} + n_{ci}' + jn_{si}' \tag{5.123}$$

where r_i' is the magnitude of the fading variable and φ_i' is its angle. The in-phase (cosine) additive term is given by n_{ci}' and n_{si}' is the quadrature (sin) term. Using capital letters to represent complex variables, we can write for the reference vector

$$V' = R' + N' \tag{5.124}$$

and for the received vector

$$V = R + N \tag{5.125}$$

where the subscripts i are dropped off to simplify the notation. The complex fading variable R includes the modulated phase angle which can be assumed to be zero for the analysis given below.

For the fast fading case, we have

$$E[R\,R^*] = E[R'\,R'^*] = S^2 \qquad \text{(signal power)}$$

and

$$E[R'\,R^*] = E[R\,R'^*] = \rho\, e^{j\beta} S^2 \tag{5.126}$$

where ρ and β are the magnitude and phase of the channel correlation coefficient between successive frames.

For a complex Gaussian process, the effects of the time variations in R can be modeled exactly by assuming

$$R = e^{-j\beta/2} R_0 + Z$$

and

$$R' = e^{j\beta/2} R_0 + Z' \tag{5.127}$$

where R_0 is the completely correlated part of R and R' and Z and Z' represent the zero-mean independent parts of R and R'. Thus, we have

$$E[R\,R'^*] = e^{-j\beta}\, E\left[R_0 R_0^*\right] = \rho\, e^{-j\beta} S^2 \tag{5.128}$$

The variance of the independent portions of R are given by

$$E[Z\,Z^*] = E\left[(R - R_0)(R^* - R_0^*)\right]$$

$$= S^2 - 2\rho S^2 + \rho S^2 \tag{5.129}$$

or

$$E[Z\,Z^*] = S^2(1 - \rho) \tag{5.130}$$

Using the above results, we can reduce the fast fading results to an equivalent slow fading result by noting that

$$V = R + N = R_0 + Z + N \tag{5.131}$$

Therefore, we can define an equivalent SNR by

$$\Gamma_{eq} = \frac{E\left[R_0 R_0^*\right]}{E[Z\,Z^*] + E[N\,N^*]} \tag{5.132}$$

or

$$\Gamma_{eq} = \frac{\rho S^2}{S^2(1-\rho) + \frac{N_0}{T}} \tag{5.133}$$

where T is the pulse duration.

The slow fading SNR is

$$\Gamma = \frac{S^2 T}{N_0} \tag{5.134}$$

Thus, the equivalent SNR can be expressed in terms of the slow fading SNR by

$$\Gamma_{eq} = \frac{\rho\Gamma}{(1-\rho)\Gamma + 1} \tag{5.135}$$

Since ρ is the correlation coefficient between successive frames, then ρ is very near to 1, and $1 - \rho \approx \frac{1}{2}\pi^2 B^2 T^2$. Therefore, the equivalent SNR can be approximated by

$$\Gamma_{eq} = \frac{\Gamma}{\Gamma\left(\frac{1}{2}\pi^2 B^2 T^2\right) + 1} \tag{5.136}$$

The irreducible SNR is the limit of (5.136) as $\Gamma \to \infty$. That is,

$$\Gamma_{irr} = \frac{1}{\frac{1}{2}\pi^2 B^2 T^2} \tag{5.137}$$

The irreducible error rate is then found by using Γ_{irr} as the mean SNR. Figure 5.20 is a block diagram of the irreducible error rate estimator. The estimation procedure is as follows. The data signal is transmitted over the channel, picked off at RF (or IF) in the receiver, and sent to one of the rms Doppler spread estimators analyzed in Section 4.3.2. This estimate of the rms Doppler spread is used to estimate the irreducible SNR, which is then combined with irreducible SNR estimates of the other diversity branches to form an estimate of the irreducible error rate.

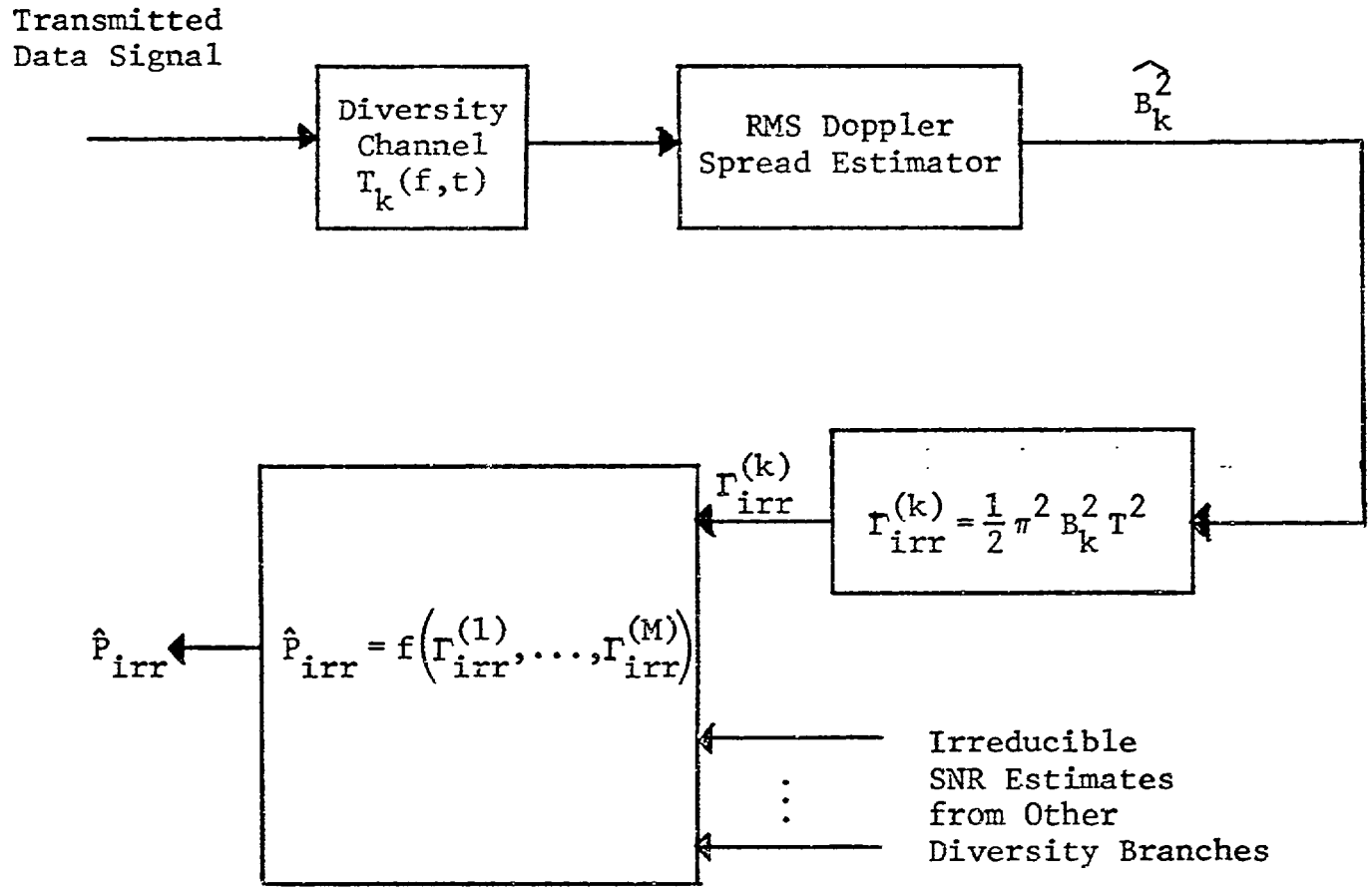

Figure 5.20 Estimation of Irreducible Error Rate Due to Time Selective Fading

As an example of the irreducible error rate estimator performance, we will determine the ability of the estimator given by Figure 5.20 to estimate the irreducible error rate for the case where the irreducible error rate is related to the irreducible SNR's on the diversity branches by

$$P_{irr} = \frac{S}{\prod_{k=1}^{M} \Gamma_{irr}^{(k)}} \tag{5.138}$$

Therefore, we will estimate P_{irr} by

$$\hat{P}_{irr} = S\left(\frac{1}{2}\pi^2 T^2\right)^M \prod_{k=1}^{M} \hat{B}_k^2 \tag{5.139}$$

where $\hat{B}_k^2$ is the estimate of B^2 on the k^{th} diversity branch.

We will consider two subcases of this example. The first will assume that all the diversity branches have the same rms Doppler spread and that one Doppler spread estimation is performed. For this case, we have

$$\hat{P}_{irr} = S\left(\frac{1}{2}\pi^2 T^2\right)^M \hat{B}^{2M} \tag{5.140}$$

For the rms Doppler spread estimators analyzed in Section 4.3.2, we can express B^2 by

$$\hat{B}^2 = E\{\hat{B}^2\} + \alpha \tag{5.141}$$

where $E\{\alpha\} = 0$ and $E\{\alpha^2\}$ depends upon the rms Doppler spread estimations technique employed. Thus, the irreducible error rate estimate can be represented by

$$\hat{P}_{irr} = S\left(\frac{1}{2}\pi^2 T^2\right)^M \left(E\{\hat{B}^2\} + \alpha\right)^M \tag{5.142}$$

Assuming that a sufficiently long enough estimation time is used such that the irreducible error rate estimate can be

accurately approximated by the first- and second-order moments of α, then

$$E\{\hat{P}_{irr}\} \approx S\left(\frac{1}{2}\pi^2 T^2\right)^M E^M\{\widehat{B^2}\}\left[1 + \frac{M(M-1)}{2}\frac{E\{\alpha^2\}}{E^2\{\widehat{B^2}\}}\right] \tag{5.143}$$

Since $E\{\alpha^2\}$ decreases as the time used to estimate B^2 increases, then $E\{\alpha^2\}/E^2\{\widehat{B^2}\}$ will probably be much less than 1 and it follows that

$$\boxed{E\{\hat{P}_{irr}\} \approx S\left(\frac{1}{2}\pi^2 T^2\right)^M E^M\{\widehat{B^2}\}} \tag{5.144}$$

For the rms Doppler spread estimation techniques considered in Section 4.3.2, the estimate of $\widehat{B^2}$ is biased. Therefore, the irreducible error rate estimate will also be biased.

The variance of the irreducible error rate estimate is given by

$$\sigma^2_{\hat{P}_{irr}} = S^2\left(\frac{1}{2}\pi^2 T^2\right)^{2M} M^2\left[E\{\widehat{B^2}\}\right]^{2M-2} E\{\alpha^2\} \tag{5.145}$$

Recalling that $E\{\widehat{B^2}\}$ and $E\{\alpha^2\}$ are the mean and variance for estimating B^2, then it should be noted that the effectiveness of estimating P_{irr} depends upon the rms Doppler spread estimation technique used.

The second example to be considered using (5.139) is the case in which the rms Doppler spread on each branch is estimated separately. For this example we have

$$\widehat{B_k^2} = E\{\widehat{B_k^2}\} + \alpha_k \tag{5.146}$$

where it will be assumed that the α_k are independent. Substituting (5.146) into (5.139) and averaging gives

$$E\left\{\hat{P}_{irr}\right\} = S\left(\frac{1}{2}\pi^2 T^2\right)^M \prod_{k=1}^{M} E\left\{\widehat{B_k^2}\right\} \tag{5.147}$$

Since $E\left\{\widehat{B^2}\right\}$ does not necessarily equal B^2, then in general the irreducible error rate estimate is biased. The variance of the estimate can be easily found to be given by

$$\sigma^2_{\hat{P}_{irr}} = S^2\left(\frac{1}{2}\pi^2 T^2\right)^{2M} \left[\prod_{k=1}^{M} E^2\left\{\widehat{B_k^2}\right\}\right] \sum_{k=1}^{M} \frac{E\left\{\alpha_k^2\right\}}{E^2\left\{\widehat{B_k^2}\right\}} \tag{5.148}$$

where higher than second-order moments of α_k were considered to be negligible.

A comparison of (5.145) with (5.148) can be made for the case where all the B_k are equal as are all the $E\left\{\alpha_k^2\right\}$. For this case, (5.148) reduces to

$$\sigma^2_{\hat{P}_{irr}} = S^2\left(\frac{1}{2}\pi^2 T^2\right)^{2M} M\left[E\left\{\widehat{B_k^2}\right\}\right]^{2M-2} E\left\{\alpha_k^2\right\} \tag{5.149}$$

Since one would expect that

$$E\left\{\alpha^2\right\} = \frac{E\left\{\alpha_k^2\right\}}{M} \tag{5.150}$$

then for this case the variance given by (5.145) will be equal to that given by (5.148).

Using the differentiation technique to estimate B^2 and for nondiversity operation, the fractional bias and estimation SNR can be found from Section 4.3.2* to be given by

*When the bias uncorrected estimates of $|T(f,t)|^2$ are used to estimate B^2, then Appendix A should be used to modify (5.151).

$$\frac{E\{\hat{P}_{irr}\} - P_{irr}}{P_{irr}} = \frac{\epsilon_p^2}{\pi^2 (\Delta t)^2 B^2}$$

$$\frac{P_{irr}}{\sigma_{\hat{P}_{irr}}} = \left[\frac{K}{6\left(1 + \frac{\epsilon_p^2}{\pi^2 B^2 (\Delta t)^2}\right)^2} \right]^{1/2} \qquad (5.151)$$

where ϵ_p is the rms fractional error in estimating the magnitude squared of the channel transfer function, K is the number of independent samples of $|T(f,t)|^2$, and Δt is the spacing between samples of $|T(f,t)|^2$ used to approximate the derivative. As mentioned in Section 4.3.2, we must have $\pi^2 B^2 (\Delta t)^2 \ll 1$.

Figure 5.21 presents the performance of the irreducible error rate estimator for first-order diversity. In this figure, it was assumed that an independent sample of $|T(f,t)|^2$ can be taken approximately every 1/B seconds; that is, that $K = B T_e$, where T_e is the time interval over which the irreducible error rate is estimated.

5.4.2 Irreducible Error Rate for FDM-FM Transmission

In this section we will address the problem of predicting the irreducible error rate for FDM-FM troposcatter systems. The frequency-selective fading causes the appearance of an intermodulation distortion noise at the discriminator output and will produce an error rate that cannote be reduced by increasing the signal-to-noise ratio, i.e., it produces an irreducible error rate.

Theories concerning intermodulation distortion in FM troposcatter systems have been developed independently by several authors [5.5] - [5.7]. We shall utilize the theory developed in [5.5], which includes the effects of diversity combining and is applicable to scatter communication channels with general delay power spectrum $Q(\xi)$. As with the others, this theory is limited to the case in which the degree of frequency selectivity in the rf signal bandwidth is small.

The intermodulation distortion is a realization of a stationary stochastic process. As such, it can be described in terms of its probability density functions of all orders. In particular, it can be shown [5.5] that the function f(R) defined by:

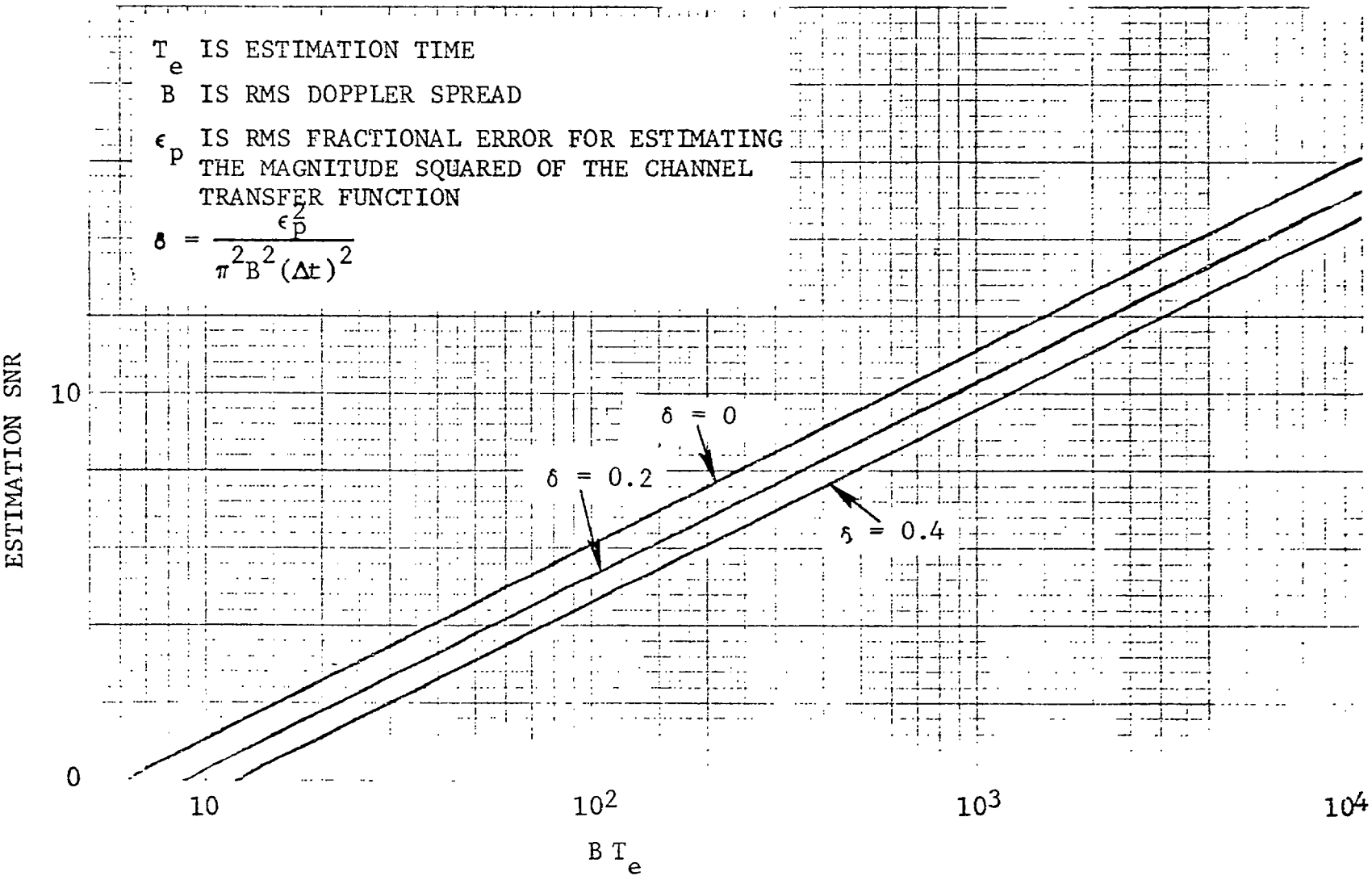

Figure 5.21 Performance of Irreducible Error Rate Estimator (Nondiversity, Differentiation Technique to Estimate RMS Doppler Spread)

$$f(R) = R^2 + \frac{\mu_3}{\Delta^3}R + \frac{1}{4}\left(\frac{\mu_4}{\Delta^4} - 1\right) \tag{5.152}$$

where μ_3/Δ^3 and μ_4/Δ^4 are the skewness and excess of the tropo-scatter channel's Delay Power Spectrum, exists such that, for M^{th} order maximal ratio predetection diversity combining $\gamma(t)$, the normalized (unity rms value) second-order intermodulation distortion has a first-order probability density function, $W(\gamma)$, given by:

$$W(\gamma) = \frac{1}{2\pi\sqrt{\gamma}} \int_{-\infty}^{\infty} \frac{M\,dR}{\sqrt{f(R)}\left[1 + R^2 + \frac{\gamma}{4f(R)}\right]^{M+1}} \tag{5.153}$$

Equation (5.153) for the intermodulation noise probability density function when maximal ratio predetection combining is used has been derived previously by Bello and Nelin [5.5] and will not be repeated here. The probability density function and cumulative distribution for selection diversity combining has been derived in [5.2], where it was noted that for M independent random variables having a continuous cumulative distribution function $P(\gamma)$ and a probability density function $w(\gamma)$, the probability that the smallest of these variables, γ_1, is less than a value Γ is:

$$\text{Prob}\{\gamma_1 \le \Gamma\} = 1 - \left[1 - P(\Gamma)\right]^M \tag{5.154}$$

and the probability density function associated with (5.154) is:

$$w_1(\gamma) = \frac{d}{d\Gamma}\left\{1 - \left[1 - P(\Gamma)\right]^M\right\}_{\Gamma=\gamma} = M\left[1 - P(\gamma)\right]^{M-1} w(\gamma) \tag{5.155}$$

Equations (5.154) and (5.155) can be applied directly to determine the distribution of intermodulation noise in a selection diversity FM system. The probability density function cf γ for one branch is given by (5.153) with $M = 1$, and, by integrating it, $P(\gamma)$ can be found. Then, direct substitution into (5.154) and (5.155) results in the cumulative distribution and density function of the smallest of N intermodulation noises. As a selection diversity combiner is designed to choose the receiver with the smallest of the input noises, the resulting

statistics are those of the selection diversity intermodulation noise.

Equations (5.153) and (5.154) have been evaluated numerically in [5.2] and the resulting noise distributions are shown in Figure 5.22. It is seen that as the order of diversity increases, the selection diversity cumulative distribution lies uniformly to the left of the maximal ratio cumulative distribution, which implies that the irreducible error due to intermodulation distortion will be lower for selection combining than for maximal ratio combining.

A quantity of importance in practical application is the ratio of the intermodulation distortion power to signal power in a narrow frequency band located at some specified baseband frequency, f. Denoting this quantity by $\eta(f,t)$, we may write [5.5]:

$$\eta(f,t) = \frac{P_{x\dot{x}}(f)\ L^4\gamma(t)}{P_x(f)\ 4} \tag{5.156}$$

where L is the rms multipath spread of the channel and, for a modulating signal x(t), $P_{x\dot{x}}(f)$ is the power spectrum of $x(t)\dot{x}(t)$, and $P_x(f)$ is the power spectrum of x(t). As an example [5.5], consider the case of a Gaussian x(t) with a flat power spectrum extending from aW to W Hz, and zero elsewhere. For this case, $\eta(f,t)$ for $aW < f < W$ is given by

$$\eta(f,t) = \frac{\gamma(t)}{2(1-a)}\left(L^2\pi^2 f_{dev} f\right)^2\left[\delta_B\left(\frac{f}{2W} - a\right) + \delta_A\left(1 - a - \frac{f}{W}\right)\right] \tag{5.157}$$

where

$$\delta_A = \begin{cases} 1\ , & \text{if}\quad aW < f < (1-a)W \\ 0\ , & \text{otherwise} \end{cases}$$

$$\delta_B = \begin{cases} 1\ , & \text{if}\quad 2aW < f < W \\ 0, & \text{otherwise} \end{cases}$$

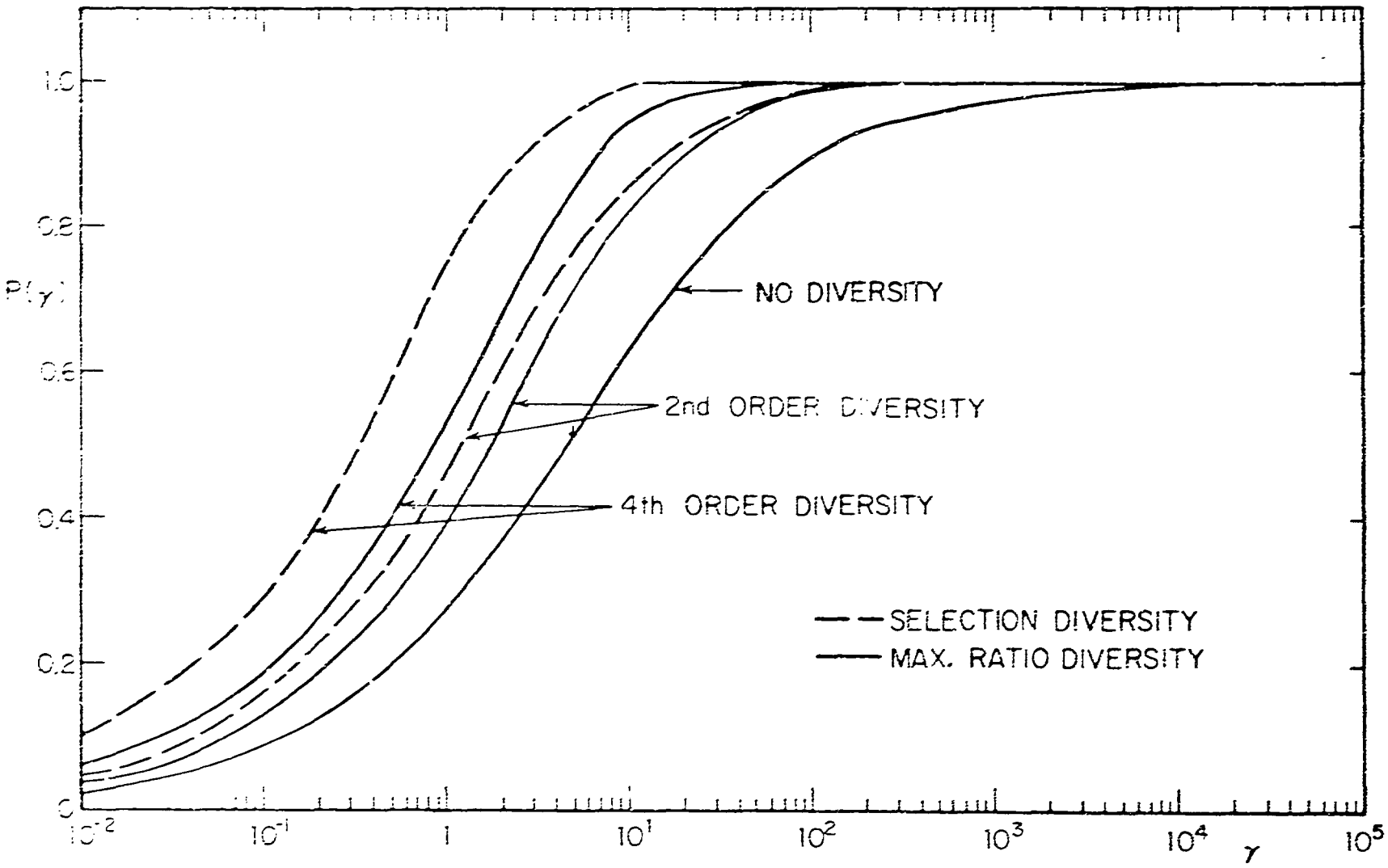

Figure 5.22 Cumulative Distribution of Intermodulation Noise, 24-Channel FDM-FM (from Ref. [5.2])

Equation (5.157) can be expressed as

$$\eta(f,t) = \gamma(t)\, L^4\, D(f) \tag{5.158}$$

where

$$D(f) \triangleq \frac{\left(f_{dev}\, f\, \pi^2\right)^2}{2(1-a)} \left[\delta_B\left(\frac{f}{2W} - a\right) + \delta_A\left(1 - a - \frac{f}{W}\right)\right]$$

Thus, the rms multipath spread is the only channel parameter required to specify the distribution of $\eta(f,t)$.

The error probability due to intermodulation noise can be expressed in terms of the conditional probability of error as

$$P_e = \int_0^\infty P_e\left[\frac{1}{\eta(f,t)}\right] W(\gamma)\, d\gamma \tag{5.159}$$

where $W(\gamma)$ is the probability density function of the normalized intermodulation distortion and $P_e(\cdot)$ is the conditional probability of error.

Figure 5.23 is a block diagram of a technique for estimating the irreducible error rate due to frequency selective fading. The estimator uses estimates of the rms multipath spread to estimate the irreducible error rate.

As an example to illustrate the performance of the estimator, we will consider the systems analyzed in [5.2]. The systems are called the Bell 301B and the Lenkurt 26B, and the irreducible error rate was found in [5.2] to be given by Figure 5.24.

From Figure 5.24 the irreducible error rate can be estimated by

$$\hat{P}_{irr} = A\, \widehat{L^2}^{\,C} \tag{5.160}$$

where A and C are constants. From Figure 5.24 we note that C approximately equals the order of diversity. In a manner similar to the procedure used to evaluate the irreducible error rate due to time selective fading [Eqs. (5.140) to (5.145)], it follows that

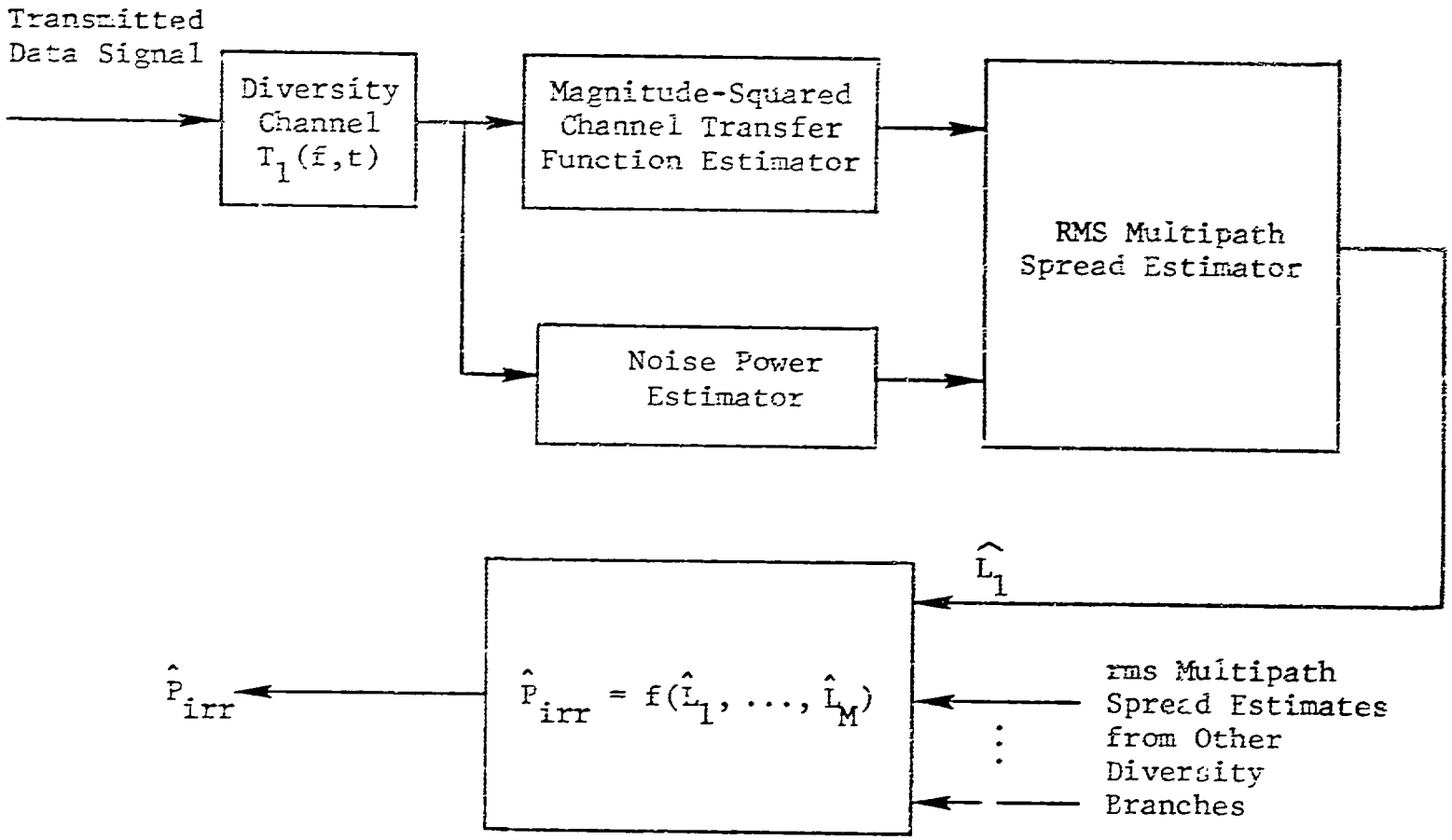

Figure 5.23 Estimation of Irreducible Error Rate Due to Frequency Selective Fading

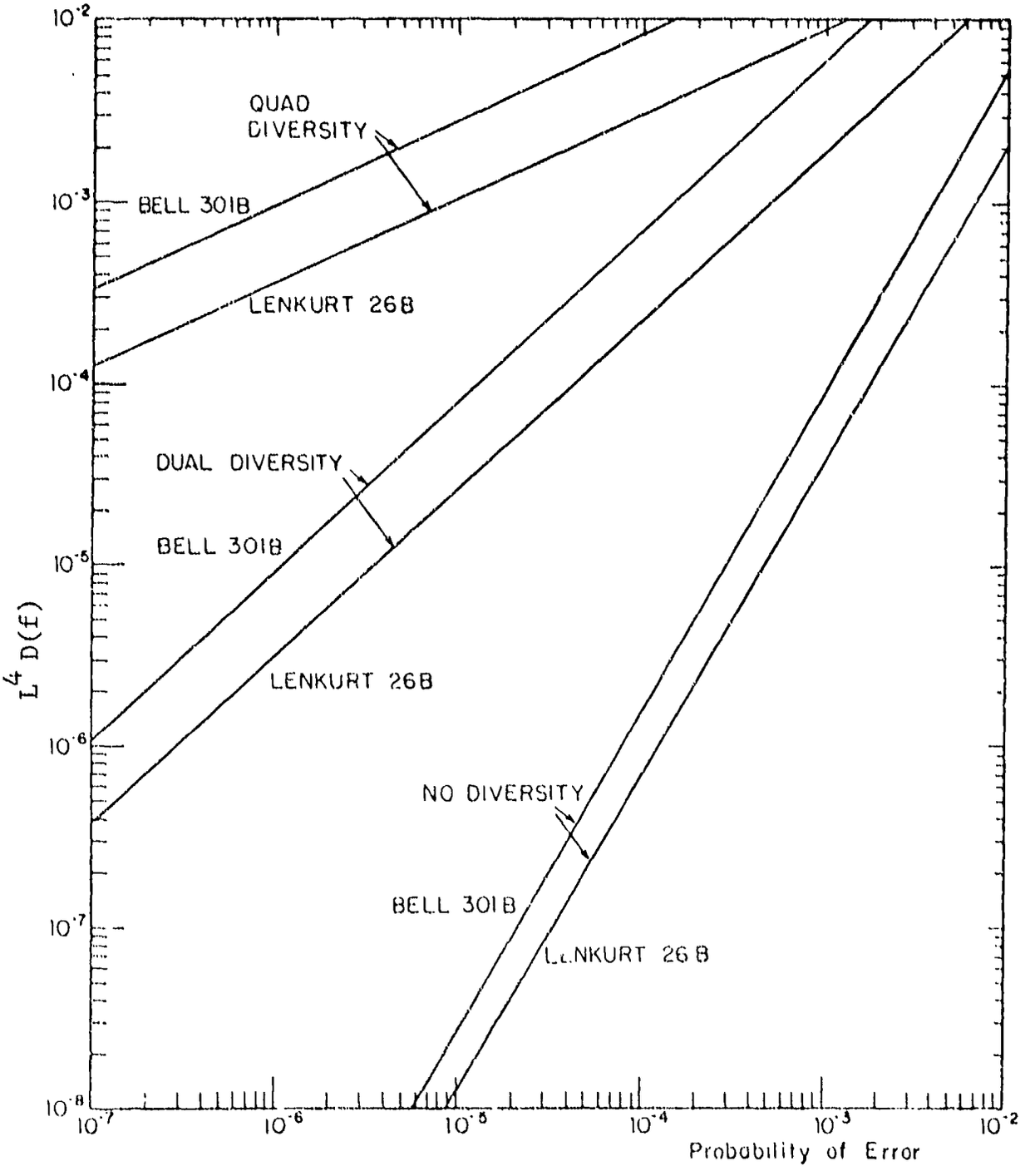

Figure 5.24 Irreducible Error Probability, 24-Channel FDM/FM System: Bell 301B and Lenkurt 26B Selection-Diversity Combining (from Ref. [5.2])

$$E\left\{\hat{P}_{irr}\right\} = A\, E^{C}\left\{\widehat{L^2}\right\}$$

$$\sigma^2_{\hat{P}_{irr}} = A^2 C^2 E\left\{\widehat{L^2}\right\}^{2C-2} \sigma^2_{\widehat{L^2}} \qquad (5.161)$$

where $E\left\{\widehat{L^2}\right\}$ and $\sigma^2_{\widehat{L^2}}$ are the mean and variance of the estimates of $\widehat{L^2}$ (see Section 4.3 and Appendix A).

5.5 FDM/FM Error Rate Estimation

5.5.1 Introduction

This section considers the problem of estimating the error rate of an FDM/FM system. The error rate for an FDM/FM system can be approximately determined by separately finding the error rate due to nonselective fading (i.e., due to additive noise) and the error rate due to selective fading (i.e., due to intermodulation noise). The latter constitutes an irreducible error rate from the point of view that it cannot be reduced by increasing signal power. In order to approximate the error rate due to additive noise and selective fading acting together, one may sum the error rates due to these disturbances acting separately.

5.5.2 Flat Fading Error Rate Estimation

In this section we present techniques for estimating the flat fading error rate of an FDM/FM system from the received data signal.

Using the results of Rice [5.8], Bello [5.9] was able to derive an expression for the discriminator output SNR. He showed that if the typical signaling element is a sinusoidal burst and the instantaneous predetection combined input SNR, ρ, is greater than about 1 dB, the discriminator output instantaneous SNR after coherent matched filter detection, s, is given by

$$s(\rho) = \frac{\sigma^2\left(1 - e^{-\rho}\right)^2}{2W(1-a)e^{-\rho}\sqrt{\dfrac{r^2 + 2\sigma^2\rho}{\pi\rho} + \dfrac{W f_d^2 (1-a)}{B\rho}}} \qquad (5.162)$$

where

σ^2 = mean-squared frequency deviation of modulation signal

B = IF bandwidth

r = $B/\sqrt{12}$ (baseband assumed flat)

f_d = location of data subcarrier

and the baseband extends from aW to W Hz. In calculating (5.162) it was assumed that there are enough baseband FDM signals so that their sum has close to Gaussian statistics.

The SNR at the input to the discriminator is distributed according to

$$W_M(\rho) \approx \frac{\rho^{M-1}}{(M-1)! \prod_{k=1}^{M} \Gamma_k} \qquad \rho \ll \Gamma_k \tag{5.163}$$

for maximal-ratio combining and

$$W_S(\rho) \approx \frac{M\rho^{M-1}}{\prod_{k=1}^{M} \Gamma_k} \qquad \rho \ll \Gamma_k \tag{5.164}$$

for selection combining. The average error rate can be found by averaging the conditional error rate over the distribution of the instantaneous SNR. That is, we can write

$$P_e = \int_0^\infty P_e[s(\rho)]\, W(\rho)\, d\rho \tag{5.165}$$

where $P_e(s)$ is the conditional error rate.

Since the case of $\rho \ll \Gamma$ is the region where most errors occur, then the error rate can be accurately estimated from the distribution of the errors for low SNR. Therefore, using (5.163) in (5.165) we obtain

$$P_e \approx \frac{A}{\prod_{k=1}^{M} \Gamma_k} \int_0^{\infty} P_e[s(\rho)]\, \rho^{M-1}\, d\rho \tag{5.166}$$

where A is a constant dependent upon the diversity-combining technique and order or diversity. Therefore, if $P_e[s(\rho)]$ is known in a functional form, the above integral can be estimated and the error rate can be expressed as

$$P_e \approx \frac{B}{\prod_{k=1}^{M} \Gamma_k} \tag{5.167}$$

This expression has the same form as the error rates estimated in Section 5.3 [i.e., see Eq. (5.101)]. Therefore, the error rate estimation technique proposed and analyzed in Section 5.3 can be used to estimate the error rate for FDM/FM systems with no intermodulation distortion. In fact, any of the techniques analyzed in Sections 5.1.5.2 and 5.3 can be used to estimate the error rate due to noise alone.

Several FDM/FM systems were analyzed in [5.2]. The AN/GSC-4 is a 4-phase, 2400 b/s, DPSK modem. In [5.2], it was found that the conditional error probability for the AN-GSC-4 is

$$P_e[s(\rho)] \cong \frac{1}{2} \operatorname{erfc}\left[\frac{3.33\, s(\rho)}{2\sqrt{0.5 + 3.33\, s(\rho)}}\right] \tag{5.168}$$

where $s(\rho)$ is given by (5.162).

The Bell 301B is a 40.8 kb/s digital data set that accepts binary information at 40.8 kb/s and encodes it into 4-phase DPSK. The conditional error probability for the Bell 301B is [5.2]:

$$P_e[s(\rho)] = \frac{1}{2} \operatorname{erfc}\left[\frac{2.35\, s(\rho)}{2\sqrt{0.5 + 2.35\, s(\rho)}}\right] \tag{5.169}$$

Comparing the conditional error rates of the AN/GSC-4 and the Bell 301B, one would expect that the two systems would have virtually the same error rate.

The third modem to be considered in the Lenkurt 26B. The Lenkurt 26B uses a duobinary modulation technique where the information is transmitted by an FSK modulation that deviates $\pm$ 600 Hz relative to the center frequency of 1.7 kHz. The conditional error probability for the Lenkurt 26B is [5.2]:

$$P_e[s(\rho)] \cong \frac{3}{4} \operatorname{erfc}\left[\sqrt{s(\rho)}\right] \tag{5.170}$$

Thus, for the above three FDM/FM modems, the error rate due to flat fading can be estimated using any of the techniques analyzed in Sections 5.1 - 5.3.

5.5.3 FDM/FM Error Rate Estimation Due to Noise and Intermodulation Distortion

To estimate the error rate due to noise and intermodulation distortion, one may sum the flat fading error rate estimate of Section 5.5.2 with the irreducible error rate estimate given in Section 5.4.2. That is, the error rate for FDM/FM transmission can be expressed as

$$P_e \approx P_{irr} + P_{FF} \tag{5.171}$$

where P_{irr} is the irreducible error rate due to intermodulation distortion and for the Bell 301B and the Lenkurt 26B systems can be estimated by [see Eq. (5.160)]

$$\hat{P}_{irr} = A \widehat{L^2}^C \tag{5.172}$$

where A and C are constants. The flat fading error rate is given by (5.167) and can be estimated by

$$\hat{P}_{FF} = \frac{B}{\prod_{k=1}^{M} \hat{r}_k} \tag{5.173}$$

where M is the order of diversity, $\hat{\Gamma}_k$ is an estimate of the mean SNR on the k^{th} diversity branch, and B is a constant dependent upon the form of the conditional error rate.

From (5.171) - (5.173) the error rate for FDM/FM systems can be estimated by

$$\hat{P}_e = A\,\widehat{L^2}^C + \frac{B}{\prod_{k=1}^{M} \hat{\Gamma}_k} \tag{5.174}$$

This estimate can be implemented from the rms multipath spread and the mean SNR estimates proposed and analyzed in Section 4.3. Frequently, either the flat fading error rate or the irreducible error rate will dominate and, for these cases, the convergence of $\hat{P}_e$ can be directly related to the convergence of $\hat{P}_{FF}$ or P_{irr}. The estimation of P_{FF} was considered in Sections 5.1 to 5.3, while Section 5.4.2 considered the estimation of P_{irr}.

5.6 Estimation of Error Rate for High-Speed Data Transmission

5.6.1 Introduction

In this section we address the problem of estimating error rates for high-speed data transmission systems employing a multipath-resisting receiver (e.g., maximum likelihood or nonlinear equalizers). For these systems, in-band diversity increases the effective order of diversity and results in an improvement in performance.

High-speed data transmission involves reception of signaling elements corrupted by intersymbol interference. Optimum demodulation techniques exist (e.g., maximum likelihood and nonlinear equalizers) which are claimed [5.10],[5.11] to come close to eliminating the effect of intersymbol interference. The limiting performance obtainable is just that associated with the matched filter receiver for a single pulse. In this section we discuss the estimation of error probabilities for this ideal multipath-resisting receiver. For practical receivers, one must assign some degradation in SNR. However, it appears that this degradation need not be more than 1 or 2 dB. Since the number of practical implementations possible is very large, it appears most

meaningful to study the estimation of the performance of the optimum receiver and then apply correction factors for the known nonideal performance of the actual implemented receiver.

5.6.2 Single-Pulse Matched Filter System

The optimum performance we wish to compute is associated with a system in which the receiver is a coherent matched filter receiver, matched to the response of each pulse and completely eliminating the effect of intersymbol interference. For simplicity of notation, consider the pulse transmitted at $t = 0$, and let $A\,g(t), A\,G(f)$ denote the transmitted pulse and its spectrum, respectively. The information is contained in the value of A which takes on the values ± 1 according to a binary alphabet. Figure 5.25 gives the signal processing operations involved. The pulse duration is so much smaller than the fading time constant that the channel may be regarded as frozen in computing the pulse response. Confining our attention to a single diversity channel for a moment, the spectrum of the received pulse is $A\,G(f)\,T(f,0)$ and the transfer function of the matched filter is then $K^*(f)\,T^*(f,0)$. The complex sampled matched filter output is given by

$$W = A\int |G(f)|^2 |T(f,0)|^2\,df + \int N(f)\,G^*(f)\,T^*(f,0)\,df \tag{5.175}$$

where $N(f)$ is the complex spectrum of the white additive complex Gaussian noise. This spectrum is also white [5.12],

$$\overline{N^*(f)\,N(f+F)} = 2N_0\,\delta(F) \tag{5.176}$$

where N_0 is the one-sided power density of the real additive noise.

Expression (5.175) is in the form

$$W = A\,S + N \tag{5.177}$$

where N is a complex Gaussian noise whose strength is readily computed to be

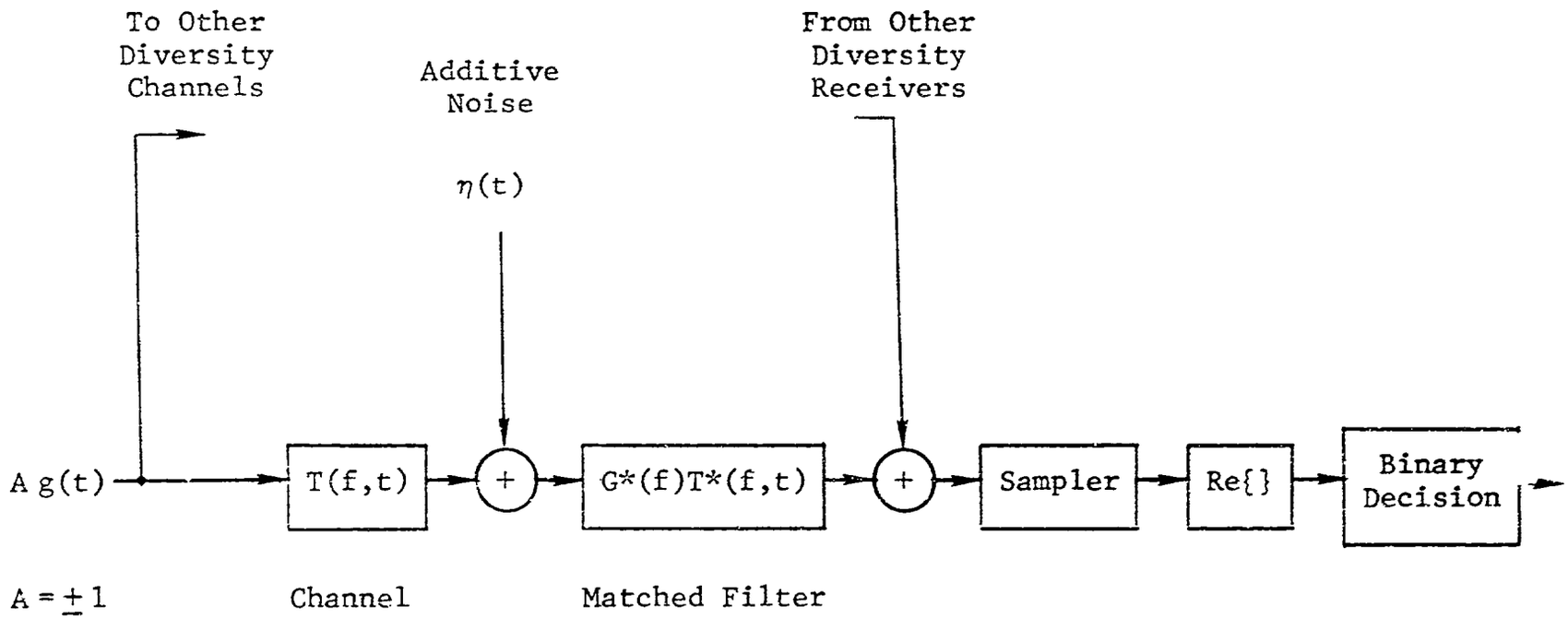

Figure 5.25 Single-Pulse Matched Filter System

$$\overline{|N|^2} = 2N_0 S \tag{5.178}$$

where

$$S = \int |G(f)|^2 \, |T(f,0)|^2 \, df \tag{5.179}$$

Of course, S is a random variable dependent upon the time of transmission, but the fading is so slow relative to the bit rate that, for purposes of analysis, we may consider S fixed for many bits. Thus, we may evaluate bit error probabilities by assuming S fixed and then subsequently averaging over the statistics of S.

When diversity channels with independent additive noises are included in the analysis, it is readily seen that we must redefine S as

$$S = \int |G(f)|^2 \sum_{k=1}^{M} |T_k(f,0)|^2 \, df \tag{5.180}$$

where $T_k(f,0)$ is the transfer function of the k^{th} diversity channel and M is the order of diversity. Equation (5.178) still applies but with the new definition of S in (5.180).

The Re{ } operation in Figure 5.25 corresponds to the coherent detection operation of the PSK system. Thus, prior to the binary ($\lesseqgtr$) decision, we use the variable

$$U = \mathrm{Re}\{W\} = A\,S + \mathrm{Re}\{N\} \tag{5.181}$$

The variable Re{N} is real Gaussian with variance

$$\overline{\mathrm{Re}^2\{N\}} = \frac{1}{2}\,\overline{|N|^2} \tag{5.182}$$

5.6.3 Estimation of S(t)

In order to estimate the bit error probability, the estimation of S(t) must be considered, where S(t) is given by

$$S(t) = \int |G(f)|^2 \sum_{k=1}^{M} |T_k(f,t)|^2 \, df \tag{5.183}$$

Two techniques for estimating S(t) from the received data signal may be used. The first approach uses samples in frequency of an estimate of the magnitude squared of the channel transfer function to express the integral as a finite sum. This approach is presented in Figure 5.26. Therefore, the estimate of $S(t_p)$ is given by

$$\hat{S}(t_p) = \Delta F \sum_{k=1}^{M} \sum_{q=1}^{Q} |\tilde{T}_k(F_q,t_p)|^2 \cdot |G(F_q)|^2 \qquad (5.184)$$

where $W = Q \cdot \Delta F$ is the bandwidth of G(f).

With the estimate of the magnitude squared of the channel transfer function given by

$$|\tilde{T}_k(F_q,t_p)|^2 = |T(F_q,t_p)|^2 (1+\epsilon_{kq}) + \delta_{kq} \qquad (5.185)$$

where δ_{kq}, ϵ_{kq} are zero mean and independent estimation errors with (see Section 4.1)

$$\sigma^2_{\delta_{kq}} = \epsilon_S^2 E^2\{|T_k(f,t)|^2\}$$

$$\sigma^2_{\epsilon_{kq}} = \epsilon^2 \qquad (5.186)$$

where ϵ and ϵ_S are given by (4.57) and (4.100), respectively. From (5.184) and (5.185), the mean and variance of $\hat{S}(t_p)$ conditioned upon the channel transfer function are given by

$$E\{\hat{S}(t_p)\} = \Delta F \sum_{k=1}^{M} \sum_{q=1}^{Q} |T_k(F_q,t_p)|^2 |G(F_q)|^2 \qquad (5.187)$$

$$\sigma^2_{\hat{S}(t_p)} = \frac{\epsilon^2 W^2}{Q^2} \sum_{q=1}^{Q} \sum_{k=1}^{M} |T_k(F_q,t_p)|^4 |G(F_q)|^4 + \frac{\epsilon_S^2 W^2}{Q^2} \sum_{q=1}^{Q} \sum_{k=1}^{M} E^2\{|T_k(F,t_p)|^2\} |G(F_q)|^4 \qquad (5.188)$$

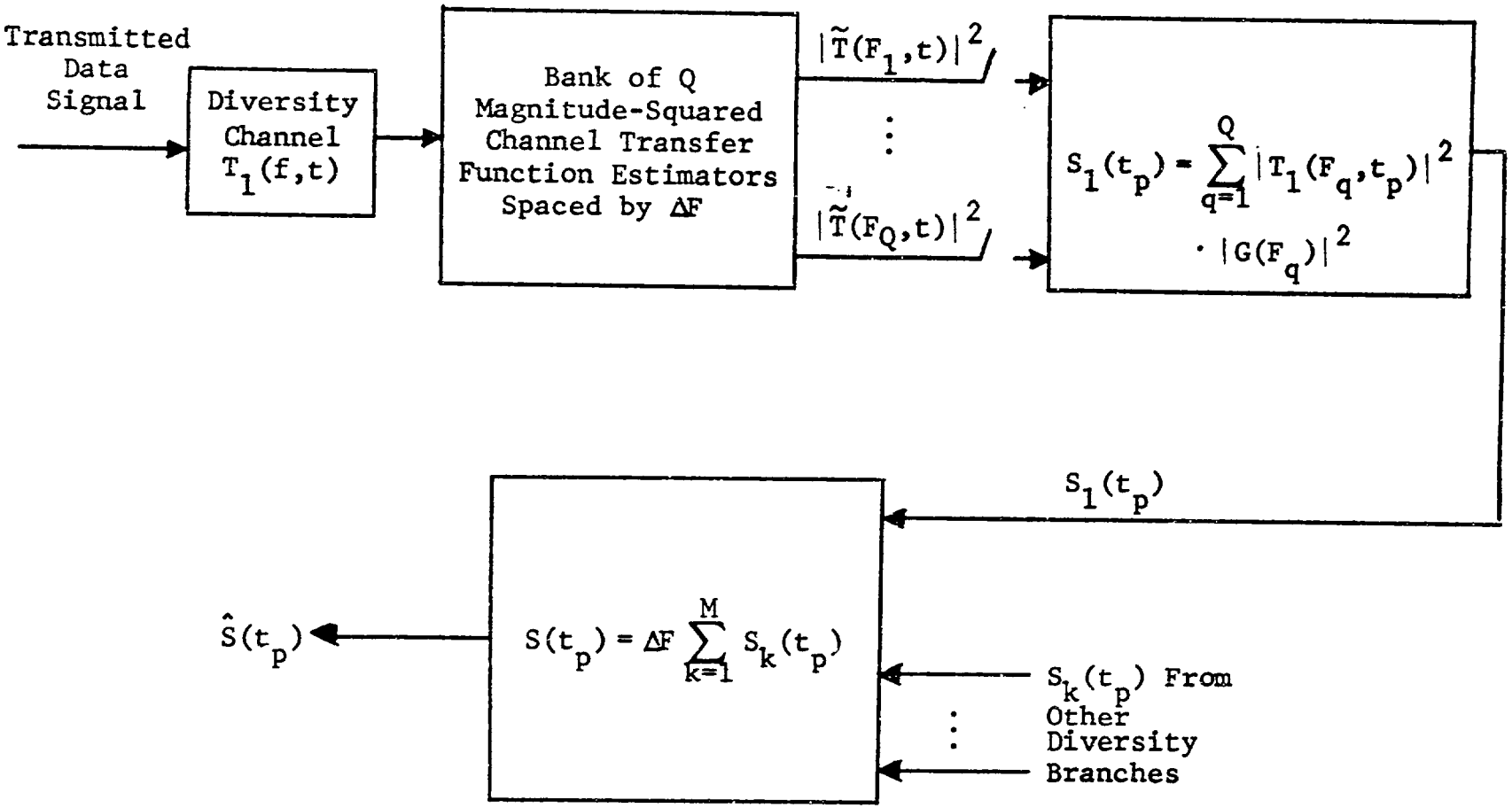

Figure 5.26 Estimation of Total Received Signal Power

For large Q, the summation of (5.187) converges to the desired integral given by (5.183) and the variance of $\hat{S}(t_p)$ becomes small. Thus, when Q is large, a good estimate of $S(t_p)^p$ can be obtained. However, a large Q means that many magnitude-squared channel transfer function estimators would be required.

The second approach for estimating $\hat{S}(t)$ that will be considered utilizes the technique employed to estimate the magnitude squared of the channel transfer function. The estimator to be considered is given by Figure 5.27 and has the same functional representation as the magnitude-squared channel transfer function estimator analyzed in Section 4.1. The averaging filter duration will be chosen long enough to average out data fluctuations, yet short enough not to filter the channel fluctuations. The bandwidth of h(t) should be large enough to pass the signal without distortion, but not so large that the amount of noise power passed is excessive.

The estimate of S(t) averaged over the data and noise can be given by

$$E\{\hat{S}(t)\} = K(0)\left[|H(0)|^2 \int_{-\infty}^{\infty} |G(f)|^2 \, |T(f,t)|^2 \, df + 2N_0 \int_{-\infty}^{\infty} |H(f)|^2 \, df\right] \tag{5.189}$$

where H(f) was assumed to be flat over the duration of G(f) and

$$K(0) = \int k(t)\, dt \tag{5.190}$$

The bias and variance of the estimator in Figure 5.27 can be computed as was done for the estimation of $|T(f,t)|^2$. Frequency-selective distortion can be neglected because an integral of $|G(f)|^2|T(f,t)|^2$ over f is computed. Thus, the output averaging filter can be adjusted to minimize the effects of time-selective fading. It appears that the desired time-variant energy can be estimated more accurately than $|T(f,t)|^2$ so that the second approach is preferred.

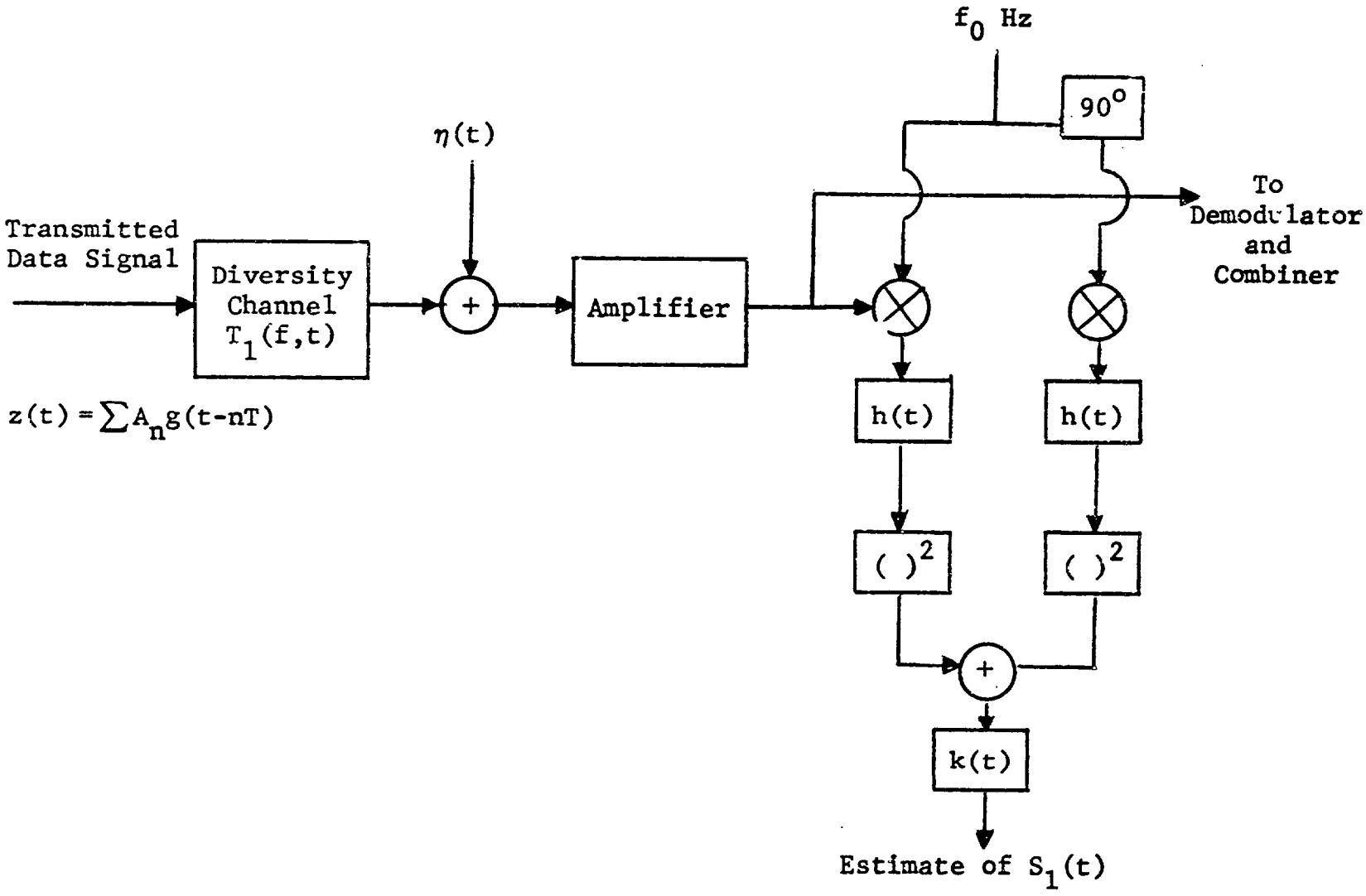

Figure 5.27 Estimation of Received Signal Power

Once S(t) is estimated by either of the two methods presented above, the error rate may be estimated from the conditional bit error probability. Figure 5.28 presents a technique for estimating error rate from estimates of S(t). As was shown in Section 5.1.4, the conditional error rate can also be used to estimate short-term error bursts.

5.7 Error Rate Estimation Based Upon Interference

In this section we describe the way that error rate estimation is affected by errors in estimating the interference parameters and channel transfer function. The error rate predictions used here are in the nature of upper and lower bounds on probability of error. This general approach is used here because of the wide variety of interference that might occur on all of the channels discussed in this report. Interference could take the form of man-made noise, naturally-occurring interference, and deliberate jamming. Due to the unpredictability of the interference, it is not feasible to attempt precise error-rate predictions at a given SNR, and any results relating to specific interference models, such as normally distributed interference, would be of extremely limited utility.

In the work reported below, the additive interference will be allowed to have general statistics. Restrictions on the interference will be minor. At first, we will describe how error rate bounds can be developed by using as the only constraints a specification of the mean value, α, and an upper bound on the values that the generalized noise variable can take on. Later, in this section, we will replace the upper bound constraint with a constraint on p, the probability that the interference variable U exceeds some fixed threshold U'. The motivation for this new approach arises from the simplicity of the schemes for estimating p and the reliability with which it can be measured, as discussed earlier in Section 4.5.4.3. In the development leading to both of these schemes, the fading, as before, is assumed to be characterizable as a complex-valued Gaussian process and is assumed to be sufficiently slow and to have a sufficiently small degree of frequency selectivity so that a received signaling element is undistorted by the channel and differs from the transmitted signaling element only in a random amplitude change and phase

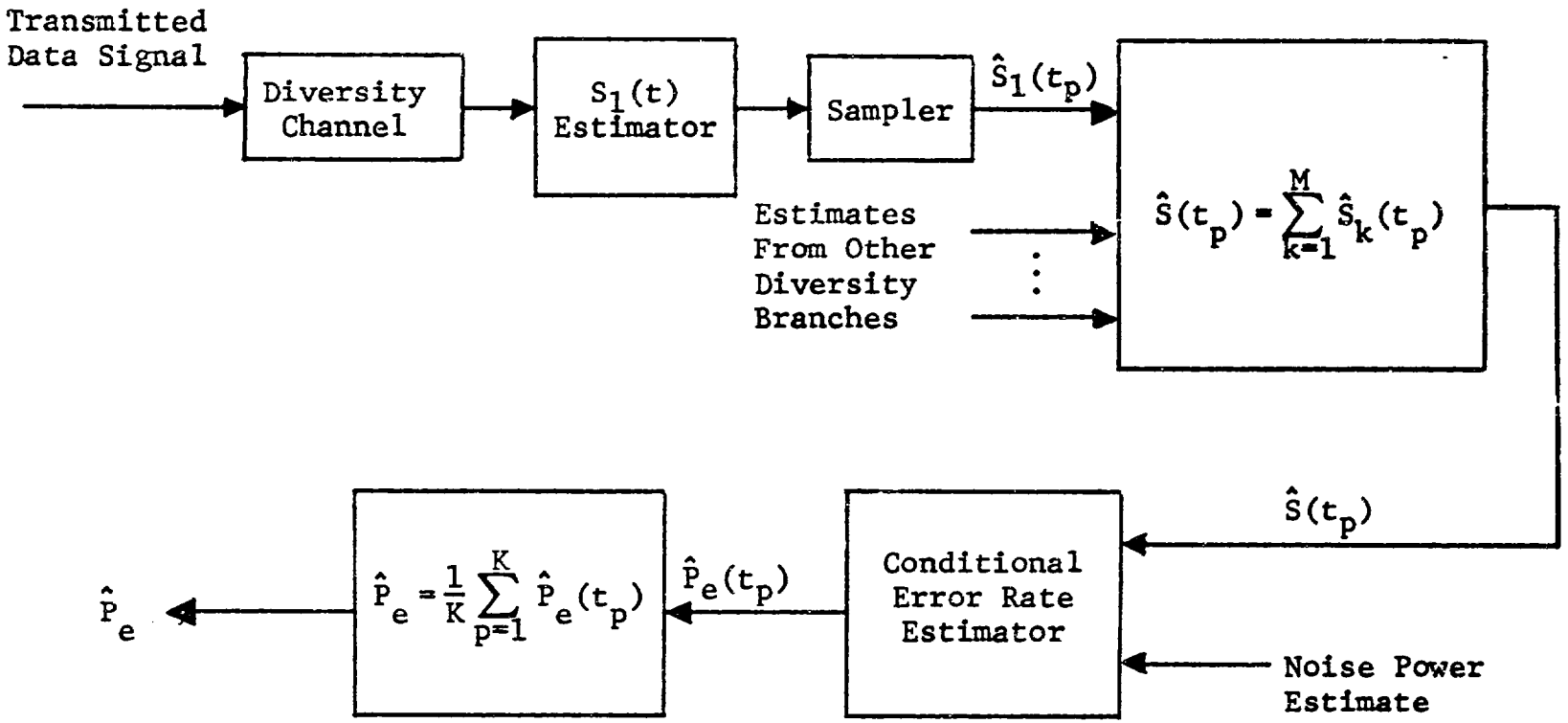

Figure 5.28 Error Rate Estimator for Multipath Resisting Receiver

shift. System degradations due to fading that is not restricted in this way have been treated elsewhere in this report. Since the effect of these distortions can be reduced to the point where system degradation is determined primarily by nonselective fading and additive interference, it is this last situation that we concentrate on. Hence, with s(t) denoting the complex envelope representation of a signaling element of duration T received in the time interval $0<t<T$ for a unit gain channel and no additive noise, we have for the received signaling element r(t), including fading and additive interference, the representation

$$r(t) = G\, s(t) + n(t) \qquad 0<t<T \tag{5.191}$$

where G is a complex-valued normally distributed variable, and n(t) is the additive interference.

It was pointed out in Section 4.5 that three important matched filter receivers are characterized well by detector operation that can be represented as the comparison of a quadratic form q_L with a zero threshold. The quantity q_L is given by

$$q_L = \sum_{p=1}^{L} |G_p + \xi_p|^2 - \sum_{p=1}^{L} |\eta_p|^2 \tag{5.192}$$

where L is the order of diversity, G_p is the complex-valued normally distributed signal term on the p^{th} diversity branch, and ξ_p and η_p are complex noise terms due to the p^{th} diversity receiver. Specific forms were given in Table 4.5. For diversity channels that fade independently, but with identical statistics, the random variables $\{G_p\}$ become mutually independent and identically distributed.

For future use, we note no loss of generality accrues if the normalization

$$\frac{1}{2}\,\overline{|G_p|^2} = 1 \tag{5.193}$$

is used which means, effectively, that the quantities U and V are "instantaneous" noise to average signal power ratios.

As shown in [5.17], the problem of determining error rate bounds is a double integral extremum problem that involves the interference only through the joint probability density function of the two interference variables, U and V,

$$U = \sum_{p=1}^{L} |\xi_p|^2 \tag{5.194}$$

$$V = \sum_{p=1}^{L} |\eta_p|^2 \tag{5.195}$$

The upper bound on the double integral is achieved when U and V are assumed to have nonzero values mutually exclusively, i.e.,

$$UV = 0 \tag{5.196}$$

and the lower bound is achieved when

$$U = V \tag{5.197}$$

It is demonstrated in [5.17] that the error probability is bounded in the following way:

$$\int F_L(A)\, G_L(A)\, dA \le p_L \le \int F_L(A)\, H_L(A)\, dA \tag{5.198}$$

where $F_L(A)$ is the probability density function for A, the arithmetic mean of U and V.

$$A = \frac{U+V}{2} \tag{5.199}$$

and $H_L(A)$ and $G_L(A)$ are given, respectively, by

$$H_L(A) = \frac{1}{2}\left[1 - e^{-A} \sum_{0}^{L-1} \frac{A^r}{r!}\right] \tag{5.200}$$

and

$$G_L(A) = \frac{1}{2}\left[1 - e^{-A} \sum_{-[L-1]}^{L-1} I_r(A)\right] \tag{5.201}$$

where $I_r(A)$ is the modified Bessel function of order r.

For the general situation being treated here, the pdf $F_L(A)$ is not known. It is clear, though, that a maximization of the right-hand side of (5.198) and a minimization of the left-hand side leads to reliable bounds on error probability.* This extremization problem only requires proper choice of the minimizing and maximizing pdf's, a task which becomes extremely simple through application of the "Completeness Theorem" proved in [5.17]. A reasonable approach to the problem, of course, requires the application of constraints, without which the bounds would be useless. The physical basis for all of the discussion in this section is that the constraints can be generated by direct interference measurement.

5.7.1 Bounds on Error Rate

In order to plot the bounds on error rate as a function of signal-to-noise ratio, it is necessary, here, to first define a composite signal-to-noise ratio.

$$\rho = \frac{\sum_{k=1}^{L} \overline{|G_k|^2}}{\frac{1}{2}\left[\sum_{k=1}^{L} \overline{|\xi_k|^2} + \sum_{k=1}^{L} \overline{|\eta_k|^2}\right]} = \frac{2L}{\alpha_L} \tag{5.202}$$

where the normalization in (5.193) has been used and α_L is defined as the mean of the noise variable U or A, i.e.,

$$\alpha_L = \overline{U} = \overline{V} = \overline{A} \tag{5.203}$$

---

*We point out that coherent PSK systems, for which U=V, require only that the left-hand side of (5.198) be dealt with, i.e., minimize and maximize $\int F_L(A)\, G_L(A)\, dA$ to get both upper and lower bounds on the error rate.

where A is just the arithmetic mean of U and V:

$$A = \frac{U+V}{2}$$

There are two constraints that are used in establishing the error bound. The first of these is the maximum allowable peak noise power to average signal power constraint defined below:

$$\gamma_L = \text{Max}\left\{\frac{\text{Peak U}}{2L}\right\} = \begin{cases} \text{Max}\left\{\frac{\text{Peak A}}{2L}\right\} & ; \; U = V \\ \text{Max}\left\{\frac{\text{Peak A}}{L}\right\} & ; \; UV = 0 \end{cases} \tag{5.204}$$

The second is the maximum allowable peak-to-average interference constraint or "crest factor":

$$\beta_L = \text{Max}\left\{\frac{\text{Peak U}}{\alpha_L}\right\} = \begin{cases} \text{Max}\left\{\frac{\text{Peak A}}{\alpha_L}\right\} & ; \; U = V \\ 2\,\text{Max}\left\{\frac{\text{Peak A}}{\alpha_L}\right\} & ; \; UV = 0 \end{cases} \tag{5.205}$$

In both of these expressions, Peak A refers to the peak or maximum value of the variable A. The first thing to be noticed about these expressions is that γ_L does not depend on α [or signal-to-noise ratio; see (5.202)] whereas β_L does. This is because the earlier constraint arises because of the finite dynamic ranges of receivers, which cause the outputs to saturate for sufficiently high input voltages, and it is safe to assume that detected noises cannot exceed the design value of output signal power by more than some factor, i.e., there is some factor γ_L for which Peak U is always less than $2\gamma_L L$. This factor, alone, places limits on the integrals in (5.198) which cannot be exceeded; this, in itself, is enough to give meaning to the extremization problem. Unfortunately, the error bounds that would result from such a formulation would be extremely weak.

The use of β_L has the effect of further constraining Peak U, and has the end effect, typically, of tightening the bounds on probability of error. As opposed to the constraint, γ_L, which arises mainly from consideration of receiver limitations, the

constraint β_L arises solely from consideration of the interference statistics. The use of some specific β_L value requires some a priori knowledge of these statistics. This knowledge could be obtained by utilizing realistic models of naturally occurring or man-made interference. Unfortunately, the interference is often of such an unpredictable nature that the only reliable way to obtain any useful information about interference statistics is through measurement. This fact, of course, was the motivation for the measurement schemes discussed in Section 4.5 and much of the work to follow.

We now review the results of the extremization procedures as reported in [5.17].

First we recall, as discussed earlier, that the left-hand side of (5.198) must be minimized and the right-hand side maximized. In the case U = V, we need only deal with the left-hand side of (5.198). This gives us the three extremization problems listed below:

I. (UV=0) Maximize the right-hand side of (5.198) to get p_1^{Max}.

II. (U=V) Maximize the left-hand side of (5.198) to get p_L^{max}.

III. (U=V) Minimize the left-hand side of (5.198) to get p_L^{min}.

The maximization problem for the UV=0 case is to maximize

$$p_L = \int_0^{\hat{A}_L} F_L(A)\, H_L(A)\, dA \tag{5.206}$$

subject to the constraint

$$\alpha_L = \int_0^{\hat{A}_L} A\, F_L(A)\, dA \tag{5.207}$$

where

$$\hat{A}_L = \text{Min}\left\{L\gamma_L,\ \frac{\alpha_L\beta_L}{2}\right\} \tag{5.208}$$

For the U=V case (problems II and III above) the extremization problem involves

$$p_L = \int_0^{\hat{U}_L} W_L(U)\, G_L(U)\, dU \tag{5.209}$$

subject to the constraint

$$\alpha_L = \int_0^{\hat{U}_L} U\, W_L(U)\, dU \tag{5.210}$$

where

$$\hat{U}_L = \text{Min}\{2L\gamma_L\,,\ \beta_L\alpha_L\} = 2\hat{A}_L \tag{5.211}$$

The results of the extremizations as a function of ρ, the SNR, are given by

$$\overset{\text{Max}}{p_L} = \left\{ \begin{array}{ll} (2/\beta_L)\ \cdot\ H_L(L\beta_L/\rho)\ ; & \rho \geq L\beta_L/\mu_L \\ (2L/\rho)\ \cdot\ H_L(\mu_L)/\mu_L\ ; & (2L/\mu_L) \leq \rho \leq L\beta_L/\mu_L \\ H_L(2L/\rho) & 2/\gamma_L \leq \rho \leq 2L/\mu_L \end{array} \right\} \quad \text{(UV=0)} \tag{5.212}$$

where μ_L is the point of tangency between a straight line emanating from the origin and the $H_L(A)$ curve, and has the values $\mu_1=0$, $\mu_2=1.8$, and $\mu_4=4.85$. For problem II, the results are:

$$\overset{\text{max}}{p_L} = \left\{ \begin{array}{ll} (1/\beta_L)\ \cdot\ G_L(2L\beta_L/\rho);\ \rho \geq 2L\beta_L/\nu_L \\ (2L/\rho)\ \cdot\ G_L(\nu_L)/\nu_L\ ; & 2L/\nu_L \leq \rho \leq 2L\beta_L/\nu_L \\ G_L(2L/\rho) & 1/\gamma_L \leq \rho \leq 2L/\nu_L \end{array} \right\} \quad \text{(U=V)} \tag{5.213}$$

where ν_L is analogous to μ_L; i.e.,

$$G_L(\nu_L)/\nu_L = \underset{U}{\text{Max}}\left\{G_L(U)/U\right\} \tag{5.214}$$

and has the values $\nu_1=0$, $\nu_2=1.8$, $\nu_4=8.8$.

The minimization in problem III is slightly more complicated and requires definition of σ_L, where σ_L is such that

$$\frac{G_L(\hat{U}_L) - G_L(\sigma_L)}{\hat{U}_L - \sigma_L} = \underset{U_L}{\text{Max}}\left[\frac{G_L(\hat{U}_L) - G_L(U_L)}{\hat{U}_L - U_L}\right] \tag{5.215}$$

Since σ_L is a function of $\hat{U}_L$, it is convenient to define

$$\sigma_L = f_L(\hat{U}_L) \tag{5.216}$$

The lower bound on error probability, as a function of SNR, is given by

$$P_L^{\min} = \begin{cases} G_L(2L\gamma_L) - 2L\left(\gamma_L - \frac{1}{\rho}\right)S_L(2L\gamma_L); & \\ \qquad\qquad \rho < \beta_L/\gamma_L & L>1 \\ G_L(2L\beta_L/\rho) - (2L/\rho)(\beta_L - 1)S_L(2L\beta_L/\rho); & \\ \qquad\qquad \beta_L/\gamma_L < \rho < 2L/\theta_L & L>1 \\ G_L(2L/\rho) \qquad\qquad \rho > 2L/\theta_L & L>1 \end{cases} \tag{5.217}$$

where θ_L is the solution to the equation

$$x = f_L(\beta_L x) \tag{5.218}$$

and where we have defined the maximum slope as

$$S_L(\hat{U}_L) = \frac{G_L(\hat{U}_L) - G_L\left[f_L(\hat{U}_L)\right]}{\hat{U}_L - f_L(\hat{U}_L)} \tag{5.219}$$

All of the results catalogued above take on considerably simpler form for the nondiversity case, L=1. We have

$$\begin{aligned} p_1^{Max} &= H_1(2/\rho) && \rho \geq 2/\gamma_1 \\ p^{max} &= G_1(2/\rho) && \rho \geq 1/\gamma_1 \\ p_1^{min} &= (2/\rho)\cdot G_1(2\gamma_1)/2\gamma_1 && \beta_1/\gamma_1 \geq \rho \geq 1/\gamma_1 \\ &= (1/\beta_1)\cdot G_1(2\beta_1/\rho) && \rho \geq \beta_1/\gamma_1 \end{aligned} \tag{5.220}$$

Some numerical results for different types of modulation and for both nondiversity and dual diversity operation are shown in Figures 5.29 - 5.31. The details of each physical situation are entered on each figure.

5.7.2 Reliability of Bounds

5.7.2.1 Preliminary Comments

The curves presented in the previous section indicate that with an extremely limited knowledge of noise statistics, i.e., the peak noise-to-average-signal ratio, γ_L, and the crest factor, β_L, one can develop meaningful bounds on probability of error as a function of the signal-to-noise ratio. In this section, we are not so much interested in how well one can generate curves of this type as we are in the question of determining how well, given a set of interference measurements (and channel transfer measurements), we can find just the two numbers which bound the error probability under the true noise condition. A schematic

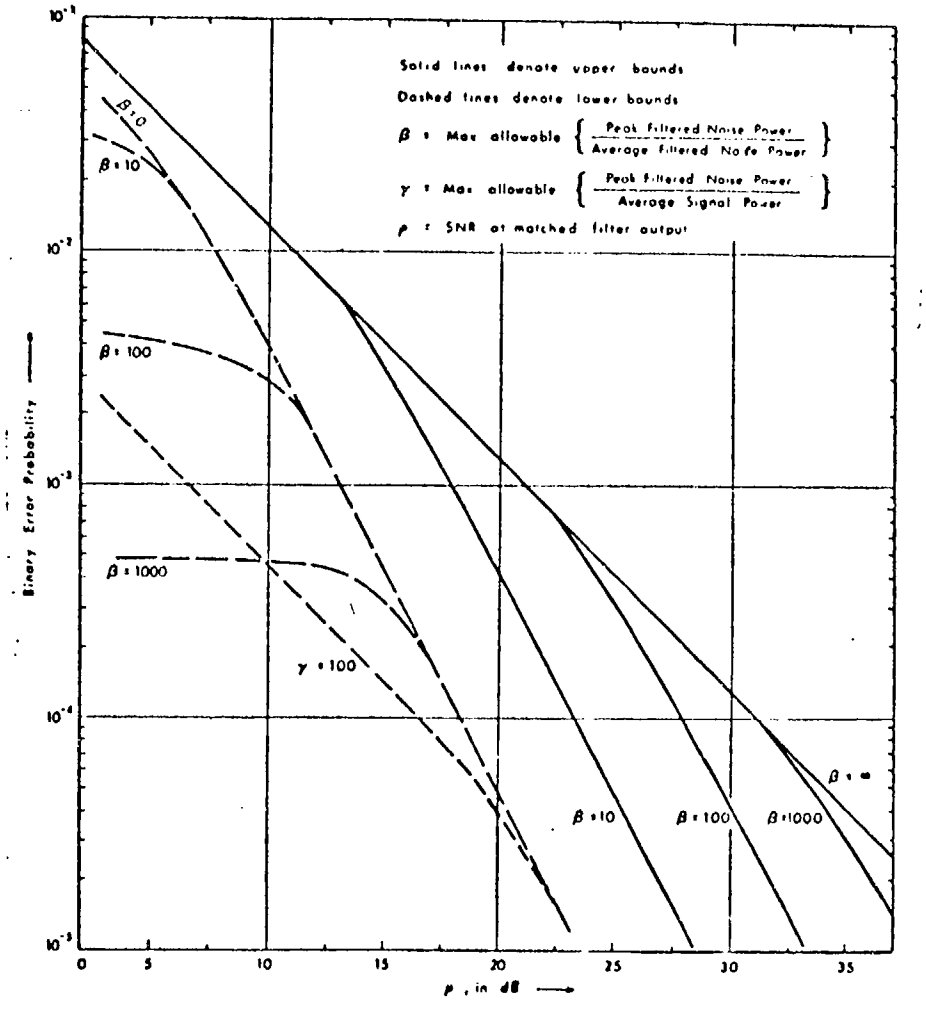

Figure 5.29 Binary Error Probability as a Function of Matched Filter Output SNR for Quaternary PSK Using a Pilot Tone as a Phase Reference. Dual Diversity Using Predetection Square Law Combining. (From Ref. [5.17])

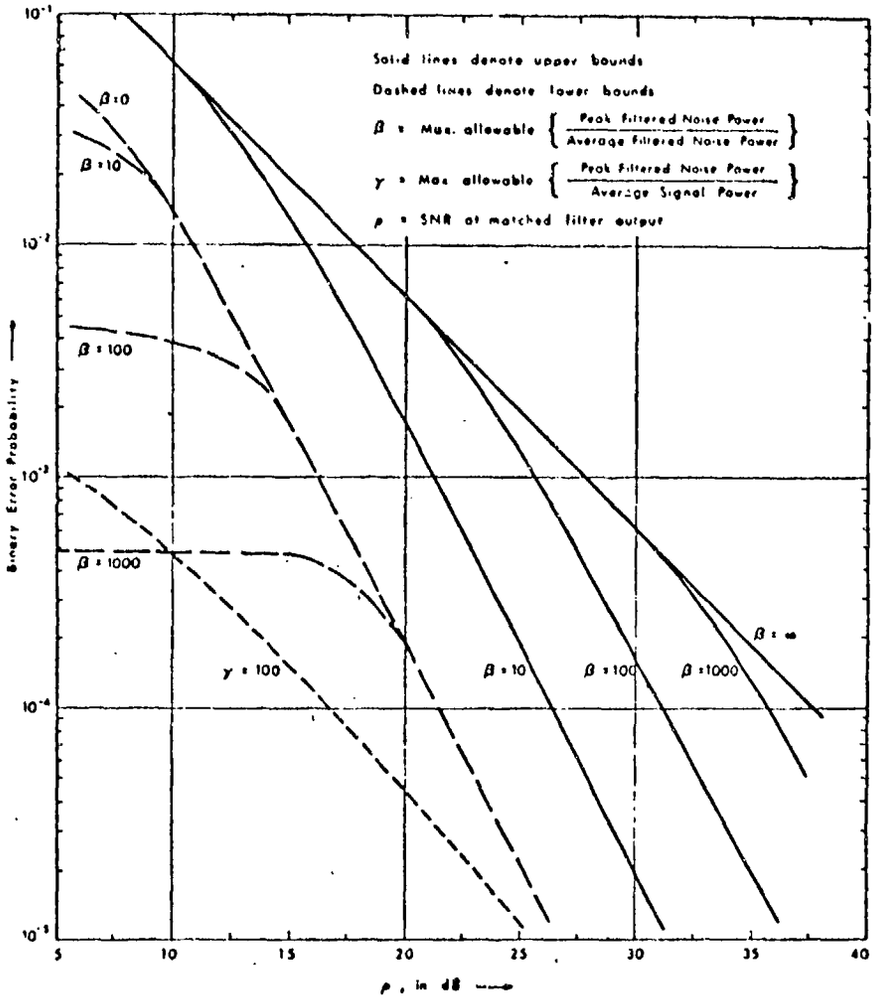

Figure 5.30 Error Probability Bounds for Binary FSK as a Function of Matched Filter Output SNR. Dual Diversity with Square Law Combining. (From Ref. [5.17])

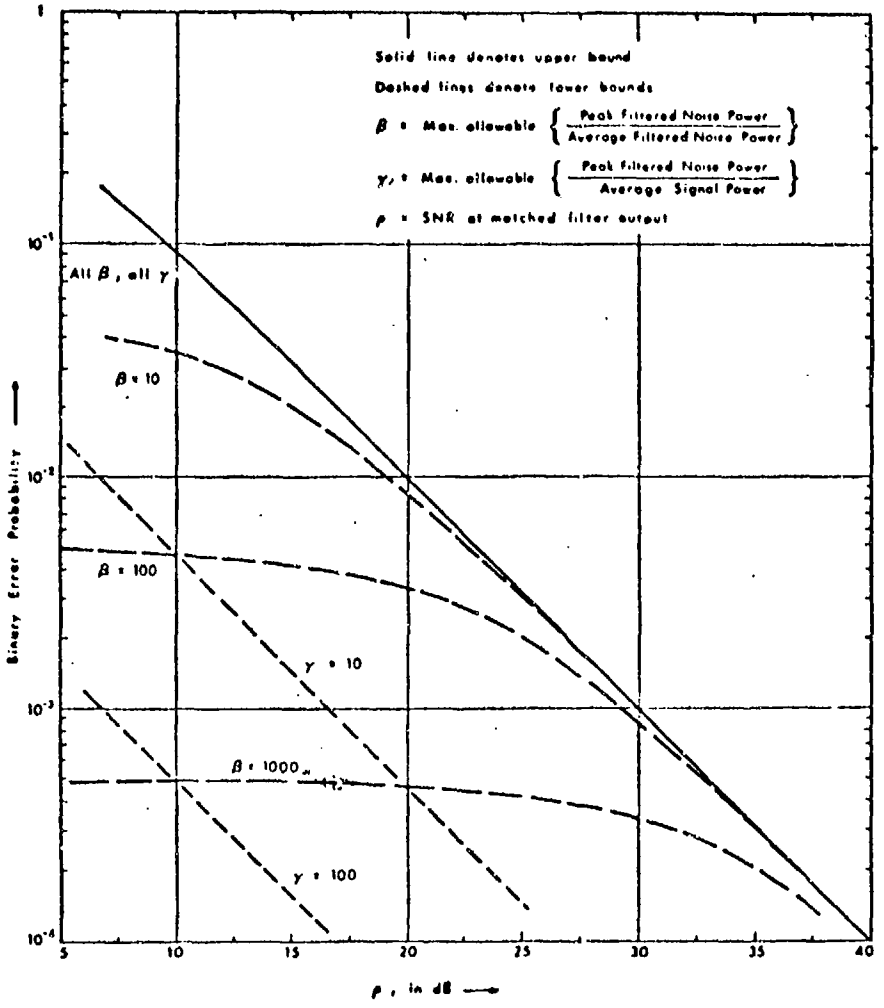

Figure 5.31 Error Probability Bounds for Binary FSK as a Function of Matched Filter Output SNR. Nondiversity Operation.

of the processing operation is given in Figure 5.32. The interference measurements are just those discussed earlier in Section 4.5. The measurements of the mean value of the magnitude-squared transfer functions can be obtained through use of the estimation schemes utilizing received data only, as discussed earlier in Section 4.1 or, alternatively, can be obtained by making use of the special probing signals discussed in Section 6. The exact details of the manner in which this latter measurement is obtained will not be of large importance in the following discussion.

As illustrated in Figure 5.32, the estimates p_L^{max} and p_L^{min} are determined by processing $\hat{\alpha}_L$, $\hat{\beta}_L$, and $\widehat{|G|^2}$. The estimates are used in different ways; $\hat{\alpha}_L$ and $\widehat{|G|^2}$ are used to estimate the signal-to-noise ratio, ρ. This, of course, specifies the point at which the function forms in (5.212) - (5.220) must be calculated. The estimate of β_L enters as a parameter affecting both the value of the bound and also the interval (and corresponding functional form) that must be used; e.g., see the first line of Eq. (5.212). The numerical processing, of course, just refers to numerical implementation of the results presented in Section 5.7.1.

Finally, we point out that the emphasis in the remainder of this section is on examining the feasibility of developing error bounds from interference measurements. It is not necessarily true that the analytical bounds presented in Section 5.7.1 constitute the best approach to the problem from the viewpoint of utilizing interference measurements. One reason for this relates to difficulties associated with estimating the interference maximum (crest factor) as discussed in Section 4.5. It would seem that alternative approaches to the general problem of bounding error rate could yield bounding curves that make more effective use of the interference measurements. An alternative approach that does not make use of the crest factor constraint is discussed in Section 5.7.3.

5.7.2.2 Bound Errors Arising from Errors in Interference Measurement

We now examine the way that the error bounds, discussed in Section 5.7.1 and illustrated in Figures 5.29 - 5.31, are affected by errors in the interference measurements. As a first step in this direction, we concentrate on determining the error in the signal-to-noise ratio measurement.

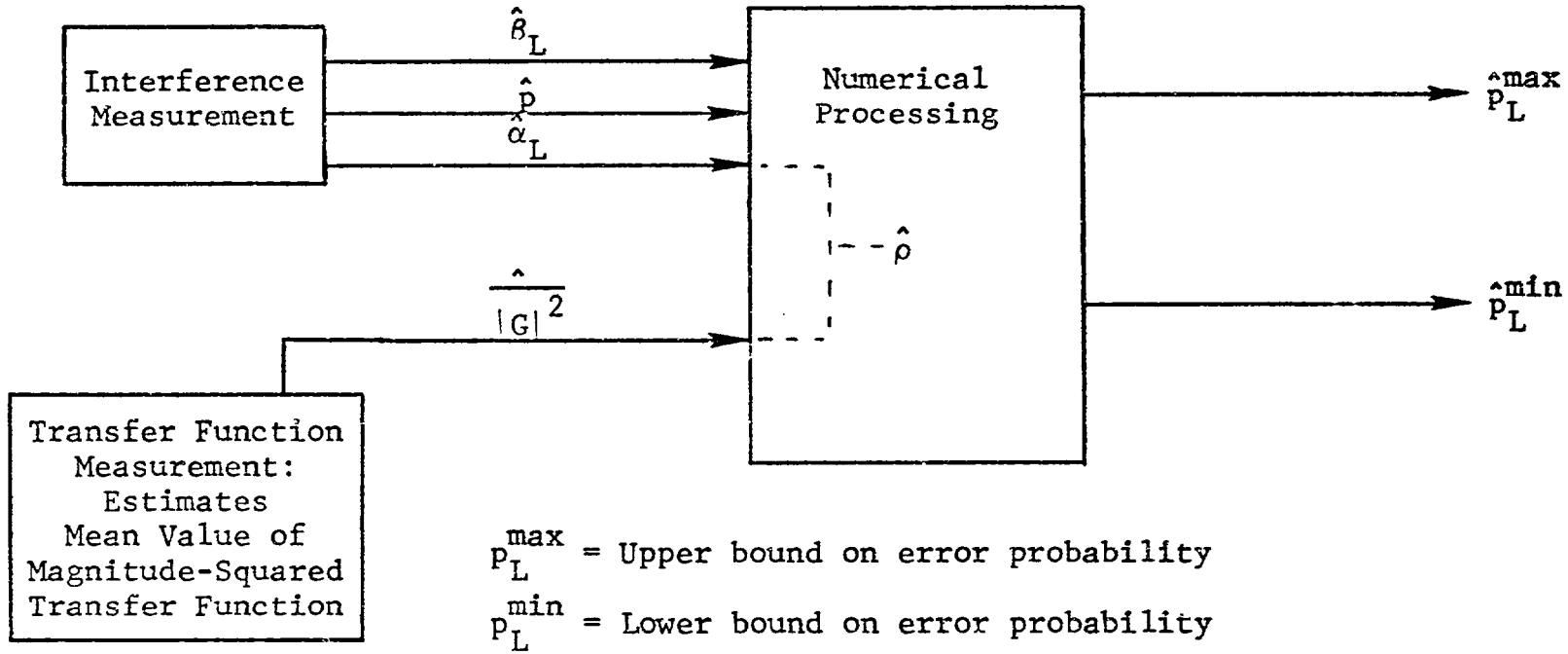

p_L^{max} = Upper bound on error probability

p_L^{min} = Lower bound on error probability

α_L = Mean value of interference

p = Probability U exceeds U'

β_L = Crest factor of interference

$\overline{|G|^2}$ = Mean value of magnitude squared of channel transfer function multiplied by T^2

ρ = Signal-to-noise ratio

Figure 5.32 Schematic for Estimating Bounds on Probability of Error

The problem of determining the degree of accuracy attainable in estimating the signal-to-noise ratio, ρ, is central to evaluating any schemes that use interference measurements to develop error rate bounds. The reliability of the signal-to-noise ratio estimate depends, of course, on the accuracy attained in estimating the mean values of the channel and interference parameters in (5.202). The assumption of identical statistics for G on each diversity branch implies that

$$\sum_{k=1}^{L} \overline{|G_k|^2} = 2\left[\frac{1}{2} L \overline{|G|^2}\right] \tag{5.221}$$

It was the assumption of identical interference statistics on each diversity branch that led to

$$\rho = \frac{2\left[L\frac{1}{2}\overline{|G|^2}\right]}{\alpha_L} \tag{5.222}$$

and finally the normalization

$$\frac{1}{2}|G|^2 = 1 \tag{5.223}$$

that led to the right-hand side of (5.202).

Here, we note from the discussion of generalized noise variables in Section 4.5 that

$$G = g(0)\,T \tag{5.224}$$

where the received signal is given by

$$y(t) = g(t)\,s(t) + n(t) \tag{5.225}$$

where g(t) just represents the time-varying complex gain, i.e., the channel transfer function. Thus,

$$\overline{|G|^2} = T^2 \overline{|g(t)|^2} \tag{5.226}$$

and its estimate is given by

$$\hat{\overline{|G|^2}} = T^2 \overline{|g(t)|^2} (1+\epsilon_T) \tag{5.22}$$

$$= \overline{|G|^2} (1+\epsilon_T) \tag{5.227}$$

where ϵ_T just represents the error in estimating the mean-squared value of the channel transfer function. This error has been discussed at great length in Section 4.1 and elsewhere in this report. Finally, using the normalization in (5.223) and the expression for ρ in (5.222), we obtain as our estimate for ρ

$$\hat{\rho} = \frac{2L}{\hat{\alpha}_L} \frac{1}{2} \hat{\overline{|G|^2}}$$

$$= \frac{2L}{\hat{\alpha}_L} (1+\epsilon_T) \tag{5.228}$$

It is convenient to define fractional errors for ρ and α and to denote them ϵ_ρ and ϵ_α, respectively. These random variables are defined according to

$$\hat{\rho} = \rho(1+\epsilon_\rho) = \frac{2L}{\alpha_L} (1+\epsilon_\rho) \tag{5.229}$$

and

$$\hat{\alpha} = \alpha(1+\epsilon_\alpha) \tag{5.230}$$

Now, substituting (5.230) in (5.228) and comparing the result with (5.229), we obtain the fractional error

$$\epsilon_\rho = \frac{\epsilon_T - \epsilon_\alpha}{1 + \epsilon_\alpha} \tag{5.231}$$

for the signal-to-noise ratio.

The other major factor on which the expressions for probability of error bounds in (5.212) and (5.213) depends is the crest factor β_L. Estimates of this quantity are formed from estimates of α_L and U_{max}, the maximum value of U, as discussed in Section 6. In fact, we recall from (4.532) that β_L has the form

$$\beta_L \stackrel{\Delta}{=} \text{Max}\left\{\frac{\text{Peak U}}{\alpha_L}\right\} \tag{5.232}$$

Defining a normalized error ϵ_β for the β_L estimate, we have

$$\hat{\beta}_L = \beta_L(1 + \epsilon_\beta) \tag{5.233}$$

and for the normalized error in estimating U_{max}

$$\hat{U}_{max} = U_{max}(1 + \epsilon_u) \tag{5.234}$$

The $\hat{\beta}_L$ estimate is obtained numerically by dividing the U_{max} estimate by the α_L estimate, i.e.,

$$\hat{\beta}_L = \frac{\hat{U}_{max}}{\hat{\alpha}_L} \tag{5.235}$$

Hence, using (5.230), (5.234), and (5.235), we obtain

$$\epsilon_\beta = \frac{\epsilon_u - \epsilon_\alpha}{1 + \epsilon_\alpha} \tag{5.236}$$

Thus, in (5.231) and (5.236) we have, respectively, expressions for the fractional measurement errors in measuring the signal-to-noise ratio, ρ, and the crest factor, β_L.

In order to focus on a goal for the calculations, we will concentrate on the reliability with which the upper bounds in (5.212) can be determined from the measurements. We note that the results that will be obtained cannot differ much from those that would follow from a similar analysis applied to (5.213); in fact, the fractional measurement error in determining p_L^{Max} and p_L^{max} is exactly the same for the "middle range" of ρ values. For the other ranges, the results would be similar because of the very similar smooth behavior of $H_L(x)$ and $G_L(x)$. For the lower bound, the situation is not as clearcut. This is due to the complexity of the expressions in (5.218). We point out, however, from Figures 5.42 - 5.45, that the slope of the lower bound is nowhere steeper than it is for the upper bound. This is a rough indication that sensitivity to errors in the ρ estimate will be less than, or comparable with, that for the upper bound. We also point out that the absolute errors, all other things being equal, will be less for the lower bound than the higher.

We now turn to direct calculation of the error in setting the bounds. We first deal with the interval $\rho \geq L\beta_L/\mu_L$. For these large ρ values, we make use of the Taylor's expansion of $H_L(x)$ about $x = 0$:

$$H_L(x) = \frac{1}{2}x^L \frac{1}{L!} - \frac{1}{2}x^{L+1}\frac{L}{(L+1)!} + \ldots. \qquad (5.237)$$

Utilizing this approximation, we obtain

$$p_L^{Max} \approx \frac{1}{\rho^L} \frac{L^{L-1}\beta_L^{L-1}}{(L-1)!} \qquad (5.238)$$

Now, using the estimates in (5.229) and (5.233) to form an estimate of p_L^{Max} at these larger ρ values, we obtain

$$\hat{p}_L^{Max} = \frac{1}{\rho^L} \frac{L^{L-1}\beta_L^{L-1}}{(L-1)!} \quad f(\epsilon_\beta, \epsilon_\rho) \tag{5.239}$$

where

$$f(\epsilon_\beta, \epsilon_\rho) = \frac{(1+\epsilon_\beta)^{L-1}}{(1+\epsilon_\rho)^L} \tag{5.240}$$

A Taylor's expansion of this function about $\epsilon_\beta = 0$ and $\epsilon_\rho = 0$ gives to first order the result

$$f(\epsilon_\beta, \epsilon_\rho) \approx 1 + (L-1)\epsilon_\beta - L\epsilon_\rho \tag{5.241}$$

Thus, the upper bound on probability of error has the form

$$\hat{p}_L^{Max} \approx p_L^{max}(1+\epsilon_1) \tag{5.242}$$

where the fractional error is given by

$$\epsilon_1 = (L-1)\epsilon_\beta - L\epsilon_\rho \tag{5.243}$$

With the totally reasonable assumption that the $\hat{\beta}$ and ρ measurements are weakly correlated, we obtain finally as the mean-squared squared fractional error the result

$$\overline{\epsilon_1^2} \lessapprox L^2\left(\overline{\epsilon_\beta^2} + \overline{\epsilon_\rho^2}\right) \tag{5.244}$$

For the "middle range" of ρ values, $(2L/\mu_L) \le \rho \le L\beta_L/\mu_L$, we note that the upper bound probability of error has the general form

$$\hat{p}_L^{Max} = \text{const}(2L/\hat{\rho}) \tag{5.245}$$

This is also true for the middle range in (5.213).

Writing

$$\hat{p}^{Max} = p^{Max}(1+\epsilon_2) \tag{5.246}$$

it is a simple matter to determine that

$$\overline{\epsilon_2^2} \approx \overline{\epsilon_\rho^2} \tag{5.247}$$

We now turn to the range of ρ consisting of the smallest values of of ρ, $2/\gamma_L \leq \rho \leq 2L/\mu_L$, we form [see (5.212)] the estimate

$$\hat{p}_L^{Max} = H_L\left[\frac{2L}{\rho(1+\epsilon_\rho)}\right] \tag{5.248}$$

With a Taylor's expansion with respect to ϵ_ρ, we obtain

$$\hat{p}_L^{Max} = H_L\left(\frac{2L}{\rho}\right)\left[1 - \left(\frac{2L}{\rho}\right)\frac{1}{H_L\left(\frac{2L}{\rho}\right)}\frac{dH_L}{dx}\left(\frac{2L}{\rho}\right)\epsilon_\rho\right] \tag{5.249}$$

The largest value of ρ in the interval of concern is $2L/\mu_L$. At this value of ρ, the factor

$$E(\rho) = \left(\frac{2L}{\rho}\right)\frac{1}{H_L\left(\frac{2L}{\rho}\right)}\frac{dH_L}{dx}\left(\frac{2L}{\rho}\right) \tag{5.250}$$

takes on unity value (by definition of μ_L); it is smaller for all other values of ρ. It follows immediately from the representation

$$\hat{p}_L^{Max} = p_L^{Max}(1+\epsilon_3) \tag{5.251}$$

that

$$\overline{\epsilon_3^2} \approx \overline{\epsilon_\rho^2}$$

is a "worst-case" approximation for the mean-squared fractional error.

From (5.231) and (5.236) we now utilize the reasonable approximations

$$\overline{\epsilon_\rho^2} \approx \overline{\epsilon_T^2} + \overline{\epsilon_\alpha^2} \tag{5.252}$$

$$\overline{\epsilon_\beta^2} \approx \overline{\epsilon_u^2} + \overline{\epsilon_\alpha^2} \tag{5.253}$$

This allows us to represent our present results in terms of the results derived earlier in Section 4.5. We obtain

$$\begin{aligned} \overline{\epsilon^2} &\approx L^2\left(\overline{\epsilon_T^2} + \overline{\epsilon_u^2} + 2\,\overline{\epsilon_\alpha^2}\right) && \rho \geq L\beta_L/\mu_L \\ &\approx \overline{\epsilon_T^2} + \overline{\epsilon_\alpha^2} && (2L/\mu_L) \leq \rho \leq L\beta_L/\mu_L \\ &\approx \overline{\epsilon_T^2} + \overline{\epsilon_\alpha^2} && 2/\gamma_L \leq \rho \leq 2L/\mu_L \end{aligned} \tag{5.254}$$

It is clear that accurate measurements of the interference mean and maximum values in combination with accurate measurements of the channel transfer function magnitude-squared value can lead to accurate determinations of the bounding curves for error rate. To give a practical feel for the effect of the measurement errors on the bounding curve, we have included in the upper left-hand corner of Figure 5.33 a plot of the 95% confidence limit versus rms fractional error in estimating the bounding probability. Also shown in this figure are the 95% confidence limits for the pulse noise jamming signal discussed in Section 4.5. It is reasonable to expect for the naturally occurring types of interference, that considerable improvement could be obtained.

Finally, we point out that the confidence limits at the break points cannot be determined exactly by analytical means. It is safe to assume, however, that the largest of the confidence limits on either side of a juncture apply over a small region about the juncture; the width of this region depends, of course, on the accuracy with which the signal-to-noise ratio can be estimated.

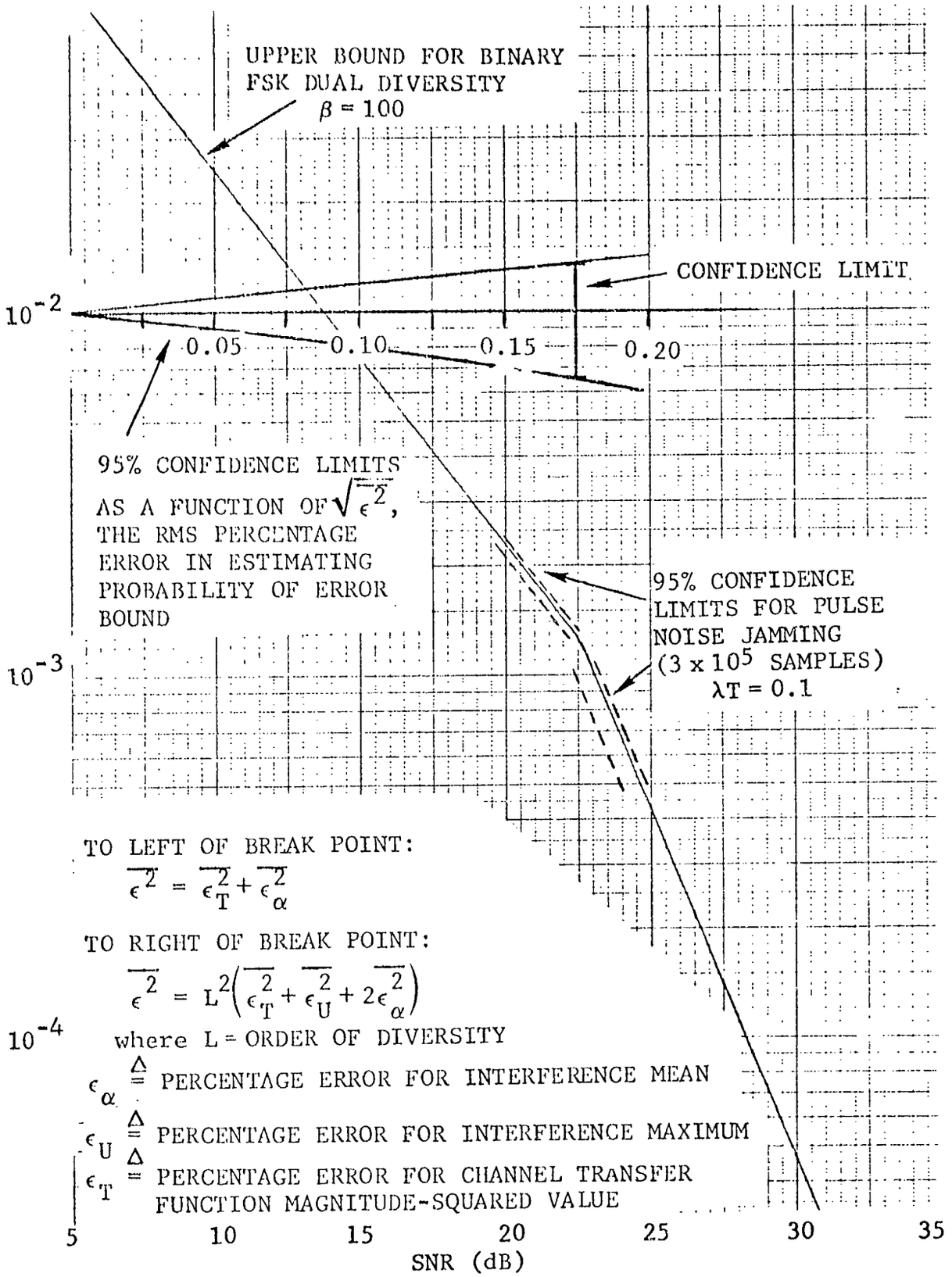

Figure 5.33 Confidence Limits (95%) for Error Probability Bounding Curves

5.7.3 An Alternative Approach

5.7.3.1 Introduction

Though estimates of β_L and α_L can be used with reasonable accuracy to develop error rate bounds by using the functional relations in Section 5.7.1, it is not necessarily true that the relations in Section 5.7.1 make the most effective use of the interference measurements. One of the major difficulties with the earlier computational scheme was that it required estimates of the probability density function maximum. Depending on the amount by which the pdf tapers off at higher values, the occurrence of a value close to the maximum can be a very low probability event. This problem was discussed earlier in connection with the work of Section 4.5. The use of the measurement maximum, as a constraint for the extremization problem, was discussed in Section 5.7.1. Here we discuss the use of a different constraint. Within a reasonable range of operational choices, this new constraint relates to events of higher probability than was the previous case.

We also note, for schemes aimed at measuring U_{max}, that there is really no way of knowing how accurate the measurements are without some a priori knowledge of the probability density function. Without some other supporting measurements, the operator of the system is to some extent working in the dark; he has no knowledge of the quality of the measurements, nor how much more time would be required to obtain more reliable measurements. This is in contrast with the simple scheme for obtaining probability estimates discussed in Section 4.5.4.3. We recall that the scheme presented there had as its goal the measurement of the probability, p, that the generalized noise variable, U, exceeds some fixed threshold, U'. The rms fractional error was given by

$$\sqrt{\overline{\epsilon_p^2}} = \sqrt{\frac{1}{M}\left(\frac{1-p}{p}\right)} \qquad (5.255)$$

We see that the measurement $\hat{p}$ itself provides some information about the number of samples required to obtain a prescribed accuracy in measurement. This leaves the operator some options, either increasing M or decreasing the threshold, U', thus increasing p and decreasing the error in (5.255).

The extra flexibility discussed above, in conjunction with the superior convergence of the p estimate (as compared to the

U_{max} estimate) motivates the use of the p measurement to develop bounds on error rate for various communication systems.

5.7.3.2 Bounds on Error Rate: Problem Statement

As pointed out in Section 5.7.1, the problem of bounding probability of error, in its most general context, is framed in terms of the integral

$$p_L = \int_0^{\hat{A}_L} F_L(A)\, H_L(A)\, dA \tag{5.256}$$

which is a precise expression for probability of error under the mutually exclusive interference condition, $UV = 0$, and in terms of the integral

$$p_L = \int_0^{\hat{U}_L} W_L(U)\, G_L(U)\, dU \tag{5.257}$$

which is the precise expression for probability of error under the identical interference condition, $U = V$. In both of these expressions, $\hat{A}_L$ and $\hat{U}_L$ are appropriately determined upper limits to be discussed below. In the first integral, A is just the arithmetic mean of U and V. In both of the integrals, $H_L(x)$ and $G_L(x)$ are the known functions given earlier in Eqs. (5.200) and (5.201), respectively, and $F_L(x)$ and $W_L(x)$ are the unknown probability density functions. Were these to be known exactly, or exactly measurable, the problem would stop here; p_L in (5.256) could provide the upper bound on the error rate, and p_L in (5.257) the lower.* In the absence of such complete statistical information, one can only develop error bounds by maximizing the integral in (5.256) and minimizing the integral in (5.257). When this approach is taken, the incomplete statistical information available from the measurements plays the important role of constraining the extremal values that either integral can take on.

As in Section 5.7.1, the first of these constraints will be on α_L, the average value of the interference variable. The second

*Actually, a single integral may be sufficient in some situations (see Section 5.7.1), in which case error rate would be known exactly.

will be on p, the probability that the interference variable exceeds some fixed threshold value. This differs from the "crest factor" constraint used in Section 5.7.1, but the work of Section 4.5 indicates that it can be more rapidly and reliably measured. The detailed forms of the new set of constraints will be presented below in Sections 5.7.3.3 and 5.7.3.4, where we use them to bound probability of error for nondiversity operation.

To determine the upper limits of integration in (5.256) and (5.257), we make use of the factor, γ_L. Recall, from Section 5.7.1, that this just puts an upper limit on the ratio of peak noise power to average signal power and arises because of the dynamic limitations of receivers; their outputs saturate when the input voltage sufficiently exceeds the average signal power for which the receiver was designed. Thus, from (5.204), we have

$$\hat{A}_L = L\gamma_L \qquad (UV = 0) \tag{5.258}$$

and

$$\hat{U}_L = 2L\gamma_L \tag{5.259}$$

In a similar vein, a probability constraint on U given by

$$p = \Pr\left\{U > \beta'\hat{U}_L\right\} \tag{5.260}$$

where β' is some number between 0 and 1, is exactly equivalent to the probability of the event $\left\{2A > \beta'\hat{U}_L\right\}$ in the mutually exclusive interference case, UV = 0. Hence, for the integrals in (5.256) and (5.257), the probability constraints will take the form

$$p = \Pr\left\{A > \beta' L\gamma_L\right\} \qquad UV = 0 \tag{5.261}$$

and

$$p = \Pr\left\{U > \beta' 2L\gamma_L\right\} \tag{5.262}$$

We close this introductory section by demonstrating that the p constraints in (5.261) and (5.262) automatically place a constraint

on α and, hence, the signal-to-noise ratio. In fact, from (5.259) we have immediately

$$\alpha_L = \bar{U} < 2L\gamma_L \tag{5.263}$$

Because of the special constraints here, however, this is not the tightest upper bound on α_L. The tightest bound will be determined below. First, however, we treat the simpler problem of determining the greatest lower bound. Utilizing the following integral forms for these constraints

$$\alpha_L \triangleq \int_0^{2L\gamma_L} U\, W_L(U)\, dU \tag{5.264}$$

$$p \triangleq \int_{2\beta'\gamma_L}^{2L\gamma_L} W_L(U)\, dU \tag{5.265}$$

and making the change of variable

$$z = \frac{U}{2L\gamma_L} \tag{5.266}$$

in (5.264) we have

$$\begin{aligned} \alpha_L &= (2L\gamma_L)^2 \int_0^1 z\, W_L(2L\gamma_L z)\, dz \\ &\geq (2L\gamma_L)^2 \beta' \int_{\beta'}^1 W_L(2L\gamma_L z)\, dz \end{aligned} \tag{5.267}$$

We note that equality is possible with an impulsive pdf. Hence this is the greatest lower bound on α_L. By making the same change of variables in (5.265), the lower bound in (5.267) can be simplified. We obtain

$$\alpha_L \geq (2L\gamma_L)\, \beta' p \tag{5.268}$$

Now, we find the largest possible value of α_L subject to the representations in (5.264) and (5.265) and the additional obvious constraint

$$1 = \int_0^{2L\gamma_L} W_L(U)\, dU \tag{5.269}$$

To do this, we make use of the cumulative distribution, $C_L(x)$, where

$$C_L(x) = \int_0^x W_L(U)\, dU \tag{5.270}$$

We note immediately from (5.269) and (5.265) that

$$C_L(2L\gamma_L) = 1 \tag{5.271}$$

and

$$C_L(2\beta' L\gamma_L) = 1 - p \tag{5.272}$$

Integrating α_L in (5.264) by parts

$$\alpha_L = 2L\gamma_L - \int_0^{2L\gamma_L} C_L(U)\, dU \tag{5.273}$$

it becomes clear that we need only minimize the integral in (5.273). Because of the fact that $C_L(x)$ may be zero until $x = 2\beta' L\gamma_L$, but then must jump to the value $1 - p$, we note that

$$\text{Min} \int_0^{2L\gamma_L} C_L(x)\, dx = \text{Min} \int_{2\beta' L\gamma_L}^{2L\gamma_L} C_L(x)\, dx \tag{5.274}$$

which, because of the fact that $C_L(x)$ is monotonically non-decreasing, has the value

$$\text{Min} \int_{2\beta' L\gamma_L}^{2L\gamma_L} C_L(x)\,dx = (1-p)\,2L\gamma_L(1-\beta') \tag{5.275}$$

Combining with (5.273) we have finally that

$$(2L\gamma_L)\,\beta' p \le \alpha_L \le (2L\gamma_L)\,[1 - (1-p)(1-\beta')] \tag{5.276}$$

In terms of the signal-to-noise ratio, this restriction takes the form

$$\frac{1}{\gamma_L[1 - (1-p)(1-\beta')]} \le \rho \le \frac{1}{\gamma_L \beta' p} \tag{5.277}$$

For decreasing β' and p, the range of possible ρ values is translated to higher values as one would expect.

5.7.3.3 Error Rate Bounds: Analysis and Numerical Results

In this section we develop the analysis leading to error rate bounds for nondiversity operation and present the results of the numerical calculations. Though only the results for nondiversity operation are presented herein, we point out that an examination of the earlier results (utilizing different constraints) and the analytical procedures indicates that the bounds for diversity operation would be even tighter than those presented here; this is especially true in the case of the upper bound.

We first deal with the problem of determining the upper bound on probability of error. In keeping with the comments accompanying (5.256), we attempt, through proper choice of $F_1(A)$, to maximize the probability of error integral

$$p_1 = \int_0^{\gamma_1} F_1(A)\,H_1(A)\,dA \tag{5.278}$$

subject to the constraints

$$\alpha_1 = \int_0^{\gamma_1} A\, F_1(A)\, dA \tag{5.279}$$

and

$$p = \int_{\beta'\gamma_1}^{\gamma_1} F_1(A)\, dA \qquad 0 < \beta' < 1 \tag{5.280}$$

and to the additional obvious constraint that the candidate pdf integrate to 1. Applying the completeness theorem in [5.17] separately to each of the intervals $(0, \beta'\gamma_1)$ and $(\beta'\gamma_1, \gamma_1)$, we find that a general form for the maximizing pdf is

$$F_1^{Max}(A) = q_1 \delta(A - A_1) + q_2 \delta(A - A_2) \tag{5.281}$$

where $A_1 < \beta'\gamma$, and $A_2 \geq \beta'\gamma_1$. We note that this candidate pdf has the four unspecified parameters, q_1, A_1, q_2, and A_2. Obviously,

$$q_1 + q_2 = 1 \tag{5.282}$$

whereas application of the constraint on α_1 in (5.279) gives

$$\alpha_1 = q_1 A_1 + q_2 A_2 \tag{5.283}$$

and application of the p constraint in (5.280) just indicates that $q_2 = p$, so that now the candidate pdf has just one unspecified parameter, A_1; i.e.,

$$F_1^{Max}(A) = (1 - p)\, \delta(A - A_1) + p\, \delta(A - A_2) \tag{5.284}$$

where

$$A_2 = \frac{\alpha_1 - (1 - p)A_1}{p} \tag{5.285}$$

Thus, the probability of error

$$p_1^{Max} = (1 - p)\, H_1(A_1) + p\, H_1(A_2) \tag{5.286}$$

must be maximized with respect to the unspecified parameter A_1. To accomplish this, we note that

$$\frac{d\, p_1^{Max}}{d\, A_1} = \frac{1}{2}(1 - p)\left[e^{-A_1} - e^{-A_2}\right] \tag{5.287}$$

and that the second derivative is negative throughout the interval (a consequence of the fact that $A_2 > A_1$). It is immediately apparent from (5.287) that p_1^{Max} is maximized at $A_1 = A_2$. Thus, from (5.285) we determine that the maximum occurs at $A_1 = \alpha_1$; the upper bound on probability of error has the value

$$p_1^{Max} = H_1(\alpha_1) \tag{5.288}$$

This is the same as the upper bound determined under the earlier constraint problem [see (5.220)].

We now turn to the problem of determining the lower bound on the probability of error. In keeping with the comments accompanying (5.257), we attempt through proper choice of $W_1(A)$, to minimize the probability of error integral

$$p_1 = \int_0^{2\gamma_1} W_1(U)\, G_1(U)\, dU \tag{5.289}$$

subject to the constraints

$$\alpha_1 = \int_0^{2\gamma_1} U\, W_1(U)\, dU \tag{5.290}$$

and

$$p = \int_{2\beta'\gamma_1}^{2\gamma_1} W_1(U)\, dU \tag{5.291}$$

and, as before, the obvious restriction that the pdf integrate to 1. Applying the completeness theorem, we have as a general form for the minimizing pdf

$$W_1^{min}(U) = q_1\delta(U) + q_2\delta(U - 2\beta'\gamma_1) + q_3\delta(U - U_1) \quad (5.292)$$

which has the four unspecified parameters, q_1, q_2, q_3, and U_1. Obviously,

$$q_1 + q_2 + q_3 = 1 \quad (5.293)$$

whereas application of the constraint on α_1 in (5.290) gives

$$\alpha_1 = q_2(2\beta'\gamma_1) + q_3U \quad (5.294)$$

and application of the probability constraint in (5.291) gives the result

$$p = q_2 + q_3 \quad (5.295)$$

Solving these three equations, we obtain the results

$$q_1 = 1 - p \quad (5.296)$$

$$q_2 = \frac{pU_1 - \alpha_1}{U_1 - 2\beta'\gamma_1} \quad (5.297)$$

$$q_3 = \frac{\alpha_1 - (2\beta'\gamma_1)p}{U_1 - 2\beta'\gamma_1} \quad (5.298)$$

This procedure leaves one degree of freedom through dependence on the variable U_1. We now minimize

$$p_1^{\min} = \left[\frac{p\,U_1 - \alpha_1}{U_1 - 2\beta'\gamma_1}\right] G_1(2\beta'\gamma_1) + \left[\frac{\alpha_1 - (2\beta'\gamma_1)\,p}{U_1 - 2\beta'\gamma_1}\right] G_1(U_1) \qquad (5.299)$$

with respect to U_1. This is best accomplished by first rearranging the terms in (5.299). We obtain

$$p_1^{\min} = p\left[\frac{U_1 G_1(2\beta'\gamma_1) - (2\beta'\gamma_1)G_1(U_1)}{U_1 - 2\beta'\gamma_1}\right]_1 + \alpha_1\left[\frac{G_1(U_1) - G_1(2\beta'\gamma_1)}{U_1 - 2\beta'\gamma_1}\right]_2 \qquad (5.300)$$

Since $G_1(U)$ is everywhere concave downward, a simple graphical construction indicates clearly that the second bracketed term in (5.300) is minimized at $U_1 = 2\gamma_1$. Evaluating the derivative of the first term, we obtain

$$\frac{d[\cdot]_1}{dU_1} = -\frac{2\beta'\gamma_1}{(U_1 - 2\beta'\gamma_1)}\left[G'(U_1) + \frac{G(U_1) - G(2\beta'\gamma_1)}{U_1 - 2\beta'\gamma_1}\right] \qquad (5.301)$$

which, because U_1 is greater than $2\beta\gamma_1$, indicates that the first term in (5.300) is minimized at $U_1 = 2\gamma_1$, and q_1, q_2, and q_3 in (5.296) through (5.298) take on the values

$$q_1 = 1 - p \qquad (5.302)$$

$$q_2 = \frac{(2\gamma_1)p - \alpha_1}{2\gamma_1(1 - \beta')} \qquad (5.303)$$

$$q_3 = \frac{\alpha_1 - (2\beta'\gamma_1)\,p}{2\gamma_1(1 - \beta')} \qquad (5.304)$$

Turning now to the dependence on α_1, we note from (5.276) that α_1 is restricted because of the constraints to values satisfying

$$\alpha_1 \geq (2\gamma_1\beta') p \tag{5.305}$$

Hence, there is no value of α_1 that allows q_3 in (5.298) to take on negative values. The situation is not as simple in the case of the second impulse which vanishes as α_1 reaches and exceeds $(2\gamma_1)p$. In this case, the only way that the constraints can be satisfied, especially the requirement for larger α_1, is that the lower impulse begins to move to the right. The minimizing pdf now has the form

$$W^{min}(U) = (1 - p)\,\delta(U - U') + p\,\delta(U - 2\gamma_1) \tag{5.306}$$

where the impulse strengths follow directly from the probability constraint and the requirement that the pdf integrate to 1. Applying the constraint on α_1, it is easy to see that

$$U' = \frac{\alpha_1 - p(2\gamma_1)}{1 - p} \tag{5.307}$$

and, hence, that

$$p_1^{min} = (1 - p)\,G_1\left(\frac{\alpha_1 - p(2\gamma_1)}{1 - p}\right) + p\,G_1(2\gamma_1)$$

$$\alpha_1 > 2\gamma_1 p \tag{5.308}$$

It would seem at first glance that the behavior of (5.308) at values of U' in excess of $2\beta'\gamma$ would require separate consideration; this is because both impulses would fall in the region $(2\beta'\gamma_1, 2\gamma_1)$ over which the integral defining the probability constraint takes place. We note, however, that a value of U' exceeding $2\beta'\gamma$ implies, from (5.307), a value of α_1 satisfying

$$\alpha_1 > p(2\gamma_1) + 2\beta'(1 - p)\gamma_1 \tag{5.309}$$

which can be rearranged to take the form

$$\alpha_1 > 2\gamma_1[1 - (1-p)(1-\beta')] \tag{5.310}$$

This places α_1 outside of the range of possible α_1 values given in (5.276). Thus, the lower bound on probability of error has been determined for all possible values of α_1.

Recalling from (5.202) that

$$\rho = 2/\alpha_1 \tag{5.311}$$

we summarize the above results in terms of the signal-to-noise ratio:

$$p_1^{Max} = H_1\left(\frac{2}{\rho}\right) \tag{5.312}$$

$$p_1^{min} = (1-p)\, G_1\left(\frac{\frac{2}{\rho} - 2p\gamma_1}{1-p}\right) + p\, G_1(2\gamma_1)$$

$$\frac{1}{\gamma_1[1 - (1-p)(1-\beta')]} < \rho < \frac{1}{\gamma_1 p} \tag{5.313}$$

$$p_1^{min} = \left[\frac{\gamma_1 p - \frac{1}{\rho}}{\gamma_1(1-\beta')}\right] G_1(2\beta'\gamma_1) + \left[\frac{\frac{1}{\rho} - \beta'\gamma_1 p}{\gamma_1(1-\beta')}\right] G_1(2\gamma_1)$$

$$\frac{1}{\gamma_1 p} < \rho < \frac{1}{\beta'\gamma_1 p} \tag{5.314}$$

Probability of error bounding curves determined from numerical calculation of these expressions are shown in Figures 5.34 - 5.37. The curves shown hold exactly for the binary FSK case but from the discussion in Section 5.7.1 can be thought of as worst-case curve both in terms of probability of error and tightness of bounds.

The first three curves are for increasing values of p, $p = 0.001$, $p = 0.01$, and $p = 0.5$, and various values of threshold β'. The increasing values of p imply increasing values of percentage measurement error of p, as discussed in Section 5.7.3.1. These

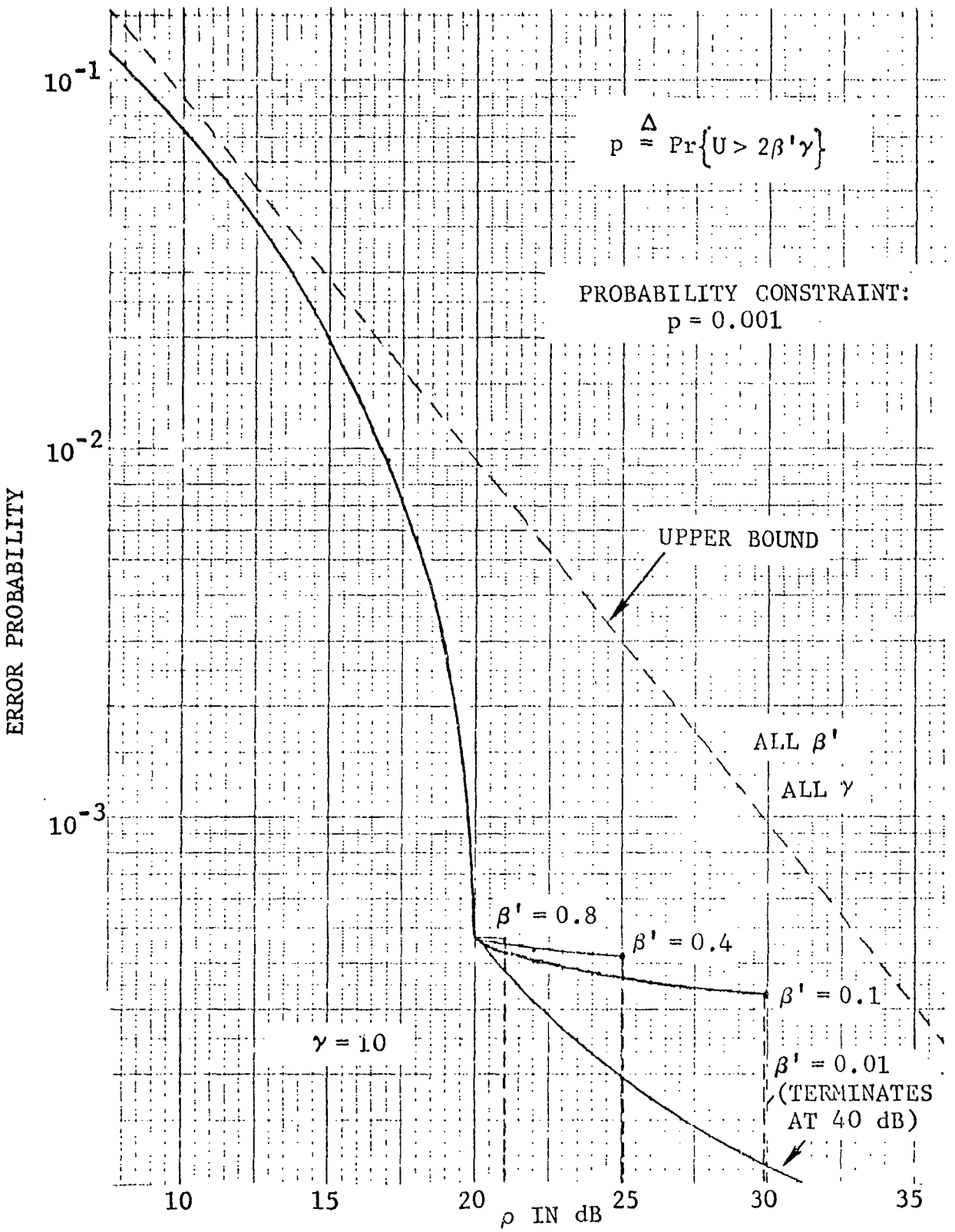

Figure 5.34 Error Probability Bounds for Binary FSK as a Function of Matched Filter Output SNR for Nondiversity Operation ($p = 0.001$, $\gamma = 10$)

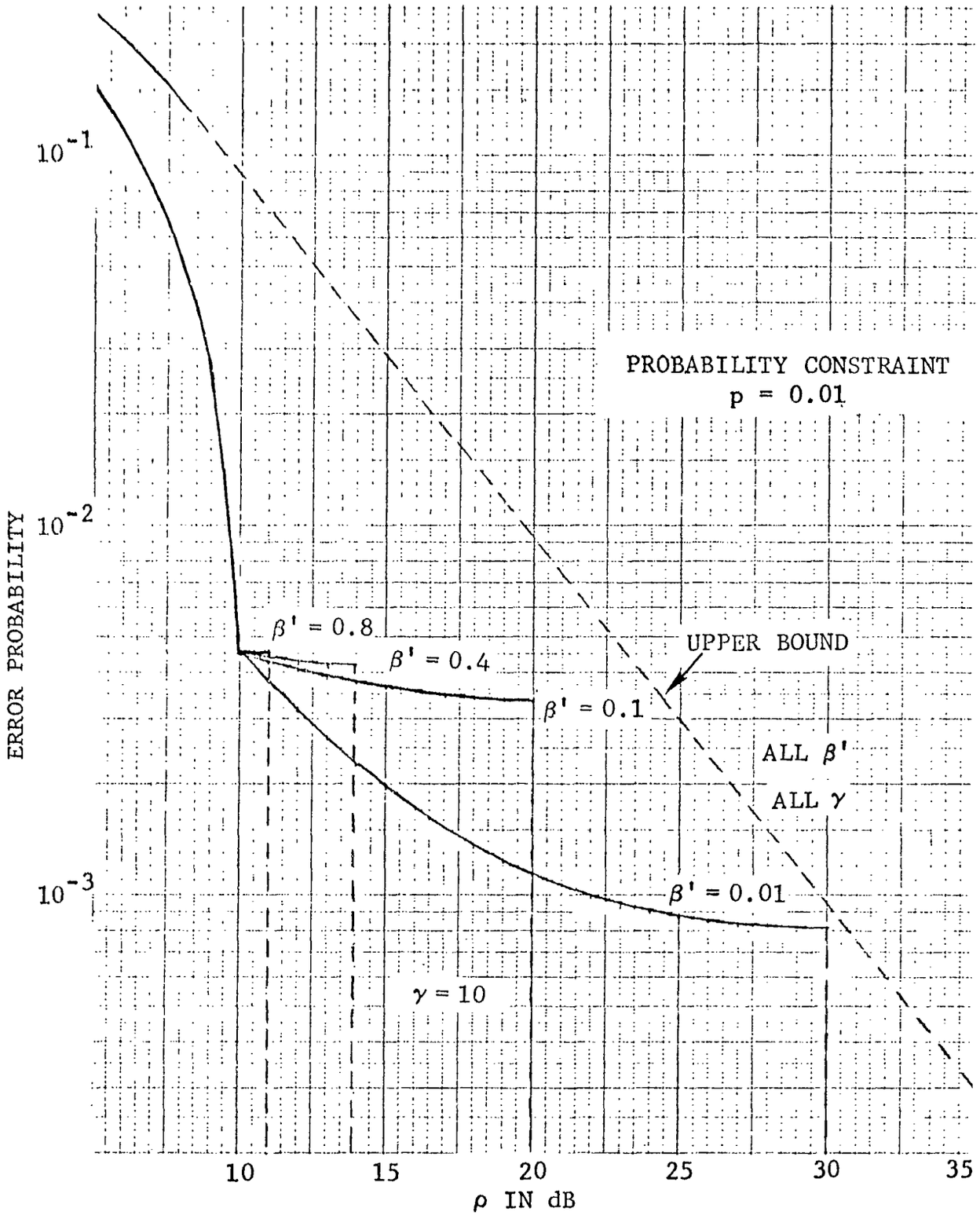

Figure 5.35 Error Probability Bounds for Binary FSK as a Function of Matched Filter Output SNR for Nondiversity Operation (p = 0.01, $\gamma = 10$)

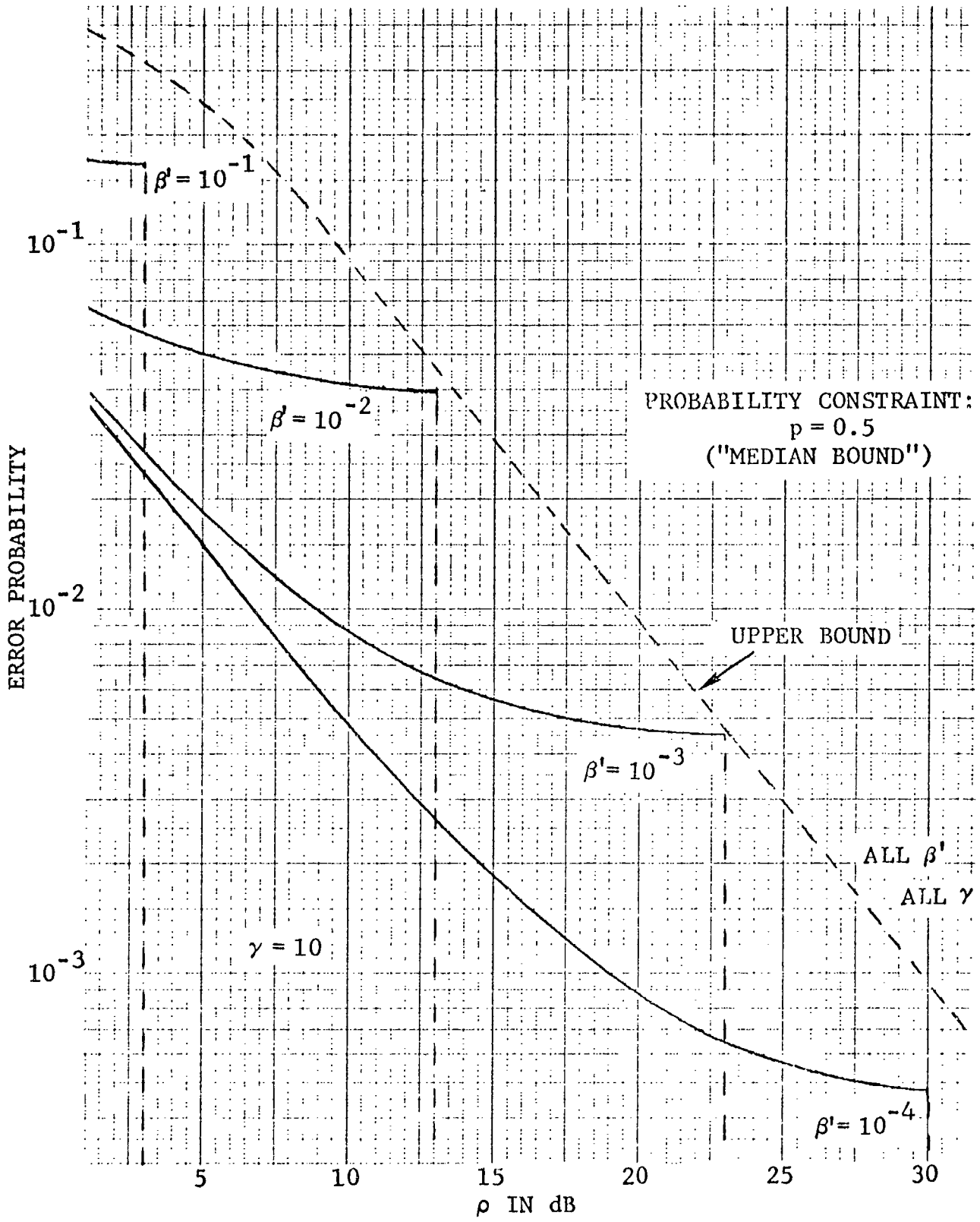

Figure 5.36 Error Probability Bounds for Binary FSK as a Function of Matched Filter Output SNR for Nondiversity Operation (p = 0.5, γ = 10 - "Median Bound")

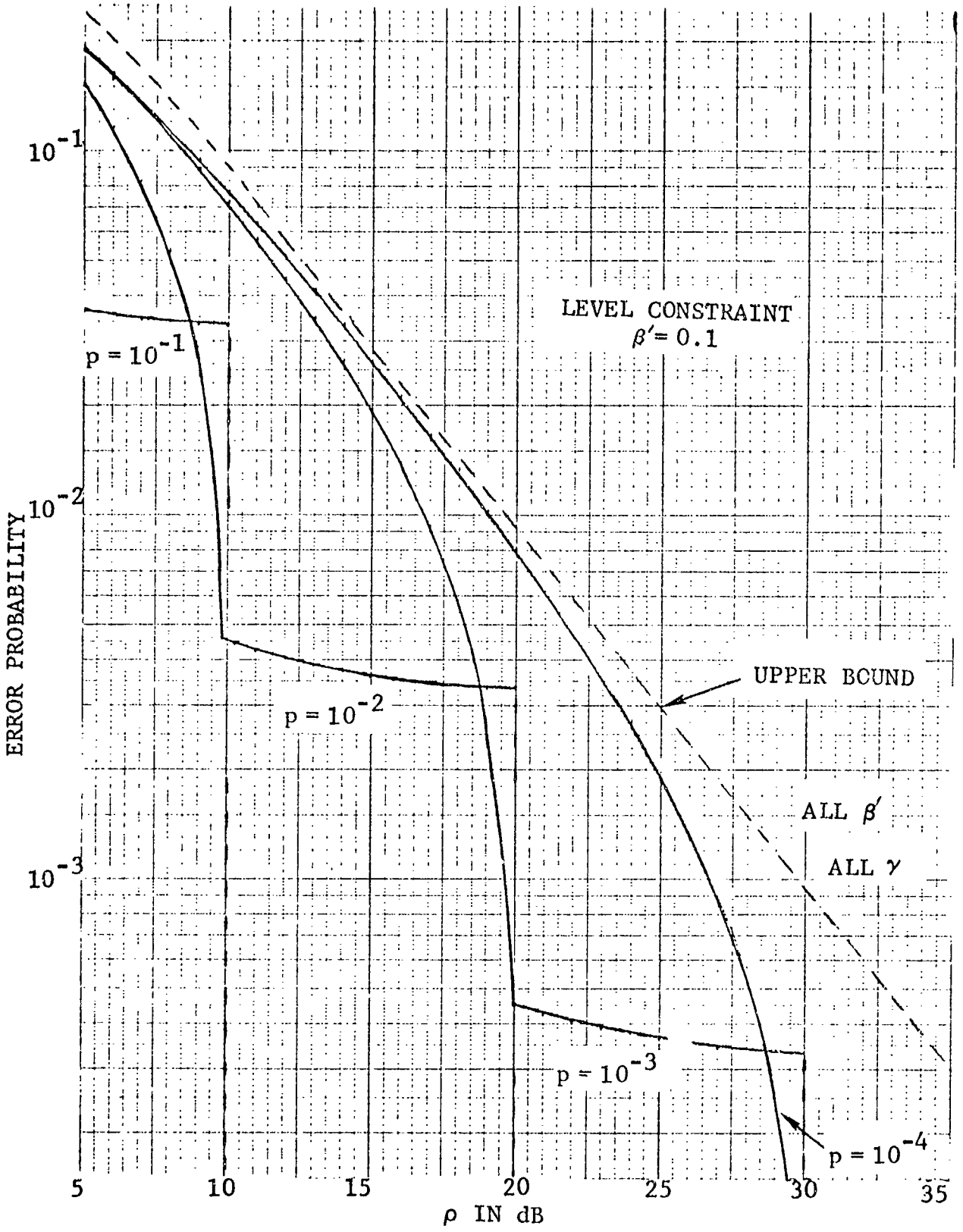

Figure 5.37 Error Probability Bounds for Binary FSK as a Function of Matched Filter Output SNR for Nondiversity Operation ($\beta' = 0.1$, $\gamma = 10$)

have, respectively, the approximate values $\sqrt{1000/M}$, $\sqrt{100/M}$, and $\sqrt{1/M}$ (exact), where M is the number of independent samples, as discussed in Section 4.5.4.3.

In each of these curves, the breakpoint [see (5.313) and (5.314)] occurs at $1/\gamma_1 p$ which is too far to the left to be illustrated in Figure 5.36.

In Figure 5.37, the curves are plotted for fixed β and various P.

These curves indicate clearly that measurements of the probability with which the noise variables exceed some threshold can be used to develop bounding curves for probability of error. The measurements are easy to obtain and with suitable operational choices can be obtained with high accuracy.

With a greater number of thresholds, the measurements would correspond to a simple histogram, and there is no doubt that one could develop considerably tighter bounds.

5.7.4 Summary

In this section we discussed the way in which the interference measurements, covered earlier in Section 4.5, can be used to develop bounds on the probability of error. To accomplish this, we drew heavily on results published earlier in [5.17]. The way in in which the error rate and the error rate bounds are related to the measurements was discussed in Section 5.7.1. In this section, we demonstrated how the probability of error integrals can be extremized by applying constraints on average interference power and on the interference crest factor. The fact that these constraints can lead to tight bounds on error probability was evidenced by the curves presented in Figures 5.29 - 5.31 which were taken from [5.17]. In Section 5.7.2 we discussed the accuracy with which the error rate bounds can be determined from the interference measurements; as one would expect, the errors in developing the bounding curves depend in direct fashion on the errors in the measurement of the interference mean value, maximum value, and on the error in estimating the mean-squared value of the channel transfer function. The relationship between the rms errors in estimating these quantities and in estimating the bound values was given in Section 5.7.2.2 [see (5.254)] and illustrated in Figure 5.33. It is clear from the work of this section that reliable interference measurements can lead to reliable bounds on error probability.

In Section 5.7.3 we tried an alternate approach to the problem of developing bounds on probability of error. This approach made use of estimates of p, the probability that the interference variable U exceeds some fixed threshold U' (see Section 4.5.4.4).

Thus, the measurements, in effect, make up a simple two bin histogram for the interference. It seems reasonable to expect that variants of this approach could be used to bound error probability when histograms with a higher number of bins are available. Although the accuracy of determining the bounds was not investigated as thoroughly as that determined earlier, the indication in Section 4.5.4.4 that p can be measured reliably indicates also that the bounds can be estimated reliably.

REFERENCES FOR SECTION 5

[5.1] M. Schwartz, W. R. Bennett, and S. Stein, Communication Systems and Techniques, McGraw-Hill, New York (1966).

[5.2] P. A. Bello, et al., "Modeling and Data Analysis - Short and Medium Range Digital Troposcatter Tests," Signatron, Inc., Final Technical Report, RADC-TR-69-233, Vol. 1 (October 1969). (AD862767)

[5.3] J. N. Pierce and S. Stein, "Multiple Diversity with Non-independent Fading," Proc. IRE, Vol. 48, pp. 89-104 (January 1960).

[5.4] P. A. Bello and T. H. Crystal, "A Class of Efficient High-Speed Digital Modems for Troposcatter Links," IEEE Trans. on Comm. Tech., COM-17, pp. 162-183 (April 1969).

[5.5] P. A. Bello and B. D. Nelin, "The Effect of Frequency Selective Fading on Intermodulation Distortion and Subcarrier Phase Stability in Frequency Modulation Systems," IEEE Trans. on Comm. Systems, pp. 87-101 (March 1964).

[5.6] E. D. Sunde, "Intermodulation Distortion in Analog FM Troposcatter Systems," BSTJ, Vol 43, pp. 399-435 (January 1964).

[5.7] C. D. Beach and J. M. Trecker, "A Method for Predicting Interchannel Modulation Distortion due to Multipath Propagation in FM and PM Tropospheric Radio Systems," BSTJ, Vol. 42, p. 1 (January 1963).

[5.8] S. O. Rice, "Noise in FM Receivers," Proc. of the Symposium on Time Series Analysis, Brown University, John Wiley and Sons, New York (1962) p. 395.

[5.9] P. A. Bello, L. Ehrman, and T. Crystal, "Troposcatter Multichannel Digital Systems Study," RADC-TR-67-218 (May 1967). (AD817211)

[5.10] G. D. Forney, "Maximum Likelihood Sequence Estimation of Digital Sequences in the Presence of Intersymbol Interference," IEEE Trans. on Inf. Theory, Vol. IT-18 (May 1972).

[5.11] P. Monsen, "Digital Transmission Performance on Fading Dispersive Channels," IEEE Trans. on Communications, Vol. COM-21, No. 1 (January 1973).

[5.12] P. A. Bello, "Time-Frequency Duality," IEEE Trans. on Information Theory, pp. 18-33 (January 1964).

[5.13] P. A. Bello, "Characterization of Randomly Time-Variant Linear Channels," IEEE Trans. on Comm. Systems, pp. 360-373 (December 1963).

[5.14] P. A. Bello, "A Troposcatter Channel Model," IEEE Trans. on Comm. Tech., Vol. COM-17, pp. 130-137 (April 1969).

[5.15] H. G. Booker and W. E. Gordon, "A Theory of Radio Scattering in the Troposphere," Proc. IRE, Vol. 38, pp. 401-412 (April 1950).

[5.16] P. L. Rice, et al., "Transmission Loss Predictions for Tropospheric Communications Circuits," National Bureau of Standards, Tech. Note 101 (Revised), Vols. I and II (1 May 1966).

[5.17] P. A. Bello, "Bounds on the Error Probability of FSK and PSK Receivers Due to Non-Gaussian Noise in Fading Channels," IEEE Trans. on Information Theory, pp. 315-316 (July 1966).

SECTION 6

TECHNIQUES UTILIZING SPECIAL PROBING SIGNALS

The previous sections have been concerned with the area of main interest to the present study, the in-service estimation of modem performance based upon propagation medium limitations alone (i.e., assuming a well-functioning modem) without the use of special probing signals. A number of concepts were developed and analyzed yielding a number of techniques of wide applicability. However, there are cases where special probing signals are needed for the most reliable performance estimation. Thus, in the case of LOS channels where deep fades can sometimes be highly frequency-selective, the complex transfer function $T(f,t)$ is needed to estimate the performance of conventional suboptimum modems which do not attempt maximum likelihood demodulation.

It is not possible to estimate a fading dispersive channel's delay power spectrum $Q(\xi)$ from $|T(f,t)|^2$. The most accurate prediction of irreducible error rate for time-gated and anti-multipath troposcatter modems is with the use of $Q(\xi)$. The measurement of $Q(\xi)$ requires the use of special probing signals if processing is to take place at RF or IF.

The HF channel was found to be the most difficult to estimate modem performance using the techniques of the previous sections. Special probing signals could reduce estimation error.

The signal distortion properties of the channel are sometimes characterized by measurements at three levels of decreasing knowledge:

1) Measurement of system functions (e.g., time-variant transfer function and impulse response).

2) Measurement of correlation functions of system functions (e.g., frequency correlation function, delay power spectrum, etc.).

3) Measurement of gross parameters of system function (e.g., coherence bandwidth, Doppler spread, etc.).

We consider each of these in order.

6.1 Out-of-Service Measurement

Here we assume that service has been interrupted and it is desired to measure the channel characteristics.

6.1.1 System Function Measurement

The problem of probing and measuring system functions for time-variant channels has been studied extensively by Bello and Esposito [6.1], Bello [6.2],[6.3], and Bello and Pinto [6.4].

It has been found that for well-designed signal processing, the accuracy in measurement of the system functions is essentially invariant to the technique used. The system function channel measurement technique used most often is the cross-correlation technique employing a periodic probing signal containing a pseudo-noise sequence of $\pm 180^{\circ}$ modulating a carrier. A simplified block diagram of the receiver processing is shown in Figure 6.1. The received multipath-distorted PN waveform is mixed with a set of delayed replicas of the transmitted sequence to extract samples of the channel's complex time-variant impulse response at the outputs of the lowpass filters. The filters have passbands flat over the spectrum occupied by the fading channel, i.e., the "total" Doppler spread.

If $z(t)$ denotes the complex envelope of the transmitted probing signal, $g(t,\xi)$ the complex envelope of the impulse response of the channel, and $\eta(t)$ the complex envelope of the received additive noise, then the received probing signal is given by

$$w(t) = \int z(t-\xi)\, g(t,\xi)\, d\xi + \eta(t) \tag{6.1}$$

The cross-correlation operation to produce a (time-varying) sample of the impulse response at $\xi = \tau$, $\hat{g}(t,\tau)$, is given by

$$\hat{g}(t,\tau) = [w(t)z^*(t-\tau)] \otimes k(t) \tag{6.2}$$

where $k(t)$ is the impulse response of the lowpass filter. For this discussion, four assumptions will be made:

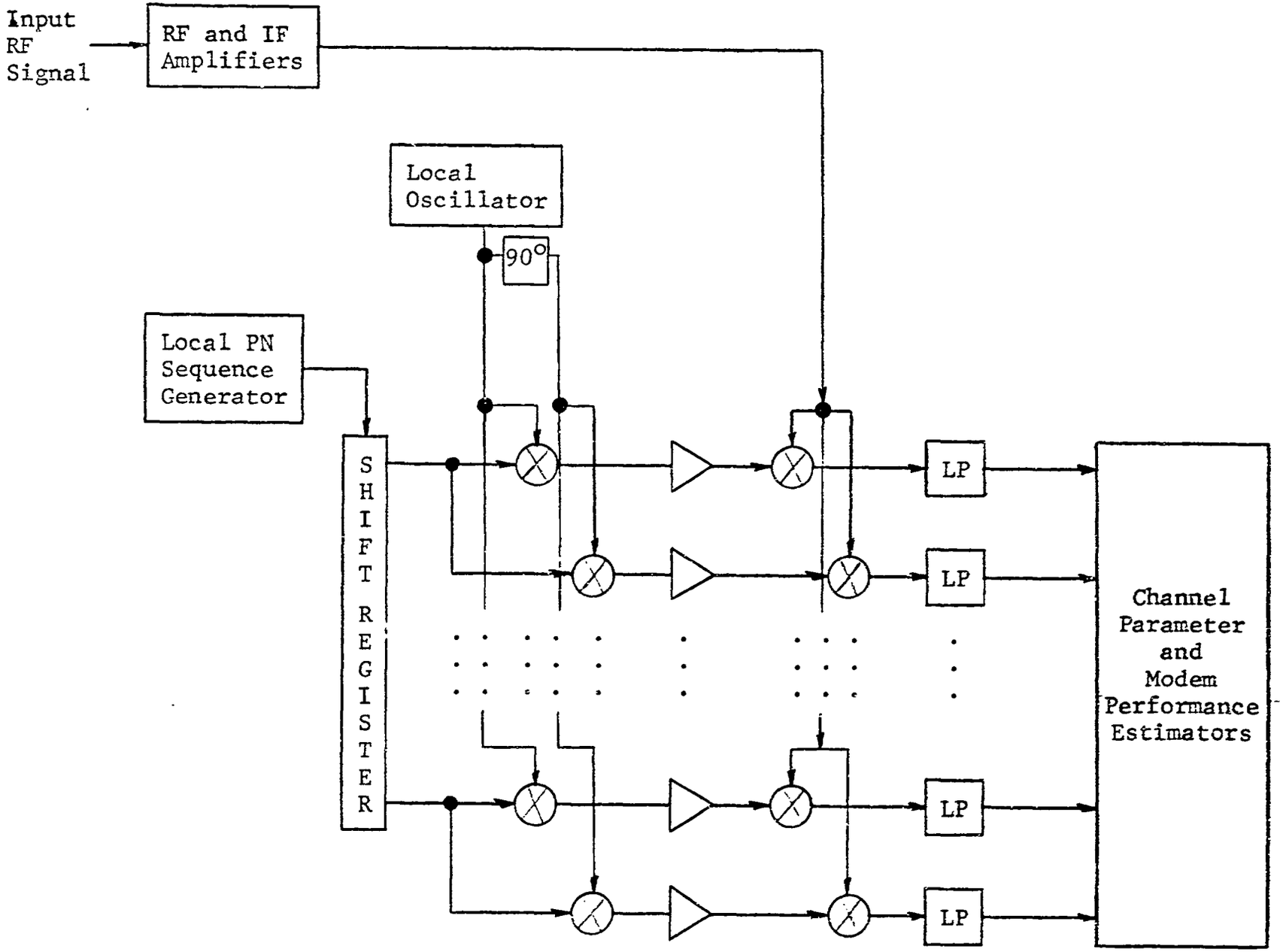

Figure 6.1 Simplified Block Diagram for Correlation Technique of Impulse Response Measurement

1) The probing signal power spectrum is flat over W, the bandwidth of the channel that it is desired to characterize.

2) The lowpass filter k(t) is nondistorting to the time-variant impulse response sample fluctuation. This means that the nondistorting bandwidth of k(t) is equal to or greater than the total Doppler spread of the channel, B_{tot}.

3) The bandwidth W is much bigger than B_{tot}.

4) The product $B_{tot}L \gg 1$, where L is the duration of the channel impulse response.

Assumptions 3) and 4) are valid for the channels under discussion. Assumptions 1) and 2) are convenient for analysis although not optimum for minimizing the estimation error due to the combined effects of additive noise and distortion. However, it will be seen below that by comparison with the incoherent probing techniques of the previous sections, the output additive noise is very much smaller so that we may be more generous here in allowing some extra noise through, to essentially remove distortion effects.

With the above assumptions, the estimated impulse response becomes

$$\hat{g}(t,\tau) = \int C_z(\tau - \xi)\, g(t,\xi)d\xi + \eta(t,\tau) \qquad (6.3)$$

where $C_z(\tau)$ is the autocorrelation function of the probing signal, and $\eta(t,\tau)$ is a noise (in effect a "noise channel") with power spectral shape (for fixed τ) proportional to $|K(f)|^2$.

All radios have filters at the transmitter and receiver which limit bandwidth. These may be defined to be part of the channel to be probed or not, depending upon the objectives of the probing. In either case, the probing signal would be designed to have a flat spectrum over the band of interest and

$$h(t,\tau) = \int C_z(\tau - \xi)\, g(t,\xi)d\xi \qquad (6.4)$$

would be the desired impulse response.

It may be shown from the referenced work by Bello that, for a dispersive channel with delay power spectrum $Q(\xi)$, the strength of the desired term to the estimation mean-squared error is is

$$\rho_{out} \approx \rho_{in} \frac{1}{B_K} \frac{Q(\tau)}{\int Q(\xi)d\xi} \tag{6.5}$$

where ρ_{in} is the input SNR measured in the bandwidth of the received signal. For a uniform delay power spectrum of width L, (6.5) becomes

$$\rho_{out} \approx \rho_{in} \frac{1}{B_K L} \tag{6.6}$$

Since B_K can be set close to B_{tot}, the total Doppler spread of the channel, and since

$$s \equiv B_{tot} L \ll 1 \tag{6.7}$$

for the channels of interest, we see that excellent measurement accuracy can be obtained with out-of-service probing because the communication system is normally designed so that ρ_{in} is $\gg 1$.

6.1.2 Correlation Function and Gross Parameter Measurement

Since, on an out-of-service basis, the system function can be measured with high accuracy for the channels of interest, the only significant contribution to the estimation error for measurement of a channel correlation function will be the channel fluctuations which must be averaged out. One may show that the rms fractional estimation error σ always takes the form

$$\delta \approx \frac{1}{\sqrt{K}} \tag{6.8}$$

where K is an effective number of independent samples of the channel during the averaging time. This may be equated approximately to the product of the observation time and the rms Doppler spread of the channel. Thus, for example, if it is desired to measure the delay power spectrum of a channel $Q(\xi)$, the rms

estimation error due to channel fluctuations can be expected to be

$$\sigma(\xi) \approx \frac{Q(\xi)}{\sqrt{K}} \tag{6.9}$$

Of course, if it is desired to measure $Q(\xi)$ where it is very small, errors due to the additive noise would have to be considered. From (6.5) - (6.7) we see that as long as

$$\frac{Q(\xi)}{Q_{max}} >> \frac{s}{\rho_{in}} \tag{6.10}$$

the noise effects may be disregarded.

The same three classes of techniques may be used for gross channel parameter measurement with special probing signals as were discussed in Section 4 for the received signal probe case. In the present case, coherent processing techniques may be used for the differentiation and level crossing approaches, and an improved correlation function estimate may be used in the correlation technique. Moreover, in addition to rms Doppler spread, a mean Doppler shift may be measured. We briefly consider these measurement techniques.

If a carrier is transmitted, the received process when referenced to the carrier frequency has the spectrum P(f). It is convenient to deal with the complex envelope of this received process z(t), which has just this low-frequency spectrum P(f). In [6.1] it is shown that the Doppler spread parameter B is given by the following operations on z(t):

$$B = \frac{1}{\pi}\sqrt{\frac{\langle |\dot{z}|^2 \rangle}{\langle |z(t)|^2 \rangle} - \left|\frac{\langle z^*\dot{z} \rangle}{\langle |z(t)|^2 \rangle}\right|^2} \tag{6.11}$$

where the triangular brackets indicate time averages.

In actuality, the operations upon z in (6.11) would most likely be carried out by operating on the "in-phase" and "quadrature" components x(t) and y(t) related to z(t) by

$$z(t) = x(t) + jy(t) \tag{6.12}$$

It is shown by Bello [6.5] that in terms of x(t) and y(t), B is given by

$$B = \frac{1}{\pi}\sqrt{\frac{\langle(\dot{x})^2 + (\dot{y})^2\rangle}{\langle x^2 + y^2\rangle} - \left|\frac{\langle x\dot{y} - y\dot{x}\rangle}{\langle x^2 + y^2\rangle}\right|^2} \tag{6.13}$$

The in-phase and quadrature components (x,y) can be determined by multiplying the received carrier by both a local carrier and a 90° shifted local carrier at the same frequency as the received carrier (or as near to the same frequency as possible) and then extracting the low-frequency components. Strictly speaking, D is independent of mean Doppler shift, and thus precise knowledge of the received carrier frequency is not necessary. However, as the local carrier frequency departs from the received carrier frequency, the extracted x(t) and y(t) increase in bandwidth, necessitating larger bandwidth filters and passing more noise. Thus, from the point of view of maximizing signal-to-noise ratio, it is desirable to keep the local carrier frequency as near as possible to the received signal frequency. An estimate of the mean Doppler shift defined as the centroid of the power spectrum is provided by

$$\overline{f} = \frac{1}{2\pi} \cdot \frac{\langle x\dot{y} - y\dot{x}\rangle}{\langle x^2 + y^2\rangle} \tag{6.14}$$

In practice, the derivatives may be approximated by differences as was done for the envelope techniques in Section 4.

The measurement of multipath spread by differentiation techniques follows an approach which is, in principle, dual to that described above for Doppler spread, where the duality involves an interchange of the roles of time and frequency. The frequency derivatives would be approximated by differences between the complex amplitudes of two received tones judiciously spaced in frequency.

For the level crossing approach, we may show from the results of Rice [6.6] that the average number of times m the in-phase or

quadrature components of narrowband Guassian noise crosses zero is given identically by the rms Doppler spread, i.e.,

$$m = B \quad . \tag{6.15}$$

Thus, by counting zero crossings in some finite time interval, we obtain an estimate of the rms Doppler spread.

Also, in an exactly analogous fashion, $\hat{m}$, the number of times/hertz that the real (or imaginary) part of the channel transfer crosses zero is identically equal to the rms multipath spread L, i.e.,

$$\hat{m} = L \tag{6.16}$$

The correlation techniques for measurement of multipath and Doppler spread were discussed in Section 4. In that section, they were based upon the channel envelope-squared time or frequency correlation functions. Here the same procedure would be used but they would be based upon the correlation function of the real or imaginary parts of the transfer function.

The estimation errors for multipath and Doppler spread would also be dependent primarily on the number of independent channel samples in the averaging interval. The rms fractional error δ would vary as $1/\sqrt{K}$, i.e.,

$$\delta \approx \frac{A}{\sqrt{K}} \tag{6.17}$$

6.2 In-Service Measurement Techniques

The previous section considered various classes of channel measurement techniques utilized in the absence of data signal transmissions. Out-of-service operation is highly undesirable.

One may obtain channel measurement information utilizing probing signals in the same frequency band and during in-service operation by multiplexing the data signal and probing signal together. We may consider four basic multiplexing arrangements:

1) Data-probing time-division multiplex
2) Data-probing frequency-division multiplex
3) Data-probing FDM/TDM
4) Nonorthogonal multiplex

In each of these arrangements, the objective is to multiplex and demultiplex the data and probing signals on an essentially noninterfering basis. In the case of time-division-multiplex, probing signals are inserted in series with data signals. Note that the method of multiplexing incoming digital data can generally be independent of the way the probing and data signals are multiplexed together. Thus, the TDM (time-division-multiplex) of probing and data signals can occur with either FDM or TDM of data subchannels. Furthermore, the multiplexing of probing and digital data can occur at baseband, RF, or IF, yielding a large number of potential combinations to be examined.

The concepts of TDM, FDM, and TDM/FDM are best understood by imagining that the available time-frequency space (either at baseband, IF, or RF) is divided up into two mutually exclusive regions assigned to the probing signal and to the data signal. In order for there to be little loss in channel capacity, the percentage of time-frequency space devoted to probing signals must be a small fraction of the total available time-frequency space.

The first three techniques are orthogonal multiplexing arrangements. The last technique has the advantage of using no additional time-frequency space. However, it cannot always be used because of the mutual interference created. We explore this point for the use of an in-band wideband probing signal. There are two requirements for utilization of this technique:

1) The probing signal must be at a low level relative to the data signal at transmission, typically 20 dB or lower to avoid degrading the communications.
2) The processing gain of the probing signal demodulator must be high enough to overcome the large interfering data signal.

Generally speaking, the probing technique can be any wideband coherent processing technique which spreads the probing signal over time-frequency space. However, care must be exercised in selection of this technique to see that discrete spectral components are either low enough or properly placed so as not to produce a local region of low data/prober power density ratio. Presuming this care has been taken, we can estimate from Eqs. (6.5) - (6.7) what the relation between channel parameters must be to allow use of the nonorthogonal multiplexing technique for measuring channel system functions. In this equation, we interpret ρ_{in} as the ratio of prober power to data power, a value we have quoted as being desirably -20 dB or smaller. If we desire at least a 20-dB measurement SNR, ρ_{out}, then from Eqs. (6.6) and (6.7) we see that the spread factor

$$s \leq 10^{-4} \tag{6.18}$$

For troposcatter links, multipath spreads are not much bigger than 1 μs, while Doppler spreads range from a fraction of 1 Hz to 10 Hz. Thus, (6.18) will be well-satisfied for troposcatter links. In the case of microwave LOS links, s is even smaller, rarely exceeding 10^{-10} to 10^{-11}. Thus, LOS links are ideally suited for in-service probing. A similar calculation for ionospheric scintillation channels reveals these suitable also. For HF channels, multipath spreads are usually less than 2 ms and Doppler spreads less than 1 Hz. This yields $s = 2 \times 10^{-3}$ which violates (6.18). Thus, some difficulty may be anticipated in utilizing a low-level probing signal in parallel with data transmission for in-service probing on HF links. In the case of HF links which are SSB, however, one or more frequency slots are usually provided for pilot tones. These may be used for accurately measuring gross channel parameters and the complex transfer function at those frequencies.

From a complexity point of view, it would be best to effect in-service probing in a way that would involve least changes in existing equipment. The two techniques that make most sense from this point of view, when applicable, are nonorthogonal multiplex with low-level wideband probing signals and tones placed at the edge of or in the signal band. Of course, a series of tones placed across the band may be regarded as a wideband probing signal. We consider the applicability of these techniques for each channel.

In the case of HF channels, we have already pointed out that a low-level PN prober would not be satisfactory because the spread factor of the channel is too large. Since SSB with parallel subcarriers is used in HF, it is a simple matter to insert probing tones in place of data subcarriers. This would always be at the cost of reducing capacity, but frequently at least one tone is provided anyway for AFC.

For the other channels, transmission signals are constant envelope and nonlinear essentially hardlimiting power amplifiers are used. In this connection we note that if a low-level probing signal p(t) plus a constant envelope data signal $\exp[j\varphi(t)]$ are fed to a hard limiter, the output may be expressed in the form

$$\frac{e^{j\varphi(t)} + p(t)}{|e^{j\varphi(t)} + p(t)|} = e^{j\omega(t)} + \frac{1}{2}p(t) - \frac{1}{2}p^*(t)e^{j2\varphi(t)} + \ldots. \tag{6.19}$$

where the missing terms are of the order of p^2. By keeping the strength of p(t) 20 - 30 dB below the constant envelope data signal, the additional terms may usually be neglected. The only proviso is the possible creation of discrete frequency components which, although small, may fall on critical parts of the data signal structure. This possibility must be examined in each case.

Assuming that the other terms may be neglected, we see that the probing signal has been reduced 6 dB by the hard limiting and a spurious term comparable in strength to the probing signal has appeared. The spurious term will only be harmful to the channel measurement if $\exp[j2\varphi(t)]$ is not a broadband signal. To take an extreme case if the data signal is binary PSK, $\exp[j2\varphi(t)]$ would be a constant and the spurious signal would be the negative conjugate of the probing signal. Barring this special case, the spurious signal would be a wideband signal contributing much smaller data noise to the channel measurement than the data signal itself. In all cases of interest, the spurious signal produces no harm to the data signal demodulation because it is of the same strength as the output probing signal which is already at a very low level.

In view of the above, it would appear that either PN or parallel in-band probing is feasible for LOS and troposcatter links, the ultimate choice being cost.

For satellite ionospheric scintillation channels, multipath is not a factor of importance and a single low-level tone placed adjacent to the data signal can be used to characterize the channel.

6.3 Error Rate Estimation

The error rate estimation techniques discussed in Section 5 based upon processing the estimated values of the squared magnitude of the transfer function may obviously be used when the actual complex transfer function or impulse response is known. Moreover, the bias errors, which were especially troublesome for HF channels, will vanish and the variances of the estimation errors will reduce. The latter reduction will not be so dramatic as the reduction of biases because the unaveraged channel fluctuations usually represent the major source of estimation error variance.

Aside from the general benefits for HF channels, perhaps the biggest bonus comes from the improved ability to estimate the irreducible error probability produced by excessive multipath in high-speed troposcatter modems and the condition error probability due to deep frequency-selective fades on LOS links. Insufficient time was available to evaluate the effectiveness of such estimation techniques.

REFERENCES FOR SECTION 6

[6.1] P. Bello and R. Esposito, "Measurement Techniques for Time Varying Dispersive Channels," Alta Frequenza, Vol. XXXIX (1970).

[6.2] P. Bello, et al., "Impact of Aeronautical Channel on Modem Specifications," Final Report Phase I, by CNR, Inc., on Contract TSC-516-1, Dept. of Transp. Report No. FAA-RD-74-54 (March 1974).

[6.3] P. Bello, et al., "Line-of-Sight Wideband Propagation," Final Report by CNR, Inc., on Contract F30602-73-C-0013 (April 1973). (AD762939)

[6.4] R. Pinto and P. Bello, "HF Channel Measurement," Final Report by CNR, Inc., on Contract N00014-74-C-0048 (July 1974).

[6.5] P. A. Bello, "Some Techniques for the Instantaneous Real-Time Measurement of Multipath and Doppler Spread," IEEE Trans. on Comm. Tech., Vol. COM-13 (September 1965) pp. 285-292.

[6.6] S. O. Rice, "Statistical Properties of a Sine Wave Plus Random Noise," BSTJ, Vol. 27 (January 1948) Sections 7 and 8, pp. 30-43.

APPENDIX A

GROSS CHANNEL PARAMETER ESTIMATION FROM BIAS UNCORRECTED ESTIMATES

A.1 Introduction

In this appendix we address the problem of estimating gross channel parameters from bias uncorrected estimates of the magnitude squared of the channel transfer function. In particular, we will estimate the rms Doppler and multipath spreads using the differentiation technique considered in Section 4.3, and the mean SNR.

It will be shown that using bias uncorrected estimates does not appreciably affect the performance of these gross channel parameter estimators. Thus, the above gross channel parameters can be accurately estimated without bias correction, and then used to correct the bias in the magnitude-squared channel transfer function estimates.

When the bias of the magnitude squared of the channel transfer function estimate is not removed, this estimate can be expressed as (see Section 4.1)

$$|\tilde{T}(F,t_p)|^2 = |T(F,t_p)|^2(1+\epsilon_p) + \delta_p \tag{1}$$

where

$$\begin{aligned} E\{\epsilon_p\} &= -\alpha = -HL^2 - KB^2 \\ E\{\delta_p\} &= \alpha\, E\{|T(f,t)|^2\} + 2N_0/P_z(F) \\ \sigma^2_{\delta_p} &= \epsilon_S^2 E^2\{|T(f,t)|^2\} \\ \sigma^2_{\epsilon_p} &= \epsilon^2 \end{aligned} \tag{2}$$

In the above expressions, $|\tilde{T}(F,t_p)|^2$ is the estimate of the magnitude squared of the channel transfer function, $|T(F,t_p)|^2$ is its actual value, and ϵ and ϵ_S are given, respectively, by (4.57) and (4.100).

A.2 Estimation of the Mean SNR

The estimation of the mean SNR is performed by using the estimates of the magnitude squared of the channel transfer function to form estimates of the instantaneous SNR, which are then averaged to give the mean SNR estimate. We can define an instantaneous SNR by

$$\gamma(t_p) = \frac{P_z(F)}{2N_0} |T(F,t_p)|^2 \tag{3}$$

and a mean SNR by

$$\Gamma = E\{\gamma(t_p)\} \tag{4}$$

Using (1) we can estimate Γ by

$$\hat{\Gamma} = \frac{P_z(F)}{2N_0} \frac{1}{K} \sum_{p=1}^{K} \left[|T(F,t_p)|^2 (1+\epsilon_p) + \delta_p \right] \tag{5}$$

Averaging over the errors and the channel fluctuations gives

$$E\{\hat{\Gamma}\} = \Gamma + 1 \tag{6}$$

where the estimation errors, ϵ_p and δ_p, were assumed to be independent of the channel fluctuations.

Therefore, no correcting for the bias in estimating $|T(F,t_p)|^2$ produces a bias in estimating Γ. However, since this bias is a known constant, it can be corrected.

The second moment of the mean SNR estimate is given by

$$E\{\hat{\Gamma}^2\} = E\left\{ \left[\frac{P_z(F)}{2N_0} \right]^2 \frac{1}{K^2} \sum_{p=1}^{K} \sum_{q=1}^{K} \left[|T(F,t_p)|^2 (1+\epsilon_p) + \delta_p \right] \cdot \left[|T(F,t_p)|^2 (1+\epsilon_q) + \delta_q \right] \right\} \tag{7}$$

After some simplification, we can express $E\{\hat{\Gamma}^2\}$ by (where a complex Gaussian scatter channel is assumed)

$$E\{\hat{\Gamma}^2\} = \frac{1}{K} 2\Gamma^2 \left[(1-\alpha)^2 + \epsilon^2 + \frac{\epsilon_S^2}{2}\right] + (\alpha\Gamma+1)^2 + 2\Gamma(1-\alpha)(\alpha\Gamma+1)$$

$$+ \frac{(1-\alpha)^2\Gamma^2}{K^2} \sum_{\substack{p=1 \\ p\neq q}}^{K} \sum_{q=1}^{K} (1+\rho_{pq})^2 \tag{8}$$

where ρ_{pq} is the magnitude of the normalized channel correlation function and is defined by

$$\rho_{pq} \triangleq \frac{\left|E\{T^*(F,t_p)T(F,t_q)\}\right|}{E\{|T(F,t)|^2\}} \tag{9}$$

Using the mean of $\hat{\Gamma}$ as given by (6) and the second moment of $\hat{\Gamma}$ as given by (8), the variance of $\hat{\Gamma}$ can be found to be given by

$$\sigma^2_{\hat{\Gamma}} = \frac{\Gamma^2}{K}\left[(1-\alpha)^2 + 2\epsilon^2 + \epsilon_S^2\right] + \frac{\Gamma^2(1-\alpha)^2}{K^2} \sum_{\substack{p=1 \\ p\neq q}}^{K} \sum_{q=1}^{K} \rho_{pq}^2 \tag{10}$$

Comparing (10) with (4.255), we note that for $2>\alpha>0$, the convergence of the mean SNR estimate using bias uncorrected estimates of $|T(F,t_p)|^2$ is faster than if these biases were not corrected. For the channels considered in Section 4.1, α is a usually positive number much less than 1 and, therefore, Eqs. (10) and (4.255) are essentially equivalent.

In summary, the use of unbiased estimates of $|T(F,t_p)|^2$ to estimate the mean SNR results in essentially the same performance as would have resulted if bias corrected estimates of $|T(F,t_p)|^2$ were used.

A.3 Estimation of the RMS Doppler Spread

The rms Doppler spread can be estimated from the bias uncorrected estimates of $|T(F,t_p)|^2$ using any of the three techniques analyzed in Section 4.3.2. In this appendix we will use the differentiation technique to determine the bias in estimating B^2 due to using bias uncorrected estimates of $|T(F,t_p)|^2$. It is felt that the convergence of the B^2 estimator will not be appreciably affected by these biases.

From (4.169), the estimate of B^2 for the differentiation technique is given by

$$\widehat{B^2} = \frac{T_1}{\pi^2(\Delta t)^2 T_2} \tag{11}$$

where

$$T_1 \stackrel{\Delta}{=} \frac{1}{K}\sum_{p=1}^{K}\left[|\tilde{T}(F,t_p+\Delta t)|^2 - |\tilde{T}(F,t_p)|^2\right]^2$$

$$T_2 = \frac{1}{K}\sum_{p=1}^{K}\left[|\tilde{T}(F,t_p)|^2\right]^2 \tag{12}$$

Using the bias uncorrected estimates of the magnitude squared of the channel transfer function as given in (1), then it follows that

$$E\{T_1\} = 2\overline{|T(f,t)|^2}^2\left[(1-\rho_{0,\Delta t})(1-\alpha)^2 + 2\epsilon^2 + \epsilon_S^2\right]$$

$$E\{T_2\} = 2\overline{|T(f,t)|^2}^2\left[1-\alpha+\frac{\alpha^2}{2}+\epsilon^2+\frac{\epsilon_S^2}{2}\right] + \frac{4N_0\overline{|T|^2}}{P_z(F)} + \frac{4N_0}{P_z^2(F)} \tag{13}$$

where $\rho_{\Omega,\tau}$ is defined by (4.156).

The mean value of $\widehat{B^2}$ can be determined in a manner analogous to that used in Section 4.3.2. Therefore, for K large it follows that

$$E\{\hat{B^2}\} = \frac{B^2(1-\alpha)^2 + \frac{2\epsilon^2 + \epsilon_S^2}{\pi^2(\Delta t)^2}}{1-\alpha+\frac{\alpha^2}{2}+\epsilon^2+\frac{\epsilon_S^2}{2}+\frac{1}{\Gamma}+\left(\frac{1}{\Gamma}\right)^2/2} \tag{14}$$

The effect of not correcting the bias when estimating $|T(F,t_p)|^2$ is to produce a bias in estimating B^2 even when the effects of ϵ and ϵ_S are negligible. By comparing (14) with (4.193), we note that if α and $\frac{1}{\Gamma}$ are negigible with respect to 1, then bias correction may not improve performance significantly.

A.4 Estimation of RMS Multipath Spread

The rms multipath spread can be estimated from the bias uncorrected estimates of $|T(F,t_p)|^2$ using any one of the three techniques analyzed in Section 4.3.3. For the differentiation techniques, the bias in estimating L^2 is the dual of (14). That is

$$E\{\hat{L^2}\} = \frac{L^2(1-\alpha)^2 + \frac{2\epsilon^2 + \epsilon_S^2}{\pi^2(\Delta F)^2}}{1-\alpha+\frac{\alpha^2}{2}+\epsilon^2+\frac{\epsilon_S^2}{2}+\frac{1}{\Gamma}+\left(\frac{1}{\Gamma}\right)^2/2} \tag{15}$$

Therefore, if α and $\frac{1}{\Gamma}$ are negligible with respect to 1, then bias correction may not improve performance significantly.

APPENDIX B

DETERMINATION OF BIAS IN ESTIMATING THE BRANCH ENVELOPE CORRELATION COEFFICIENT

B.1 Introduction

In this appendix we address the problem of determining the bias in estimating the branch envelope correlation coefficient. Four cases will be considered. For each case considered, an upper and a lower bound on the expected value of $\hat{\rho}_{kj}$ will be found. The expected value of $\hat{\rho}_{kj}$ will be bounded when the correlation coefficient formula (Figure 4.18) or the simplified formula [Eq. (4.261)] is used with or without correcting for the biases in estimating $|T(f,t)|^2$.

B.2 Simplified Approach with Bias Correction

From (4.261) of Section 4.3, the branch envelope correlation coefficient can be estimated by

$$\hat{\rho}_{kj} = \frac{T_{kj}}{T_i T_j} - 1 \tag{1}$$

where

$$T_{kj} = \frac{1}{K}\sum_{p=1}^{K}\left[|T_k(F,t_p)|^2(1+\epsilon_{kp}) + \delta_{kp}\right]\left[|T_j(F,t_p)|^2(1+\epsilon_{jp}) + \delta_{jp}\right]$$

$$T_k = \frac{1}{K}\sum_{p=1}^{K}|T_k(F,t_p)|^2(1+\epsilon_{kp}) + \delta_{kp}$$

$$T_j = \frac{1}{K}\sum_{p=1}^{K}|T_j(F,t_p)|^2(1+\epsilon_{jp}) + \delta_{jp} \tag{2}$$

The bias that we will determine is the asymptotic bias; that is, we will determine the bias assuming that the number of samples K is sufficiently large. With this assumption, the mean of $\hat{\rho}_{kj}$ is

$$E\{\hat{\rho}_{kj}\} = \frac{E\{T_{kj}\}}{E\{T_k T_j\}} - 1 \tag{3}$$

From (2) with δ and ϵ uncorrelated, we have

$$E\{T_{kj}\} = (1+\rho_{kj})\overline{|T_j(f,t)|^2}\ \overline{|T_k(f,t)|^2}\left(1+E\{\epsilon_{kp}\epsilon_{jp}\}\right) + E\{\delta_{kp}\delta_{jp}\}$$

$$E\{T_k T_j\} = \overline{|T_j(f,t)|^2}\ \overline{|T_k(f,t)|^2}\left[1+\frac{1}{K}\rho_{kj}\left(1+E\{\epsilon_{kp}\epsilon_{jp}\}\right)\right] + \frac{E\{\delta_{kp}\delta_{jp}\}}{K} \tag{4}$$

For large K

$$E\{T_k T_j\} = \overline{|T_j(f,t)|^2}\ \overline{|T_k(f,t)|^2} \tag{5}$$

Since we can bound the moments of the errors by

$$0 \le E\{\epsilon_{kp}\epsilon_{jp}\} \le \epsilon^2$$

$$0 \le E\{\delta_{kp}\delta_{jp}\} \le \epsilon_S^2\ \overline{|T_j(f,t)|^2}\ \overline{|T_k(f,t)|^2} \tag{6}$$

Using (4), (5), and (6) in (3) gives

$$\boxed{\rho_{kj} \le E\{\hat{\rho}_{kj}\} \le \rho_{kj}(1+\epsilon^2) + \epsilon^2 + \epsilon_S^2} \tag{7}$$

B.3 Simplified Approach Without Bias Correction

In this section we will assume that the biases in estimating $|T(f,t)|^2$ have not been corrected (except for the noise bias; see (2) of Appendix A). For this case, (3) is still valid except that the required expectations are given by

$$E\{T_j T_k\} = \overline{|T_j(f,t)|^2}\ \overline{|T_k(f,t)|^2}$$

$$E\{T_{kj}\} = \overline{|T_k(f,t)|^2}\ \overline{|T_j(f,t)|^2}\left[(1+\rho_{kj})\ 1 + E\{\epsilon_{kp}\epsilon_{jp}\} - 2\alpha + 2\alpha(1-\alpha)\right]$$

$$+ E\{\delta_{kp}\delta_{jp}\} \qquad (8)$$

Using (6) and (8) in (3), it follows that

$$\boxed{\rho_{kj}(1-\alpha)^2 \le E\{\hat{\rho}_{kj}\} \le \rho_{kj}\left[(1-\alpha)^2+\epsilon^2\right] + \epsilon^2 + \epsilon_S^2} \qquad (9)$$

B.4 Formula Approach with Bias Correction

In this section we will use the correlation coefficient formula and determine the bias in estimating ρ_{kj}. This approach is functionally presented in Figure 4.18 of Section 4.3. The estimate of ρ_{kj} is given by

$$\hat{\rho}_{kj} = \frac{T_{kj} - T_k T_j}{\left[\left(R_k - T_k^2\right)\left(R_j - T_j^2\right)\right]^{\frac{1}{2}}} \qquad (10)$$

where

$$R_k = \frac{1}{K}\sum_{p=1}^{K}\left[|T_k(F,t_p)|^2(1+\epsilon_{kp}) + \delta_{kp}\right]^2$$

$$R_j = \frac{1}{K}\sum_{p=1}^{K}\left[|T_j(F,t_p)|^2(1+\epsilon_{jp}) + \delta_{jp}\right]^2 \qquad (11)$$

Using bias corrected estimates of $|T(F,t_p)|^2$ and assuming K is sufficiently large, the it follows that (see Section 4.2):

$$E\{R_k\} - E\{T_k^2\} = \overline{|T_k(f,t)|^2}^2 \ (1 + 2\epsilon^2 + \epsilon_S^2)$$

$$E\{R_j\} - E\{T_j^2\} = \overline{|T_j(f,t)|^2}^2 \ (1 + 2\epsilon^2 + \epsilon_S^2) \qquad (12)$$

From (4), (5), (10), and (12) we have

$$E\{\hat{\rho}_{kj}\} = \frac{\rho_{kj} + (1+\rho_{kj})E\{\epsilon_{kp}\epsilon_{jp}\} + \dfrac{E\{\delta_{kp}\delta_{jp}\}}{\overline{|T_k(f,t)|^2}\ \overline{|T_j(f,t)|^2}}}{1 + 2\epsilon^2 + \epsilon_S^2} \qquad (13)$$

Using (6), we can bound $E\{\hat{\rho}_{kj}\}$ by

$$\boxed{\frac{\rho_{kj}}{1 + \epsilon_S^2 + 2\epsilon^2} \le E\{\hat{\rho}_{kj}\} \le \frac{\rho_{kj}(1+\epsilon^2) + \epsilon^2 + \epsilon_S^2}{1 + \epsilon_S^2 + 2\epsilon^2}} \qquad (14)$$

B.5 Formula Approach Without Bias Correction

When the formula approach given by (10) is applied using bias uncorrected estimates of $|T(f,t)|^2$, then it is easy to determine that for K sufficiently large

$$E\{R_k\} - E^2\{T_k\} = \overline{|T_k(f,t)|^2}^2\left[(1-\alpha)^2 + \epsilon_S^2 + 2\epsilon^2\right]$$

$$E\{R_j\} - E^2\{T_j\} = \overline{|T_j(f,t)|^2}^2\left[(1-\alpha)^2 + \epsilon_S^2 + 2\epsilon^2\right] \qquad (15)$$

Using (8) and (15), the expected value of $\hat{\delta}_{kj}$ is

$$E\left\{\hat{\delta}_{kj}\right\} = \frac{\rho_{kj}\left(1 + E\left\{\epsilon_{kp}\epsilon_{jp}\right\} - 2\alpha\right) + E\left\{\epsilon_{kp}\epsilon_{jp}\right\} - 2\alpha^2 + \dfrac{E\left\{\delta_{kp}\delta_{jp}\right\}}{|T_j(f,t)|^2\,|T_k(f,t)|^2}}{(1-\alpha)^2 + 2\epsilon^2 + \epsilon_S^2}$$

From (6), we can bound $E\left\{\hat{\rho}_{kj}\right\}$ by

$$\boxed{\frac{\rho_{kj}(1-\alpha)^2}{(1-\alpha)^2 + 2\epsilon^2 + \epsilon_S^2} \le E\left\{\hat{\rho}_{kj}\right\} \le \frac{\rho_{kj}\left[(1-\alpha)^2 + \epsilon^2\right] + \epsilon^2 + \epsilon_S^2}{(1-\alpha)^2 + 2\epsilon^2 + \epsilon_S^2}} \quad (17)$$

APPENDIX C

MINIMIZATION OF THE RMS ERROR IN ESTIMATING $|T(f,t)|^2$ CONDITIONAL UPON THE FADE LEVEL

In this appendix we address the problem of minimizing the rms fractional error in estimating the magnitude squared of the channel transfer function conditional upon a given fade level. The utility of this estimation is to obtain good estimates of $|T(f,t)|^2$ at a predetermined fade level. From (4.101) of Section 4.1.4 the variance of the output of the $|T(f,t)|^2$ estimator is given by

$$\delta^2 = \epsilon^2 |T_{00}(F,t)|^4 + \epsilon_S^2 \overline{|T(f,t)|^2}^2 \tag{1}$$

where $\overline{|T(f,t)|^2}$ has not been normalized to 1, as is the case in (4.101).

We can define a fade level by

$$F_L \triangleq \frac{|T_{00}(F,t)|^2}{\overline{|T(f,t)|^2}} \tag{2}$$

In Section 1 we used a fade level given by $-10 \log F_L$.

Using (2) in (1), it follows that

$$\delta^2 = |T_{00}(F,t)|^4 \left[\epsilon^2 + \frac{\epsilon_S^2}{F_L^2}\right] \tag{3}$$

The rms fractional error conditional upon a given fade level is defined as

$$\epsilon_C \triangleq \frac{\delta}{|T_{00}(F,t)|^2} = \left[\epsilon^2 + \frac{\epsilon_S^2}{F_L^2}\right]^{1/2} \tag{4}$$

We would like to determine the filter parameters that minimize (4). Assuming the functional form of the filters given by (4.105) and with $A_3 = \sqrt{A_1 A_2}$, it follows that

$$\epsilon_C \approx \frac{1}{\sqrt{2}} \left\{ \frac{5}{\pi WT} + \frac{\pi^4}{32} \left[\left(\frac{B^2 T^2 \sqrt{2}}{3F_L} - \frac{W^2 L^2 \sqrt{2}}{F_L} \right)^2 + \left(\sqrt{A_1} \frac{B^2 T^2 \sqrt{2}}{3F_L} + \sqrt{A_2} \frac{W^2 L^2 \sqrt{2}}{F_L} \right)^2 \right] \right\}^{1/2} \qquad (5)$$

Comparing (5) with (4.108) of Section 4.1.5, we note that the determination of W and T such that (5) is minimized is identical to the minimization of (4.108). In fact, it should be noted that (5) and (4.108) are identical except for a scaling of B and L. Therefore, the optimum filter parameters can be found from (4.116) and (4.117) to be given by

$$W_{opt} = \frac{F_L^{1/3}}{\pi L 2^{1/6}} \left\{ \frac{40\pi B L/\sqrt{3}}{(1+A_2)\left[\frac{1+A_2}{1+A_1}\right]^{1/4} + \left(\sqrt{A_1 A_2} - 1\right)\left[\frac{1+A_1}{1+A_2}\right]^{3/4}} \right\}^{1/6} \qquad (6)$$

and

$$T_{opt} = \frac{F_L^{1/3}}{\pi B 2^{1/6}} \left\{ \frac{360\pi B L \sqrt{3}}{(1+A_1)\left[\frac{1+A_1}{1+A_2}\right]^{1/4} + \left(\sqrt{A_1 A_2} - 1\right)\left[\frac{1+A_1}{1+A_2}\right]^{3/4}} \right\}^{1/6} \qquad (7)$$

Comparing (6) and (7) with (4.116) and (4.117) we note that when ϵ_C is minimized for a given value of F_L, as opposed to minimizing ϵ_p, W_{opt} and T_{opt} change by a factor $F_L^{1/3}/2^{1/6}$. For example, if for a given channel it is desired to minimize ϵ_C for $F_L = 0.001$ (i.e., a 30 dB fade), then W_{opt} and T_{opt} are approximately one-tenth of the values that minimized ϵ_p.

Substituting the respective optimum filter parameters into (5) and (4.108), then ϵ_C and ϵ_p can be related by

$$\epsilon_C = \frac{1}{\sqrt[3]{2 F_L}} \epsilon_p \tag{8}$$

In summary, optimum filter parameters have been found for estimating $|T(F,t)|^2$ at a predetermined fade level. Also, (8) can be used to evaluate the rms fractional error for the channels of interest.

MISSION

OF

ROME AIR DEVELOPMENT CENTER

RADC is the principal AFSC organization charged with planning and executing the USAF exploratory and advanced development programs for electromagnetic intelligence techniques, reliability and compatibility techniques for electronic systems, electromagnetic transmission and reception, ground based surveillance, ground communications, information displays and information processing. This Center provides technical or management assistance in support of studies, analyses, development planning activities, acquisition, test, evaluation, modification, and operation of aerospace systems and related equipment.

Source AFSCR 23-50, 11 May 70